



# UNIVERSIDAD MIGUEL HERNÁNDEZ

Doctorado en Bioingeniería

Departamento de Ingeniería de Sistemas y Automática

## NON-INVASIVE BRAIN-MACHINE INTERFACES FOR MENTAL TASKS CLASSIFICATION AND UPPER-LIMB MOVEMENT DECODING

TESIS QUE PRESENTA:

ANDRÉS ÚBEDA CASTELLANOS

DIRECTOR DE TESIS:

JOSÉ MARÍA AZORÍN POVEDA

Elche, Alicante, España

Octubre 2014



# AUTORIZACIÓN DE LA PRESENTACIÓN DE LA TESIS DOCTORAL

**Autor:** Andrés Úbeda Castellanos  
**Director:** Dr. José María Azorín Poveda  
**Programa de doctorado:** Bioingeniería  
**Título de la Tesis:** Non-Invasive Brain-Machine Interfaces for Mental Tasks  
Classification and Upper-Limb Movement Decoding

Como director de la tesis reseñada certifico que ha sido realizada bajo mi dirección por D. Andrés Úbeda Castellanos en el Departamento de Ingeniería de Sistemas y Automática de la Universidad Miguel Hernández de Elche y autorizo su presentación.

Elche, a            de            de 2014

**Fdo.:** D. José María Azorín Poveda





Dr. Eugenio Vilanova Gisbert, Director del Instituto de Bioingeniería de la Universidad Miguel Hernández de Elche,

HAGO CONSTAR,

Que el trabajo realizado por D. Andrés Úbeda Castellanos titulado "Non-Invasive Brain-Machine Interfaces for Mental Tasks Classification and Upper-Limb Movement Decoding", ha sido dirigido por D. José María Azorín Poveda, realizado en el Departamento de Ingeniería de Sistemas y Automática dentro del Programa de Doctorado en Bioingeniería, y se encuentra en condiciones de ser leído y defendido como Tesis Doctoral ante el correspondiente tribunal en la Universidad Miguel Hernández de Elche.

Y para que así conste y surta los efectos oportunos, firmo la presente en Elche, a                    de                    de 2014.





## AGRADECIMIENTOS

Ahora que termina esta etapa de mi vida me doy cuenta de la cantidad de gente que he conocido y las experiencias que he vivido durante estos años. Por desgracia, no tengo espacio ni memoria para reconocer a todos los que me han ayudado en mayor o menor medida a que logre terminar mi doctorado, por lo que incluyo en este párrafo a los que no nombre a lo largo de estas líneas.

En primer lugar, quiero agradecer a mi supervisor, José María Azorín, todo el esfuerzo y la confianza que ha puesto en mí a lo largo de este doctorado. Habría sido muy difícil llegar hasta dónde he llegado sin su apoyo. También debo hacer una mención especial a mi compañero y amigo Eduardo Iáñez que me ha aguantado durante todos estos años. Han sido años... Gracias Edu, y al resto de mis nakamas: Enrique, Álvaro y Dani, que hacéis de ir al laboratorio un motivo para levantarse contento. Por supuesto, extendiendo este agradecimiento al resto de compañeros del laboratorio y de la universidad: Javi, Juan, Luisda, Antonio, José Antonio y todos los demás.

Durante mi investigación, tuve la oportunidad de enriquecer mi experiencia tanto personal como laboral en el extranjero. Quiero agradecer muy especialmente a José Millán haberme acogido en el CNBI en Lausanne y darme la oportunidad de trabajar en un laboratorio puntero como el suyo. A Ricardo Chavarriaga por supervisarme y ocuparse de mí y a todos los demás compañeros de laboratorio. Mi experiencia en Suiza fue fantástica. Doy las gracias a mis amigos españoles que me hicieron sentir un poco más cerca de casa: José Luis, Ángela, José Manuel y Tamara. También a los chicos de Zenith con los que compartí el resto de mi estancia: Dani, Sanket, Silvia, Patrick, William, Nalin y el resto de gente de la resi.

Ha pasado tiempo, pero no quiero olvidarme de mi primera experiencia investigadora en Orihuela. Gracias a José Ramón Díaz por tratarme tan bien. Gracias a Gema, Amparo y al resto de compañeros. Gracias a las cabritas. Fueron cuatro meses inolvidables.

Durante estos años muchos han estado a mi lado. Gracias a los compañeros de

UNRV, el otro trozo de nuestro grupo. Pasé un año fantástico allí. Gracias a todos los que conocí en ese laboratorio y contribuyeron al buen rollo que siempre reinaba. Muchos pasaron de ser buenos compañeros a grandes amigos. En ese aspecto, gracias muy especialmente a Antonio y Andrés, a los que tengo el más profundo aprecio. Ellos lo saben. Quiero dejar para el final a mi querido Círculo: Rocío, Gaby, Ílida, Alam y Edu, por hacer ese primer año de tesis uno de los mejores de mi vida. Qué puedo decir que no sepáis.

A mis amigos... Cuando uno se cansaba del trabajo han estado allí para traerme de vuelta al mundo. A los Chewbaccas: Jose, Gabriel, Morell. Sois unos cracks. Y a los demás, Alberto, Mari, Carmen, Juanjo.

Por último, dedico esta tesis y el mayor de mis agradecimientos a mi familia. A mi madre, a mi padre y a mi hermano, que me han aconsejado, apoyado, reanimado, estimulado, espoleado y querido.

Muchas gracias.





## RESUMEN

Una Interfaz Cerebro-Máquina (del inglés, Brain-Machine Interface, BMI) es un dispositivo que permite registrar, procesar y clasificar las señales cerebrales de un sujeto para generar comandos de control. En otras palabras, una BMI permite a una persona prescindir de los caminos neuromusculares convencionales para interactuar con el entorno. Las BMI pueden ser invasivas o no invasivas. Las BMI no invasivas se basan en el análisis y la clasificación de patrones mentales sin la necesidad de realizar ningún tipo de implante quirúrgico. Un ejemplo de esta tecnología es el análisis de señales electroencefalográficas (EEG) medidas sobre el cuero cabelludo. Estos sistemas han experimentado un gran avance en su uso sobre humanos debido a su facilidad de preparación y sus ventajas éticas y de seguridad frente a las alternativas invasivas. La tecnología BMI tiene un futuro prometedor en la rehabilitación de las capacidades motoras, la restauración del control motor en pacientes con discapacidades severas o en la asistencia de personas con una pérdida total de movilidad. En esta tesis se han desarrollado varios tipos de BMI no invasivas con las que se pretende alcanzar una mejor comprensión de la comunicación cerebro-máquina y que sirven como base de futuras herramientas de rehabilitación y asistencia para personas con discapacidad motora.

En un primer estudio, el concepto de mapeado EEG se ha aplicado a una BMI espontánea en tiempo real basada la imaginación motora para obtener clasificadores precisos de dos tareas mentales. El clasificador se basa en una correlación de imágenes entre mapas EEG. Los parámetros del clasificador se han optimizado para obtener una clasificación robusta y fiable. Este clasificador se ha probado en la clasificación en tiempo real de tareas mentales y posteriormente se ha empleado con éxito para

controlar un robot planar asistivo para alcanzar objetivos en un entorno bidimensional. Para ello, se han diseñado varias estrategias de control del robot y se han probado en tiempo real para maximizar la fiabilidad del sistema BMI.

En un segundo estudio, se ha analizado la decodificación del movimiento del miembro superior de la persona aplicando técnicas de regresión lineal a las componentes EEG de baja frecuencia. Se han llevado a cabo distintos procedimientos experimentales para mostrar las posibilidades reales de usar métodos de regresión lineal para decodificar la cinemática del miembro superior a partir de señales EEG. Se ha estudiado la actividad neural asociada al movimiento real e imaginado del miembro superior para mostrar correlaciones significativas entre la cinemática real y decodificada. Adicionalmente, la decodificación continua de la cinemática del miembro superior se ha simplificado a una alternativa discreta para clasificar diferentes objetivos alcanzados mostrando ventajas prometedoras en relación a la precisión y fiabilidad del proceso. También se ha estudiado la influencia del movimiento del brazo realizado en relación a su velocidad, trayectoria y variabilidad. Finalmente, el método de decodificación se ha aplicado en tiempo real para detectar movimientos horizontales de la mano.

Esta tesis proporciona metodologías que se pueden emplear en multitud de aplicaciones asistivas o de rehabilitación de personas con discapacidad motora. Esta tesis ha permitido además avanzar en la comprensión de las correlaciones neuro-motoras y proporciona nuevos conocimientos para investigaciones futuras.

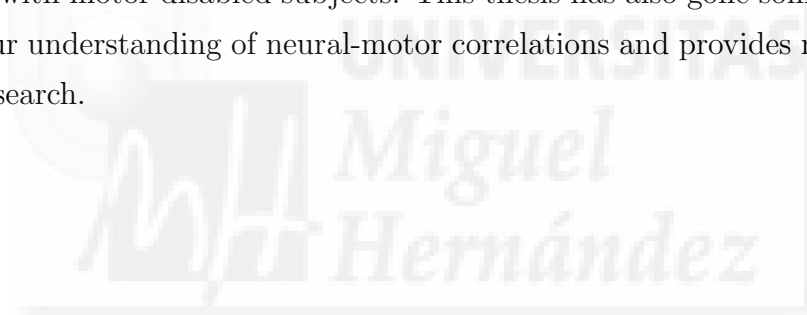
## ABSTRACT

A Brain-Machine Interface (BMI) is a device that allows registering, processing and classifying the brain signals from a person to generate control commands. In other words, a BMI allows a person to bypass the conventional neuromuscular pathways to interact with the environment. A BMI can be invasive or non-invasive. Non-invasive BMIs are based on the analysis and classification of brain patterns without the need of any surgical implant. An example of this technology is the analysis of electroencephalographic (EEG) recordings from the scalp. The use of these systems has experienced a great progress in humans due to their short-term preparation and their advantages in terms of ethics and safety compared to invasive approaches. BMI technology has a promising future in rehabilitating motor capabilities, restoring motor control of severely disabled patients and assisting people with a total motor loss. In this thesis, different BMI-based techniques have been developed to achieve a better understanding of brain-machine communication and to serve as base of future rehabilitation and assistive tools for motor disabled people.

In a first study, the concept of EEG mapping has been applied to a real-time spontaneous motor imagery BMI to obtain accurate classifiers for two mental tasks. The classifier is based on an image correlation between EEG maps. The classifier parameters have been optimized to obtain a robust and reliable classification. This classifier has been tested in a real-time classification of mental tasks and then used to successfully control an assistive planar robot to reach targets in a bidimensional setup. To that end, several robot control strategies have been designed and tested in real-time to maximize the reliability of the BMI system.

In a second study, upper-limb movement decoding has been analyzed by applying linear regression techniques to low frequency EEG components. Different experimental procedures have been undertaken to assess the real possibilities of using linear regression methods to decode upper limb kinematics from EEG signals. Neural activity in imagined and actual upper-limb movements has been studied to show significant correlations between decoded and real kinematics. Additionally, continuous decoding of upper-limb kinematics has been simplified to a discrete approach for the classification of reached targets showing promising advantages in terms of accuracy and reliability. The influence of the performed arm movement has been also studied in terms of velocity, trajectory and variability. Finally, the decoding method has been applied in real-time to decode horizontal hand movements.

This thesis provides methodologies to be applied in many rehabilitation and assistive applications with motor disabled subjects. This thesis has also gone some way towards enhancing our understanding of neural-motor correlations and provides new knowledge for future research.





# CONTENTS

<b>AGRADECIMIENTOS</b>	<b>vii</b>
<b>RESUMEN</b>	<b>x</b>
<b>ABSTRACT</b>	<b>xii</b>
<b>CONTENTS</b>	<b>xv</b>
<b>LIST OF TABLES</b>	<b>xix</b>
<b>LIST OF FIGURES</b>	<b>xxiii</b>
<b>LIST OF ACRONYMS</b>	<b>xxvii</b>
<b>1 INTRODUCTION</b>	<b>1</b>
1.1 Background and Motivations . . . . .	1
1.2 Thesis Contributions . . . . .	4
1.3 Thesis Structure and Publications . . . . .	5
<b>2 BRAIN-MACHINE INTERFACES</b>	<b>7</b>
2.1 Introduction . . . . .	7
2.2 Causes of Motor Impairment . . . . .	8

2.2.1	Stroke . . . . .	8
2.2.2	Spinal Cord Injury . . . . .	11
2.2.3	Other Causes of Motor Impairment . . . . .	13
2.3	What is a Brain-Machine Interface? . . . . .	14
2.4	Methods for Measuring Brain Activity . . . . .	16
2.4.1	Invasive Recordings . . . . .	16
2.4.2	Partially Invasive Recordings. Electrocorticography (ECoG) . . . . .	17
2.4.3	Non-Invasive Recordings . . . . .	18
2.4.3.1	Functional Magnetic Resonance Imaging (fMRI) . . . . .	18
2.4.3.2	Magnetoencephalography (MEG) . . . . .	18
2.4.3.3	Electroencephalography (EEG) . . . . .	19
2.5	EEG-Based Brain-Machine Interfaces . . . . .	20
2.5.1	Mental Task Recognition . . . . .	21
2.5.2	Evoked Potentials . . . . .	21
2.5.3	Other Potentials . . . . .	22
2.6	Brain-Machine Interfaces for Assistance and Rehabilitation . . . . .	22
<b>3</b>	<b>EEG MAPPING CLASSIFICATION</b>	<b>25</b>
3.1	Introduction . . . . .	25
3.2	EEG Mapping Classifier . . . . .	27
3.2.1	Image Correlation Classifier . . . . .	27
3.2.2	Classifier Parameters . . . . .	30
3.3	Analysis of the EEG Mapping Classifier . . . . .	33
3.3.1	EEG Data Used . . . . .	33
3.3.2	Frequency Study . . . . .	34
3.3.3	Time Interval Study . . . . .	37
3.3.4	Uncertainty Study . . . . .	37
3.3.5	Discussion and Conclusions . . . . .	40
3.4	Real-Time Application . . . . .	45
3.4.1	Materials and Methods . . . . .	45
3.4.1.1	Register . . . . .	45
3.4.1.2	Processing . . . . .	47

3.4.1.3	EEG Mapping Classifier . . . . .	48
3.4.1.4	Classifier Adjustment Protocol . . . . .	49
3.4.1.5	Visual Interface and Trajectory Application . . . . .	50
3.4.2	Results and Discussion . . . . .	52
3.4.3	Conclusions . . . . .	55
3.5	Control of an Assistive Planar Robot . . . . .	56
3.5.1	Materials and Methods . . . . .	57
3.5.1.1	Hierarchical Control . . . . .	57
3.5.1.2	Directional Control . . . . .	58
3.5.2	Results and Discussion . . . . .	60
3.5.3	Conclusions . . . . .	64
3.6	Conclusions . . . . .	65
<b>4</b>	<b>UPPER LIMB MOVEMENT DECODING</b>	<b>67</b>
4.1	Introduction . . . . .	67
4.2	Continuous and Discrete Decoding in Center-Out Tasks . . . . .	70
4.2.1	Materials and Methods . . . . .	71
4.2.2	Experimental Tests . . . . .	71
4.2.2.1	Preprocessing . . . . .	72
4.2.2.2	Decoding . . . . .	74
4.2.2.3	Analysis . . . . .	74
4.2.3	Results . . . . .	76
4.2.3.1	Continuous Decoding . . . . .	76
4.2.3.2	Discrete Decoding . . . . .	79
4.2.3.3	Decoding passive movement . . . . .	82
4.2.4	Discussion and Conclusions . . . . .	85
4.3	Analysis of Movement Variability . . . . .	89
4.3.1	Materials and Methods . . . . .	89
4.3.1.1	Subjects . . . . .	89
4.3.1.2	Experimental Paradigm . . . . .	90
4.3.1.3	EEG Recordings and Preprocessing . . . . .	90
4.3.1.4	Data Decoding Procedure . . . . .	91

4.3.1.5	Participant Survey . . . . .	92
4.3.2	Results . . . . .	92
4.3.3	Discussion . . . . .	97
4.3.4	Conclusions . . . . .	99
4.4	Real-Time Decoding . . . . .	100
4.4.1	Materials and Methods . . . . .	100
4.4.1.1	Experimental Procedure . . . . .	100
4.4.1.2	Register and Preprocessing . . . . .	101
4.4.1.3	Decoding Method and Classification of Targets . . . . .	101
4.4.2	Results and Discussion . . . . .	103
4.4.3	Conclusions . . . . .	104
4.5	Conclusions . . . . .	106
<b>5</b>	<b>CONCLUSIONS AND FUTURE WORK</b>	<b>109</b>
5.1	Conclusions . . . . .	109
5.2	Future Works . . . . .	112
<b>6</b>	<b>CONCLUSIONES Y TRABAJOS FUTUROS</b>	<b>115</b>
6.1	Conclusiones . . . . .	115
6.2	Trabajos Futuros . . . . .	118
	<b>BIBLIOGRAPHY</b>	<b>121</b>
<b>A</b>	<b>Hardware and Equipment</b>	<b>137</b>
A.1	EEG Acquisition Devices . . . . .	137
A.1.1	gUSBamp BMI System . . . . .	137
A.1.2	BioSemi ActiveTwo BMI System . . . . .	140
A.2	Planar Robot Arm . . . . .	142

## LIST OF TABLES

2.1	Methods for measuring brain activity: a comparative . . . . .	16
3.1	EEG Mapping success rate (%) with a time interval of 5 seconds . . . .	36
3.2	Subject 1, results with uncertainty (Frequency: 10 Hz, Time Interval: 3 seconds) . . . . .	41
3.3	Subject 2, results with uncertainty (Frequency: 10 Hz, Time Interval: 2 seconds) . . . . .	42
3.4	Subject 3, results with uncertainty (Frequency: 12 Hz, Time Interval: 3 seconds) . . . . .	43
3.5	Optimal parameters of the image correlation classifier for each subject .	44
3.6	Training results with the BMI based on EEG Mapping . . . . .	54
3.7	Tests results with the BMI based on EEG Mapping . . . . .	56
3.8	Experimental results using the BMI based on EEG Mapping to control the planar robot . . . . .	62
4.1	Accuracy percentages (%) for different disc speeds (mm/s) and sizes (diameter in pixels) . . . . .	95
4.2	Pearson correlation coefficients after decoding hand trajectories performed with the planar robot for different disc speeds (mm/s) and sizes (diameter in pixels) . . . . .	96

4.3 Success rate (%) obtained for the classification of two targets . . . . . 104







## LIST OF FIGURES

1.1	Cerebro-Vascular Disease (CVD) burden across the world . . . . .	2
1.2	Brain-Machine Interfaces publications . . . . .	3
2.1	Types of stroke: (a) Ischemic stroke. (b) Hemorrhagic Stroke . . . . .	9
2.2	Consequences of SCI depending on the location of the injury . . . . .	12
2.3	General structure of a Brain-Machine Interface. . . . .	15
2.4	International System 10/20 (left). International System 10/10 (right). . . . .	20
3.1	Classification algorithm . . . . .	29
3.2	Optimization protocol . . . . .	31
3.3	Electrodes position for BCI Competition using International 10/10 System (left). Example of an EEG map from Subject 1, 12 Hz, Word Task (right) . . . . .	35
3.4	Average success rate after cross-validation for different frequencies . . . . .	36
3.5	Average success rate after cross-validation for different time intervals with the selected frequencies . . . . .	37
3.6	Subject 1 - Evolution of the success (SR), error (ER) and uncertainty rate (UR) for different uncertainty thresholds and selection of thresholds using the three methods proposed (M1, M2 and M3) . . . . .	38

3.7	Subject 2 - Evolution of the success (SR), error (ER) and uncertainty rate (UR) for different uncertainty thresholds and selection of thresholds using the three methods proposed (M1, M2 and M3) . . . . .	39
3.8	Subject 3 - Evolution of the success (SR), error (ER) and uncertainty rate (UR) for different uncertainty thresholds and selection of thresholds using the three methods proposed (M1, M2 and M3) . . . . .	39
3.9	Real-time Brain-Machine Interface environment . . . . .	46
3.10	Electrodes location on the motor cortex (left). Example of EEG map (right) . . . . .	47
3.11	Visual interface for BMI training . . . . .	51
3.12	Offline BMI register timing paradigm . . . . .	52
3.13	Several trajectories performed by the volunteers using a BMI based on EEG Mapping . . . . .	52
3.14	Evolution of the success rate for left and right mental tasks during the online training for Subject 1 . . . . .	55
3.15	Experimental environment of the planar robot . . . . .	58
3.16	Hierarchical control protocol . . . . .	59
3.17	Hierarchical control interface (left). Directional control interface (right) . . . . .	60
3.18	Example of test with the hierarchical control protocol . . . . .	60
3.19	Results with the directional control strategy for goals 1, 2 and 3 (scale in mm) . . . . .	63
4.1	Experimental setup . . . . .	73
4.2	Continuous decoding of center-out trajectories for motor imagery center-out (A) and real center-out movement (B) for the frequency band 0.1-2 Hz . . . . .	77
4.3	Continuous decoding of kinematics using the linear regression decoding method (Subject 3 - Real Center-out Movement) . . . . .	78
4.4	Continuous decoding of center-out trajectories comparing different experimental data: motor imagery center-out, real center-out movement, shuffled data and random data . . . . .	80

4.5	Comparison between different frequency bands: 0.1-2 Hz (low frequencies), 8-12 Hz (alpha band), 14-30 Hz (beta band) and 0.1-40 Hz . . . .	81
4.6	Discrete decoding of center-out trajectories for motor imagery center-out (A) and real center-out movement (B) . . . . .	83
4.7	Discrete decoding of center-out trajectories comparing different experimental data: motor imagery center-out, real center-out movement, shuffled data and random data . . . . .	84
4.8	Continuous (A) and discrete (B) decoding of center-out trajectories for passive center-out movement . . . . .	86
4.9	Continuous (A) and discrete (B) decoding of center-out trajectories comparing active center-out movement and passive center-out movement . .	87
4.10	Experimental environment showing the subject performing the tracking movements in front a screen . . . . .	91
4.11	Example of trajectory followed by a subject . . . . .	93
4.12	Example of a decoded trajectory for subject 4 . . . . .	93
4.13	Decoding performance regarding speed (mm/s) and disc size (small, medium, big) . . . . .	97
4.14	Radial representation of the volunteers general impressions . . . . .	97
4.15	System architecture to decode horizontal hand movements . . . . .	101
4.16	Experimental environment where the subject performs horizontal trajectories with the computer mouse . . . . .	102
4.17	Example of the decoded X position during horizontal hand movements	103
4.18	Average classification rates for each subject compared to chance level rates	105
A.1	gUSBamp technical specifications . . . . .	138
A.2	gUSBamp passive 16-electrodes system . . . . .	138
A.3	gUSBamp active 16-electrodes system . . . . .	139
A.4	BioSemi ActiveTwo active 64-electrodes system . . . . .	141
A.5	Pneumatic planar robot: Parts. . . . .	142
A.6	Pneumatic planar robot: Components. . . . .	143



## LIST OF ACRONYMS

<b>BMI</b>	Brain-Machine Interface
<b>BCI</b>	Brain-Computer Interface
<b>EEG</b>	Electroencephalography
<b>CVA</b>	Cerebro-Vascular Accident
<b>SCI</b>	Spinal Cord Injury
<b>ALS</b>	Amyotrophic Lateral Sclerosis
<b>ECoG</b>	Electrocorticography
<b>fMRI</b>	Functional Magnetic Resonance Imaging
<b>MEG</b>	Magnetoencephalography
<b>SCP</b>	Slow Cortical Potentials
<b>ERD</b>	Event Related Desynchronization
<b>PSD</b>	Power Spectral Density
<b>GSR</b>	Global Success Rate



## 1.1 Background and Motivations

According to the European Commission in the VI Framework Programme of Research and Development (2002-2006) [1], the number of people with disability in Europe is around 50 million people (10% of the population) affected by different deficiencies: wheelchair users (2.8 millions), deaf people (1.1 millions), hearing impaired (80 millions), blind people (1.1 millions), other visual impairments (11.5 millions), speech difficulties (5.5 millions), cognitive impairment (30 millions) and reduced strength (22.5 millions). From this statistics, it can be concluded that more than 25 million people in Europe have disability related to motor impairment.

In the particular case of Spain, according to the Olivenza Report in 2010 [2], there are around 3.8 million people with a disability. From this total, 25.9% are affected by vision problems, 28.1% from hearing limitations, 19.5% have problems with communication, 16.6% suffer from cognitive impairment, 67.2% have a reduced mobility, 48.4% have self-care limitations, 55.3% have domestic problems and 16.4% suffer from difficulties in personal relationships. This means that in Spain there are around 2.5 million people with mobility or motor limitations.

One of the main causes of motor limitation is stroke (Figure 1.1). The World Health Organization estimates that more than 17.3 million people died of cardiovascular diseases such as heart attack or stroke in 2008 [3]. For people who survive a stroke (around 85% of the total), the rehabilitation of the affected side is crucial to maintain

or even regain motor and cognitive capabilities. In Spain, the number of stroke survivors was around 329.500 in 2008 (8.7% of the total disabled population) [4].

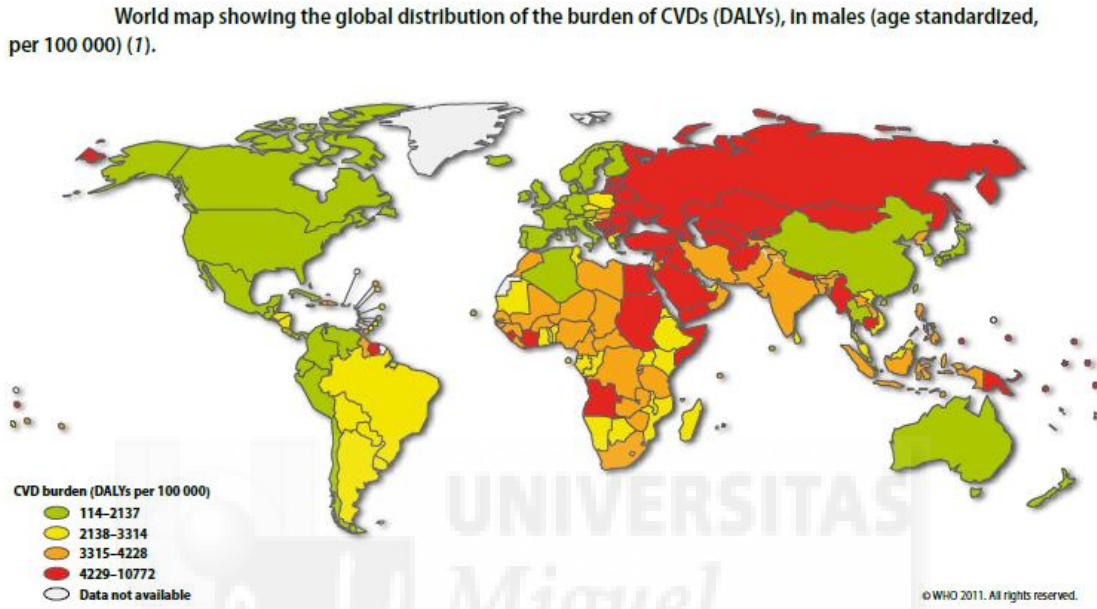


Figure 1.1: Cerebro-Vascular Disease (CVD) burden (Disability-Adjusted Life Year, DALY) across the world (Source: World Health Organization [3]).

In recent years, the interest for solving and reducing the limitations caused by motor problems of disabled people has been accompanied by a very important development of assistive and rehabilitation technologies. Focusing on the specific case of motor disability, the main goal is to rehabilitate the motor capabilities of a patient with movement limitations or, if this is not possible, to replace the natural movement by a commanded action over an external device. In this sense, Brain-Machine Interfaces (BMIs) allow, through voluntary thoughts of the subject, interacting with the environment without the need of any actual motor activity or physical effort. The field of Brain-Machine Interfaces has seen an impressive development during the last few years (Figure 1.2). Only in the present decade, the number of publications about BMIs has almost doubled. It is particularly remarkable the interest of applying this technology for assistive and re-

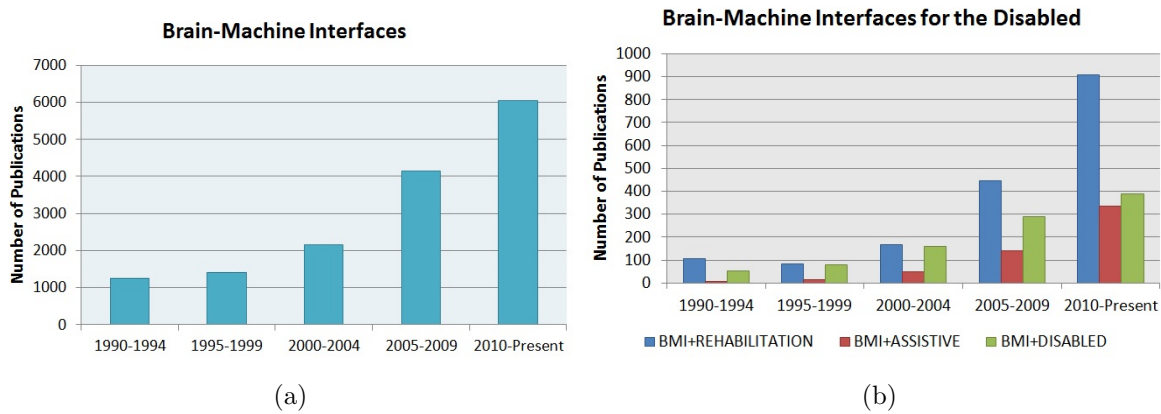


Figure 1.2: Brain-Machine Interfaces publications (Source: Science Direct [5]): (a) Search criteria: Brain-Machine Interface. (b) Search Criteria: Brain-Machine Interface + Rehabilitation/Assistive/Disabled.

habilitation purposes, which has become one of the most important fields of application of BMIs in current research.

In this thesis, the main motivation is to achieve a better understanding of brain-machine communication to serve as base of future rehabilitation and assistive tools for motor disabled people, particularly for people suffering from stroke. Other causes of motor impairment will also benefit from the contributions of this work (a further review on stroke and these other causes is undertaken in Chapter 2). This thesis is part of the BRAIN2MOTION Project supported by Ministerio de Economía y Competitividad of the Spanish Government (DPI2011-27022-C02-01). The main goal of BRAIN2MOTION project is to develop a new hybrid Exoskeletal Robot/Motor Neuro-Prostheses (ER-MNP) for the upper limb interfaced to the users by means of non-invasive brain-machine interfaces (BMIs). This thesis serves as a methodological support for future experimental procedures with the ER-MNP and disabled subjects. The robotic hybrid system combines a light and kinematically compatible ER, and a textile-based surface MNP. In this combined ER-MNP, hardware and control strategies are being developed to combine the action of the ER and MNP while preserving motor latent capabilities of the user. A non-invasive EEG-based Brain-Machine Interface is being used to differentiate between several mental tasks. This is achieved by incorporating new adaptive classifiers into the

BMI. Learning strategies are being developed in order to improve the performance and versatility of the BMI. The hybrid ER-MNP controlled by the BMI is being used to perform reaching and grasping operations. The system is being validated with patients suffering from neurological conditions leading to severe motor disorders, in particular cerebrovascular accident (CVA). This thesis has also been supported by the predoctoral grant VALi+d ACIF/2012/135 and the research visitor grant BEFPI/2013/043 both from Conselleria d'Educació, Cultura i Esport of Generalitat Valenciana of Spain.

## 1.2 Thesis Contributions

This thesis has led to the following contributions to the current literature:

- This thesis presents a **novel classification of mental tasks method based on the correlation of EEG maps**. This classifier has been successfully tested in non-invasive spontaneous Brain-Machine Interfaces.
  1. The EEG mapping classifier has been optimized by designing a proper parameter adjustment methodology.
  2. The EEG mapping classifier has been successfully tested with healthy subjects in real-time environments.
  3. The EEG mapping classifier has been successfully tested with healthy subjects in a real world scenario by controlling an assistive robot arm.
- This thesis gives **additional evidence** with respect to the **decoding of upper limb kinematics from low frequency EEG components**.
  1. Continuous decoding of hand kinematics has shown significant correlations not related to muscular artifacts between real and decoded kinematics during the performance of center-out movements.
  2. Discrete decoding of center-out movements has been applied to report an advantage in future real-time applications.

3. The influence of the performed arm movement has been studied in terms of velocity, trajectory and variability.
4. The discrete decoding method has been successfully applied to a real-time application to detect horizontal arm movements.

This research will serve as a base for future studies and provides useful methodologies to be applied in rehabilitation and assistive applications with motor disabled subjects. This thesis has also gone some way towards enhancing our understanding of neural-motor correlations and provides new knowledge for future research.

### 1.3 Thesis Structure and Publications

The thesis document is organized as follows:

- **Chapter 2** describes Brain-Machine Interfaces and their applications. First, it shows a brief description of the causes of motor disability that may lead to the need of assistive and rehabilitation systems such as Brain-Machine Interfaces. Then, the chapter reviews the different types of Brain-Machine Interfaces and their applications in the field of assistive and rehabilitation technologies.
- **Chapter 3** describes a non-invasive spontaneous Brain-Machine Interface based on the correlation of EEG maps. On a first section, the EEG mapping classifier is presented in detail. This has led to the publication of two conference papers [6, 7] and a journal article [8]. Afterwards, the system has been successfully tested in a real-time environment. This has led to the publication of a journal article [9]. Finally, the classifier has been applied to a real world scenario, particularly, to the control of a planar robot arm in an assistive application. This has led to the publication of two conference papers [10, 11].
- **Chapter 4** gives new evidences of the decoding of upper limb kinematics from low frequency EEG components. To that end, different experimental procedures have been undertaken to assess the real possibilities of using linear regression methods

to decode upper limb kinematics from EEG signals. First, continuous and discrete decoding of center-out movements have been analyzed. This has led to the submission of a journal article [12]. Afterwards, the influence of the performed arm movement in terms of velocity, trajectory and variability has been studied. This has led to the submission of a journal article [13]. Finally, the discrete decoding method has been tested in real-time. This has led to the preparation of a conference paper [14].

- **Chapter 5 and 6** contain the conclusions and future work related to the contents and contributions of this thesis.
- **Appendix 1** contains information about the hardware and equipment used in this thesis.



## BRAIN-MACHINE INTERFACES

### 2.1 Introduction

In recent years, the interest for solving or, at least, reducing the limitations caused by motor problems of disabled people has been accompanied by a very important development of assistive technologies. These technologies can be defined as the use of any assistive, adaptive and rehabilitation device that enables disabled people to perform tasks that they were formerly unable to accomplish. In the case of motor disability, these devices can replace the natural movement by a commanded action over a external device such as a prosthesis or orthosis (motor substitution), but also can help in the rehabilitation of the motor capabilities of a patient with movement difficulties. A more common way to improve the interaction between the subject and the environment consists of establishing alternative communication channels with external devices such as a computer or a robot through the so-called human-machine interfaces (HMIs). Amongst these devices, there is a great number of possibilities such as ocular interfaces, voice control, adapted mechanical switches and many more. A particular case of this kind of devices, which will be explained in detail throughout the chapter, are brain-machine interfaces (BMIs) which allow, through voluntary thoughts of the subject, interacting with the environment without the need of any actual motor activity or physical effort.

## 2.2 Causes of Motor Impairment

Motor disability may be caused by many different conditions. The most common one is a cerebrovascular accident (CVA), which occurs when the blood supply to the brain stops [15, 16]. If the length of this interruption is longer than several seconds, brain cells can die causing a permanent damage in the patient. When this damage occurs in the brain areas responsible for motor control, the patients may suffer permanent or temporal loss of mobility, coordination and control of their limbs. Another important cause of motor disability is due to Spinal Cord Injury (SCI), which provokes the total loss of sensibility and movement capability below the level of the injury [16, 21, 22]. In this case, the patient assistance must be purely based on motor substitution, given that it is impossible to perform a rehabilitation procedure. Finally, less frequent illnesses and diseases may cause motor disfunctions, such as cerebral palsy, spina bifida, muscular dystrophy, amyotrophic lateral sclerosis (ALS) or central nervous system diseases such as Parkinson syndrome or Huntington disease [16].

### 2.2.1 Stroke

A stroke or cerebrovascular accident (CVA) happens when blood flow to a part of the brain stops. If blood flow is stopped for longer than a few seconds, the brain cannot get blood and oxygen. When this happens, brain cells can die, causing permanent damage [15, 16].

There are two major types of stroke: ischemic stroke and hemorrhagic stroke (Figure 2.1). Ischemic stroke is the most common one (85% of cases). It occurs when a blood vessel that supplies blood to the brain is blocked by a blood clot. Ischemic strokes may be caused by clogged arteries. Fat, cholesterol, and other substances collect on the artery walls, forming a sticky substance called plaque. A hemorrhagic stroke occurs when a blood vessel in part of the brain becomes weak and bursts open, causing blood to leak into the brain. Some people have defects in the blood vessels of the brain that make this more likely.

Some strokes result in death whereas others cause permanent or temporary disability. About 2 out of 10 people who have a stroke die within the first month, 3 out of 10

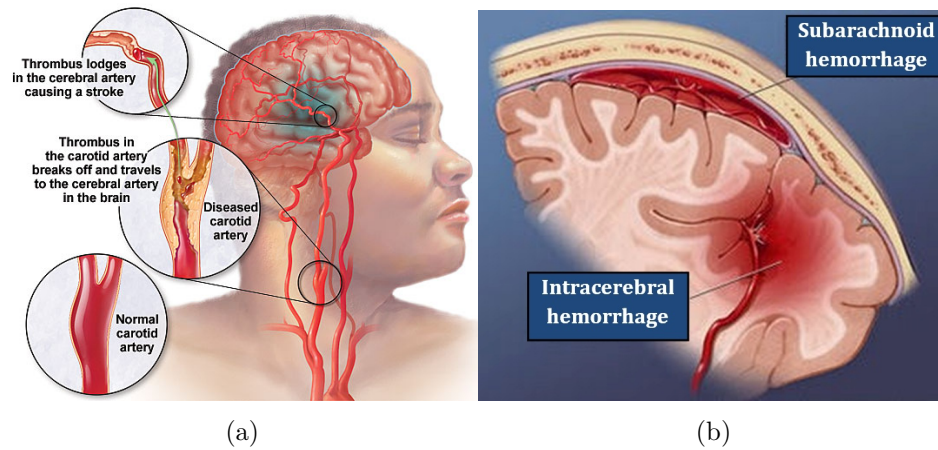


Figure 2.1: Types of stroke: (a) Ischemic stroke (Source: Mayo Foundation for Medical Education and Research). (b) Hemorrhagic stroke (Source: Barrow Neurological Institute).

die within the first year, and 5 out of 10 die within the first 5 years. The more time that passes after a stroke, the lesser is the risk of dying from it. People who have a subarachnoid or intracerebral hemorrhage as the cause of their stroke are more likely to die than people who have an ischemic stroke.

High blood pressure is the main risk factor for strokes. Other major risk factors are: atrial fibrillation, diabetes, familiar history of stroke, high cholesterol, increasing age or race. People who have heart disease or poor blood flow in their legs caused by narrowed arteries are also more likely to have a stroke. Also, the chance of suffering stroke is higher in people who live an unhealthy lifestyle. Birth control pills can increase the chances of having blood clots. The risk is highest in women who smoke and are older than 35.

The symptoms of stroke depend on what part of the brain is damaged. In some cases, a person may not know that he or she has had a stroke. Symptoms usually develop suddenly and without warning. Or, symptoms may occur on and off for the first day or two. Symptoms are usually most severe when the stroke first happens, but they may slowly get worse. The main symptom is the headache suffered due to the bleeding in the brain. Other symptoms depend on how severe the stroke is and what

part of the brain is affected. Symptoms may include changes in feeling, hearing, taste or alertness, clumsiness, confusion, memory loss, difficulty swallowing, reading or writing and motor symptoms such as loss of balance and coordination, muscle weakness and lack of control.

The goal of treatment after a stroke is to help the patient recover as much function as possible and prevent future strokes. Problems moving, thinking, and talking often improve from weeks to months after a stroke. A number of people who have had a stroke will keep improving in the months or years after the stroke. The recovery time and need for long-term treatment is different for each person and it is generally divided into four phases [17]:

1. Treatment: This begins when a person first enters the hospital. Doctors will determine the type of stroke and will provide the appropriate treatment. This may consist of drugs to break up clots, tPA, and thin the blood or surgery to repair a broken blood vessel. Treatment is aimed at preventing another stroke from taking place and limiting the amount of brain damage that occurs.
2. Recovery: After a stroke, some spontaneous recovery takes place for most people. Abilities that may have been lost will begin to return. This process can take place very quickly over the first few weeks, and then, it may begin to taper off.
3. Rehabilitation: This phase usually takes place while the patient is still in the hospital. Various therapists and specialists will work with the stroke victim to bring back lost skills.
4. Returning home: In this phase, the patient usually continues the rehabilitation procedures that started in the hospital.

Motor impairment after stroke is the major cause of permanent disability. This kind of subjects usually suffer from upper limb movement limitations in their affected side, and the recovery of the arm movement is often variable and incomplete [18]. This recovery is crucial in order to perform activities of the daily life. In this sense, the use of non-invasive BMIs may be useful to support traditional motor restoration procedures [19, 20].

### 2.2.2 Spinal Cord Injury

A spinal cord injury is a damage to the spinal cord that may result from direct injury to the cord itself or indirectly from disease of the surrounding bones, tissues or blood vessels [16, 21, 22]. Spinal cord trauma can be caused by a number of injuries to the spine, including: assault, falls, gunshot wounds, industrial accidents, motor vehicle accidents or sports injuries. Most spinal cord trauma happens to young, healthy individuals so people ages 15 - 35 are most commonly affected. The death rate tends to be higher in young children with spinal injuries.

A minor injury can cause spinal cord injury if the spine is weakened (such as from rheumatoid arthritis or osteoporosis) or if the spinal canal protecting the spinal cord has become too narrow (spinal stenosis) due to the normal aging process. More often, a direct injury, such as cuts, can occur to the spinal cord, especially if the bones or the disks have been weakened. Direct damage can also occur if the spinal cord is pulled, pressed sideways, or compressed. Bleeding, fluid buildup, and swelling can occur inside or outside the spinal cord (but within the spinal canal). The buildup of blood or fluid can press on the spinal cord and damage it.

Symptoms vary depending on the location of the injury (Figure 2.2). Spinal cord injury causes weakness and loss of feeling at, and below the injury. How severe symptoms are depends on whether the entire cord is severely injured (complete) or only partially injured (incomplete).

- When spinal cord injuries occur in the neck area, symptoms can affect the arms, legs, and middle of the body. The symptoms may occur on one or both sides of the body. Symptoms can also include breathing difficulties from paralysis of the breathing muscles, if the injury is high up in the neck.
- When spinal injuries occur at chest level, symptoms can affect the legs. Injuries to the cervical or high thoracic spinal cord may also result in blood pressure problems, abnormal sweating, and trouble maintaining normal body temperature.
- When spinal injuries occur at the lower back level, symptoms can affect one or both legs, as well as the muscles that control the bowels and bladder.

Injuries near the top of the spine lead to more disability than injuries low in the spine. Paralysis and loss of sensation of part of the body are common. This includes total paralysis or numbness, and loss of movement and feeling. Death is possible, especially if there is paralysis of the breathing muscles. A person who recovers some movement or feeling within one week usually has a good chance of recovering more function, although this may take 6 months or more. Losses that remain after 6 months are more likely to be permanent.

Patients who have suffered from spinal cord injuries are incapable of performing daily life activities and they generally need modifications in their homes to adapt them to their needs. Most of the SCI paralyzed make use of wheelchairs and assistive devices so the application of non-invasive BMIs can be very useful to assist them in daily life activities.

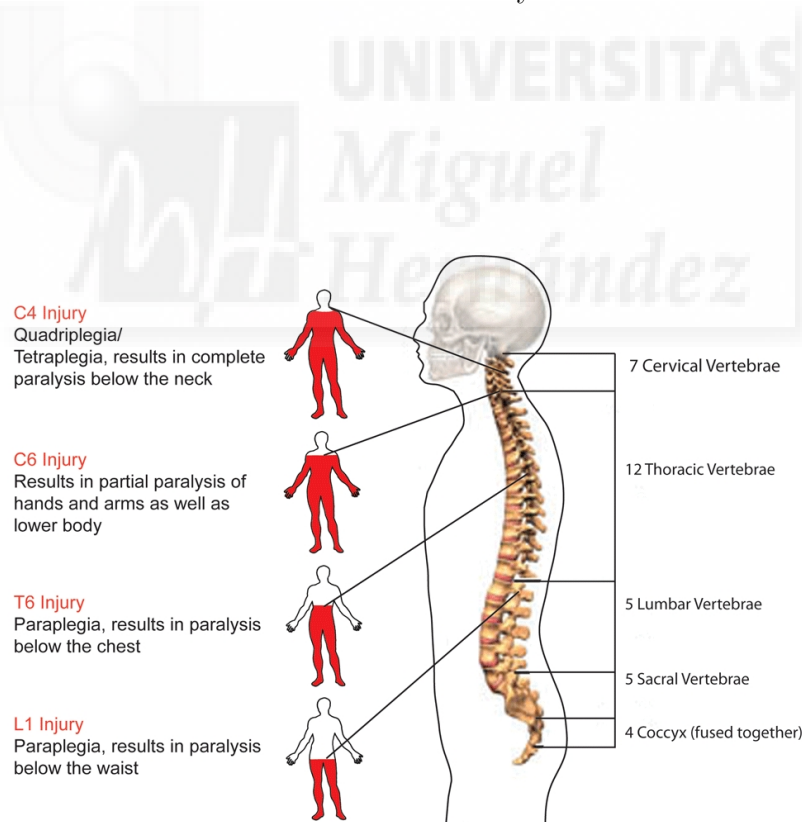


Figure 2.2: Consequences of SCI depending on the location of the injury (Source: Internet, Unknown Author).

### 2.2.3 Other Causes of Motor Impairment

Stroke and spinal cord injuries are not the only causes of a partial or complete paralysis of the limbs. Cerebral palsy, spina bifida, muscular dystrophy or multiple sclerosis are pathologies that affect motor capabilities to a greater or lesser extent and the people affected by these diseases may require external assistance to develop their activities.

- **Cerebral palsy:**

Cerebral palsy is caused by injuries or abnormalities of the brain [16]. Most of these problems occur as the baby grows in the womb. But they can happen at any time during the first 2 years of life, while the brain of the baby is still developing. In some people with cerebral palsy, parts of the brain are injured due to a low level of oxygen (hypoxia) in the area. Premature infants have a slightly higher risk of developing cerebral palsy. Cerebral palsy may also occur during early infancy as a result of several conditions such as bleeding in the brain, infections or head injury. The effects of cerebral palsy are diverse including muscle weakness, abnormal gait, tremors, loss of coordination, speech and hearing problems and even seizures.

- **Spina bifida:**

Spina bifida occurs when there is birth defect involving incomplete closure of the spine [16]. It is thought that the main cause of spina bifida may be a lack of folic acid in the body of the woman before and during early pregnancy. The effects of this malformation are partial or total loss of sensations, partial or total paralysis of lower limbs and loss of motor control in hips and legs.

- **Muscular dystrophy:**

Muscular dystrophy is a disorder that involves muscle weakness and loss of muscle tissue, which get worse over time [16]. As any other degenerative illness, the muscular capabilities change depending on the stage of the disease. The loss of muscle tissue leads to a progressive motor limitation as strength and muscular control decreases, generating problems in walking and frequent falls. In severe cases, people who suffer from muscular dystrophy cannot look after themselves,

but symptoms can be generally slowed down and controlled through proper rehabilitation therapies.

- **Multiple sclerosis:**

Multiple sclerosis is caused by damage to the myelin sheath, the protective covering that surrounds nerve cells [16]. When this nerve covering is damaged, nerve signals slow down or stop. It provokes problems with coordination, spasticity, fatigue and loss of mobility in severe cases, often when the illness is not treated in time.

- **Other diseases that affect the nervous system:**

Parkinson syndrome, Huntington disease and other illnesses that affect the central nervous system [16] may lead to tremors and involuntary movements in the upper limb that, in advanced stages, may cause important limitations in daily life activities.

## 2.3 What is a Brain-Machine Interface?

A Brain-Machine Interface (BMI) is a system that processes brain signals and translates them into useful information that can be used to generate control commands without performing any muscular movement. The general structure of a BMI can be seen in Figure 2.3. After the proper signal processing, external devices or applications can be controlled with the only help of our thoughts. The use of a BMI has a potentially wide range of useful outcomes. However, in terms of usability and reliability there are still great prospects for improvement [23].

The system architecture of a BMI is generally structured according to four main blocks: data acquisition, preprocessing, feature extraction and classification.

- **Data acquisition:** Neural information is recorded through specific equipment. The analog data of the brain activity is translated into a digital output that can be processed to identify the intention of the subject.

- **Preprocessing:** To obtain reliable outputs, neural information is processed to improve the quality of the signal or filter specific features of the brain activity. After this preprocessing, the valuable information can be extracted.
- **Feature extraction:** From the preprocessed signals, the feature extractor obtains the most representative characteristics of the neural information that identify the particular brain process.
- **Classification:** The classifier differentiates between different brain processes by computing the signal features and generates an output command.

During the last decade, the field of BMIs has seen an outstanding progress in many fields: communication, assistance, rehabilitation, games, device control and many more. In the following sections, we will briefly explain the different types of BMI and its applications, particularly in assistive and rehabilitation procedures.

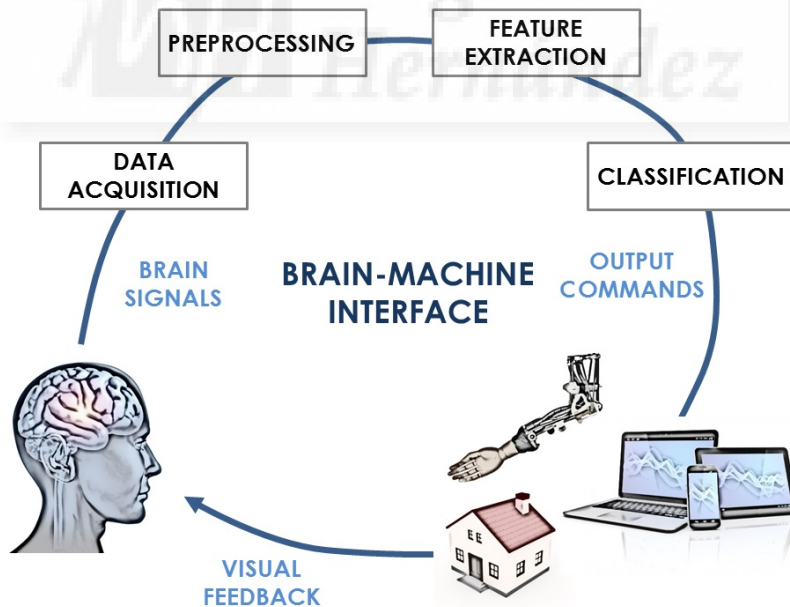


Figure 2.3: General structure of a Brain-Machine Interface.

## 2.4 Methods for Measuring Brain Activity

There are several methods for measuring brain activity. Depending on the invasiveness of the recordings they can be divided into invasive, partially invasive and non-invasive. Table 2.1 shows a comparative between methods stating advantages and disadvantages in terms of spatial and temporal resolution, cost and complexity.

	INTRACORTICAL	ECoG	EEG	fMRI	MEG
Invasiveness	High	Medium	Low	Low	Low
Spatial Resolution	Very High	Medium	Very Low	Low	Very Low
Temporal Resolution	High	Medium	Medium	Low	High
Measurement	Neuronal Activity	Cortical Activity	Cortical Activity	Oxygen Level Blood Flow	Neuronal Activity
Cost	High	High	Low	High	High
Facilities	Little Space	Little Space	Little Space	Large Space	Large Space

Table 2.1: Methods for measuring brain activity: a comparative (ECoG: Electro-corticography, EEG: Electroencephalography, fMRI: Functional Magnetic Resonance Imaging, MEG: Magnetoencephalography).

### 2.4.1 Invasive Recordings

Invasive BMI approaches are based on recordings of individual neurons (single units), groups of them (multi-units) or local field potentials (LFPs). When a neuron generates an action potential, the signal propagates down the neuron as a current which flows in and out of the cell through excitable membrane regions in the soma and axon. This activity can be measured with precise microelectrode systems that are implanted directly on the brain cortex. The first experiments began in the 1960s, where monkeys learned to control their cortical activity voluntarily supported by a biofeedback of the

firing rate of single neurons [24]. In 1980, Schmidt suggested the possibility of obtaining a voluntary motor control of a prosthetic device extracted from the information of cortical activity [25]. These findings opened a promising future in the restoration of motor functions of the paralyzed.

During the last few years, the development of invasive approaches has importantly increased, mainly centered in the experimentation with non-human primates. Further research has been undertaken to study the number of cortical implants, the cortical location of these implants and the type of neural signal measured (local field potentials or single/multi units). Particularly remarkable are the works from Nicolelis team, engrossing the knowledge about neural ensembles physiology [26, 27, 28, 29]. Other important studies have also given account of intracortical experiments in monkeys [30, 31]. Invasive approaches have been successfully used in people with motor disabilities to perform reaching and grasping tasks [32, 33].

Intracortical recordings provide the highest resolution and signal quality of brain recording methods. The main problem of invasive recordings is the high complexity of the intracranial operation to implant the electrodes arrays. This leads to risk of tissue damage and infection, and the stability and durability of the implants during long-term recordings is still a problem to be solved.

### **2.4.2 Partially Invasive Recordings. Electrocorticography (ECoG)**

Electrocorticography (ECoG) consists of recording electroencephalographic (EEG) activity directly from the surface of the brain cortex. ECoG was first used to treat epilepsy by Penfield and Jasper in 1950. Despite being less invasive than single unit or LFP recordings, this methodology still requires the use of surgery to implant the electrodes and, as a consequence, entails the same risks and disadvantages of invasive procedures. Another drawback is that ECoG is usually applied to short-term studies as it is generally associated to the clinical needs of the patients [34]. However, this technique keeps good signal to noise ratio and improves the quality of EEG recorded signals (electrodes are closer to the source of information). Also, the surgery is far less complex providing a very interesting tool for BMI research. In this sense, recent works have obtained significant results by applying this measurement technique for BMI

applications [35, 36, 37, 38].

## 2.4.3 Non-Invasive Recordings

### 2.4.3.1 Functional Magnetic Resonance Imaging (fMRI)

Functional Magnetic Resonance Imaging (fMRI) is a functional neuroimaging procedure that uses magnetic resonance imaging to measure brain activity by detecting associated changes in blood flow. In 1890, Roy and Sherrington found a link between brain function and blood flow. In 1990, Ogawa discovered that mental activity could be assessed by measuring blood oxygenation. The blood oxygen level dependent (BOLD) could be measured through MRI and near-infrared spectroscopy (NIRS). This correlation with neural activity has been widely studied in current research [39, 40, 41]. The main advantage of fMRI is its high spatial resolution. Researchers have successfully trained subjects to volitionally control brain regions using feedback from a real-time fMRI [42]. Recent work has even shown the possibility of controlling a two-dimensional robotic arm through motor imagery tasks [43]. The main drawback of this technology is the high cost and big space needed for the equipment which makes fMRI non-portable and unsuitable for commercial purposes.

### 2.4.3.2 Magnetoencephalography (MEG)

Magnetoencephalography (MEG) consists of the recording of the magnetic fields produced in the brain. MEG signals were first measured by Cohen in 1968. This technique is based on the fact that electrical currents inside the brain generate associated magnetic fields. This effect is clearly measurable on the brain cortex. MEG has been recently used as a potential source to operate BMIs [44, 45]. This procedure is not invasive and has a slightly higher spatial resolution than other non-invasive methods such as EEG. MEG-based BMI systems have been applied in the rehabilitation of stroke patients [46] and for two-dimensional control of computers [47]. The main drawback is the high cost of the equipment and the need of magnetic shielding to prevent external magnetic sources to interfere with the measurements which reduces the portability of these devices.

### 2.4.3.3 Electroencephalography (EEG)

Electroencephalography (EEG) is the recording of the activity of the cerebral cortex through electrodes placed on the surface of the scalp. Hans Berger recorded the first EEG in 1924. During the last century, EEG recordings were mainly used to detect epilepsy, but in the 90s, the application of this technique experimented a huge progress for all sorts of applications. To the date, EEG recordings have seen a rapid development and are widespread for BMI-based applications as the equipment is relatively cheap and portable and it has a good temporal resolution. However, the signal to noise ratio and the spatial resolution of the signals is still quite low compared to other recording methods. Current research has successfully designed EEG-based BMIs for the control of external devices, communication, clinical applications, assistance and rehabilitation [48, 49, 50, 51].

The EEG is usually described in terms of rhythmic activity and this activity has been divided into several frequency bands. Although this characterization is still a matter of discussion, the following list shows some of the most common frequency bands applied to EEG processing:

- Delta band (<4 Hz): it usually appears in frontal regions and it is characterized by high-amplitude waves found during sleep or, sometimes, continuous-attention tasks [52]. It can be a symptom of subcortical lesions and other brain pathologies [53].
- Theta band (4-7 Hz): it reflects drowsiness and it is sometimes associated with inhibition of elicited responses and with cognitive control [54]. It can be a symptom of subcortical lesions and other brain pathologies [55].
- Alpha band (8-15 Hz): it is usually located in posterior regions of both sides of the cortex and appears when closing the eyes or relaxing. It is also common in comatose states [56].
- Beta band (16-31 Hz): beta activity is symmetrically distributed over the cortex with a higher activity in frontal regions and characterized by low-amplitude waves. It reflects active thinking, focusing and stress [57].

- Gamma band ( $>32$  Hz): located in the somatosensory cortex it usually appears during dual tasks that involve more than one sense and short-term memory matching [58].
- Mu band (8-12 Hz): located in the sensorimotor cortex it reflects the activity of the motor neurons [59].

To measure EEG activity, a standard criteria for the placement of electrodes has been agreed. The International System 10/20 is an internationally recognized method to describe the location of scalp electrodes in the context of an EEG test or experiment [60]. This system is based on the relationship between the location of an electrode and the underlying area of cerebral cortex. One of its modifications, the International System 10/10, is widely used in current BMI research (Figure 2.4).

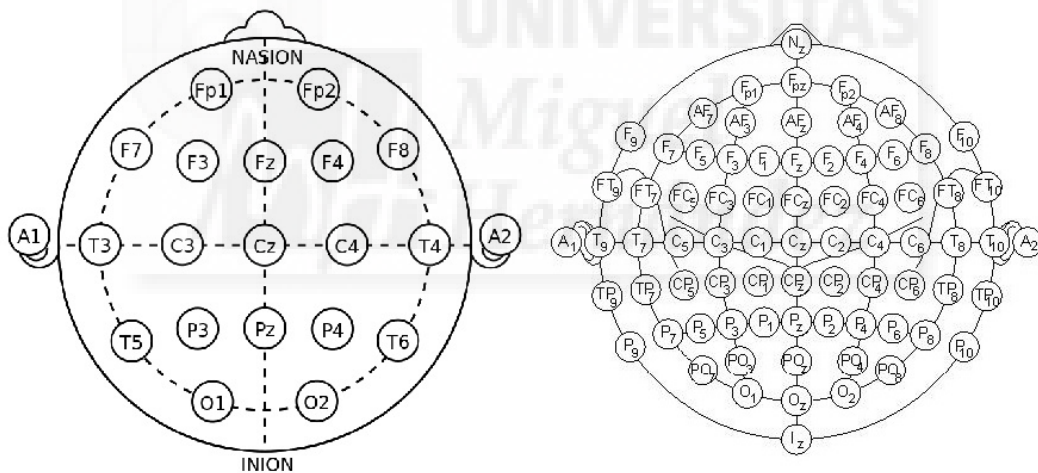


Figure 2.4: International System 10/20 (left). International System 10/10 (right).

## 2.5 EEG-Based Brain-Machine Interfaces

There are several techniques that have been applied to EEG-Based Brain-Machine Interfaces. Non-invasive BMIs have been traditionally divided into spontaneous and evoked systems. However, current development in EEG signal analysis has opened a

wide range of methodologies to detect neural patterns. In this section, some of the most important ones are briefly described.

### 2.5.1 Mental Task Recognition

Spontaneous BMIs have a great advantage when using applications where performing voluntary commands is necessary. In these systems, the user performs a volitive cognitive action, i.e., thinks of a particular mental task, generating a command willingly. This approach has been used to control a robot arm [61, 62] or a virtual keyboard [63]. Motor imagery consists of the imagination of real motor movement performed by the user. According to Decety and Lindgren, the mental activity of an actual and an imagined motor movement follows the same pattern [64]. The analysis of the activity in regions destined to motion action may allow the detection of different mental tasks such as motor imagery. Moreover, other kinds of mental activity (e.g., concentration tasks) can be studied in order to obtain a better differentiation between mental tasks. The use of these EEG signals can allow patients with mobility impairments to control systems that provide an improvement in their quality of life.

### 2.5.2 Evoked Potentials

Evoked BMIs are based on the extraction of a characteristic EEG signal pattern produced automatically in the brain as a response to some external stimuli [65].

One evoked potential widely explored in the field of BMI is the P300 [66]. P300 is a potential evoked by an awaited infrequent event and it is characterized by a positive deflection in the EEG signal approximately produced 300 milliseconds after receiving a visual stimulus and mostly located covering the parietal lobe. This paradigm was first used in 1998 to develop a speller application [65]. However, this paradigm has been used recently on other applications, such as controlling a wheelchair [67] or an Internet browser [68, 69]. In these applications, in order to evoke the P300, subjects are given a sufficiently large number of options (e.g., letters of the alphabet or icons) from which they choose one by paying attention to the desired one. These options are pseudo-randomly flickering in a screen and it is possible to determine which choice the

subject intended as a target, simply by selecting the stimulus that elicits the largest P300. This technique is known as oddball paradigm.

Another example of evoked potential is the N2PC, which is a negative deflection in the EEG approximately produced 200 milliseconds after a visual stimulus that appears in the visual cortex contralateral to the side where the stimulus is attended. This potential has been widely studied to prove its relationship with selective attention [70, 71]. There are also other visual evoked potentials, such as Steady State Visually Evoked Potentials (SSVEP), which are signals that are natural responses to visual stimulation at specific frequencies [72, 73, 74].

### 2.5.3 Other Potentials

Slow Cortical Potentials (SCPs) are slow EEG changes that last between a second to several seconds. Researchers have discovered that it is possible to self-regulate these brain potentials with the help of a proper feedback [75, 76]. This kind of potentials have also been applied to the decoding of upper and lower limb kinematics [77, 78]. Other event-related potentials such as Event-Related Desynchronization have been studied [79]. The standard measure of ERD quantifies the induced change in signal band power as the difference between a baseline prior to the event and a post-event period. By convention an ERD corresponds to a negative value, i.e., a decrease in power, while event-related synchronization (ERS) refers to an increased signal power. This paradigm has been used to study gait onset [80].

## 2.6 Brain-Machine Interfaces for Assistance and Rehabilitation

As it has been reported, Brain-Machine Interfaces suppose a novel way to enhance human capabilities beyond the neuromuscular system. This opens a promising path to the development of tools to help people with severe motor disabilities to rehabilitate their motor capabilities or to replace their natural movement with the use of a commanded device. In this section, current applications of BMIs both for rehabilitation [49] and

assistive purposes [51] are analyzed.

Brain-Machine Interfaces have been widely used to command communication and control systems [48]. Birbaumer et al. developed a spelling device system that could be operated by people suffering from Amyotrophic Lateral Sclerosis (ALS) [76]. Other BMI-driven devices have been developed to work either synchronously [62] or asynchronously [81, 82]. Some web browsers are based on evoked potentials such as P300 [68, 83]. This kind of potentials have been also tested with ALS patients using a four odd-ball paradigm for task selection [84].

Another important application of brain interfaces is assisting mobility. BMI-driven wheelchairs enable quadriplegic patients to move around on their own [67, 85]. Also, telepresence robots have been mentally controlled [86]. These robots are equipped with sensors to detect obstacles and reconstruct pathways. In both cases, a shared-control approach is necessary to evaluate the user intention along with the information provided by the sensors and cameras.

One of the main challenges of BMIs is motor substitution. Mental commands can control hand and arm prostheses and orthoses or even lower-limb exoskeletons. This is extremely useful for people with a complete paralysis such as SCI patients. Intracortical BMIs have taken the lead of current applications. In some studies, the motor cortical activity of monkeys was used to perform reaching and grasping activities with a robot arm [30], or to perform three dimensional movements that included force grasping for self-feeding using a mechanical device [31]. By using implanted electrodes, it is also possible to control a computer cursor [87, 88]. Recently, non-invasive approaches have been used in the research of clinical applications. Wolpaw et al. have demonstrated that it is possible to achieve one, two and three dimensional control of a cursor from EEG signals [89, 90]. In other study, a hand orthosis was controlled by tetraplegic patients by learning to generate separable motor imagery tasks [91].

The use of BMIs to support rehabilitation procedures has been recently explored with promising expectations [49]. The use of these systems during motor recovery is still in its early stages [92]. Nevertheless, according to Mak and Wolpaw, the application of BMI systems can augment the current rehabilitation therapies by reinforcing and increasing effective use of impaired brain areas and connections [50]. An example

of this reinforcement is the use of neuroprostheses guided through Functional Electrical Stimulation (FES) and motor imagery classification [81]. In another study, the BMI was guided by a four-class SSVEP, which controlled a hand prosthesis [93]. With these techniques it would be possible to restore motor capabilities such as grasping in severely impaired patients. However, the system bit rate is still quite low and it is necessary to develop intelligent controllers to avoid system errors. An interesting approach to post-stroke recovery has also shown that motor imagery can activate sensorimotor networks affected by the lesion. In this study, hand motor imagery led to a simultaneous contralateral ERD and ipsilateral ERS after some training sessions [94]. The main drawback of these procedures is the lack of information of how the brain cortex behaves when an injury occurs. In those cases, further research should explore and particularize the neural activity of stroke patients.



## MENTAL TASK CLASSIFICATION FROM EEG SIGNALS USING EEG MAPPING

### 3.1 Introduction

In recent years, there has been an increasing interest in performing an accurate classification of mental tasks in non-invasive spontaneous BMIs [95, 96, 97]. The classification of mental activity related to motor imagery is very common in literature. When a motor movement is performed, a particular band of frequencies between 8 and 12 Hz (Mu band) is activated. The classification of this kind of mental tasks has been proved to be quite accurate. The most common mental task classification methods in spontaneous BMIs are usually based on mathematical algorithms like LDA (Linear Discriminant Analysis) or SVM (Support Vector Machine) which are used to find a combination of features to separate two or more classes [96]. There are also techniques based on neural networks [98, 99] or methods using k Nearest Neighbours (kNN) and probabilistic Bayesian classifiers [97, 95]. Different methods for motor imagery classification have also been studied [100, 101, 102].

The main purpose of this chapter is to apply the concept of EEG mapping to a real-time spontaneous motor imagery BMI. To that end, a classification algorithm based on image correlation between EEG maps has been developed. EEG mapping was mainly used related to clinical diagnosis of mental diseases whose origin is located in EEG alterations such as epilepsy [103, 104] or schizophrenia [105]. It was also used in electrotherapy [106]. This technique consists of obtaining a visual plotting

of the brain activity (usually in terms of frequency), which is a more representative method for determining EEG alterations. In these clinical works, each session processed consisted of several minutes of recording. This processing time is totally useless for a BMI, which works with small windows of time to be able to perform commands in real time. An alternative to EEG mapping is the use of EEG microstates, which are transient patterned states of EEG that are associated with initializations of human neurological tasks. This approach has been used to decode visual-related stimulus [107] or to analyze timing of exploratory and exploitation decisions [108]. Regarding motor imagery classification, EEG microstates have been applied to provide feedback about relevant task-related mental patterns [109]. However, the use of short processing time windows may affect the stability of classification.

In this chapter, we first present a classifier based on EEG mapping (Section 3.2). The classification algorithm is based on an image correlation between the EEG maps obtained from the EEG data processed. To test the classifier, we have used data provided by IDIAP Research Institute for BCI Competition 2003, based on the performance of mental tasks related to motor imagery (Section 3.3). The classifier depends on several parameters that affect the overall accuracy. An in-depth analysis of these parameters (the frequency chosen for each subject, the time interval processed, and an uncertainty threshold) previously introduced in the classifier, has been undertaken to optimize the method and obtain a suitable configuration protocol for tests in a real BMI environment.

Afterwards, the EEG mapping classifier is tested in real time (Section 3.4). For this purpose, the EEG maps are obtained after a suitable processing of the raw EEG data registered from 4 healthy subjects who have participated in the experiments. Two mental tasks related to motor imagery are classified, including an uncertainty state to prevent errors in classification. To measure the accuracy and reliability of the EEG mapping classifier, the subjects have performed several trajectories in order to control the cursor position in a visual interface using the BMI. An in-depth analysis of the frequency and uncertainty threshold chosen for each subject has been performed to optimize the method and to obtain a better performance of the classification.

Finally, the classifier has been applied to a real world scenario (Section 3.5). A BMI

based on the correlation of EEG maps has been used to control a pneumatic planar robot arm in an assistive application. The application designed consists of moving the end effector of the robot in a plane in order to reach a certain target. The subject sits in front of a screen located in the robot environment. A visual interface showed the different movement options. The first strategy is based on a hierarchical control where the subject can decide the axis and the direction of movement. The second strategy is based on a directional control, where the subject can continuously decide the direction of the movement and the command is generated periodically. Both strategies have been tested by performing trajectories to reach several goals on a plane. The results show that the subject is able to successfully reach the goals and suggest that the system is capable of performing more complex tasks in a realistic environment, for example, grasping daily objects with a gripper.

## 3.2 EEG Mapping Classifier

In this section, we present a classifier based on EEG mapping. The classification algorithm is based on an image correlation between the EEG maps obtained from the EEG data processed. The classifier depends on several parameters that affect the overall accuracy. An in-depth analysis of these parameters (the frequency chosen for each subject, the time interval processed, and an uncertainty threshold) introduced in the classifier, has been undertaken to optimize the method and obtain a suitable configuration protocol for future tests in a real BMI environment.

### 3.2.1 Image Correlation Classifier

The EEG maps obtained from EEG data are used to perform the classification. The EEG mapping consists of the geometrical representation of the activity of the recorded electrodes in terms of frequency. Each EEG map shows a particular frequency and mental task. Figure 3.1 shows an example of the classification process for three mental tasks. This classification is divided into two main parts: models obtention and the classifier itself. The data used to test the classifier has been split into model sessions and test session. The model data has been used to obtain suitable EEG models to perform

the classification. These models, together with the test session, are the input of the image correlation classifier. The input data takes into account two main parameters: processing time interval and frequency. The election of these parameters is critical for a good classification and the protocol to obtain them, as well as the uncertainty threshold used in the classifier block, will be explained in detail later.

In the top block of the classification algorithm (Figure 3.1) the models for each mental task are obtained by processing the data registered in the model sessions. To that end, several EEG maps are created using a particular frequency and a particular processing time interval (between 1 and 5 seconds). The selection of these two parameters is critical as they affect the accuracy of the classification.

For each mental task, the data are processed in windows of an specific duration (time interval) and several images of the same task are created. These images are averaged to obtain a unique image for each mental task so the final output of this block will be a set of several images (model EEG maps) corresponding to the mental tasks trained (one EEG model map for each task).

After obtaining the models, a different set of data is used to test the classification. To that end, the data are processed in trials (with the selected time interval and frequency) to obtain the EEG map. This image is compared using a *normalized cross-correlation* [110] with the models obtained before as it is explained in Figure 3.1. This kind of comparison between images improves substantially the accuracy of the classification of a previous work based on simpler methods of image comparison [6].

The correlation between two signals (cross correlation) is a standard approach to feature detection and also a component of more sophisticated techniques [110, 111]. However, there are several disadvantages of using this technique for template matching or in this case, in image comparison:

- If the image varies with position, matching can fail.
- The range is dependent on the size of the feature. In this case the size of the shape.
- The algorithm is not invariant to changes in image amplitude, which are common in the EEG maps obtained as the amplitude of the signal is not stable.

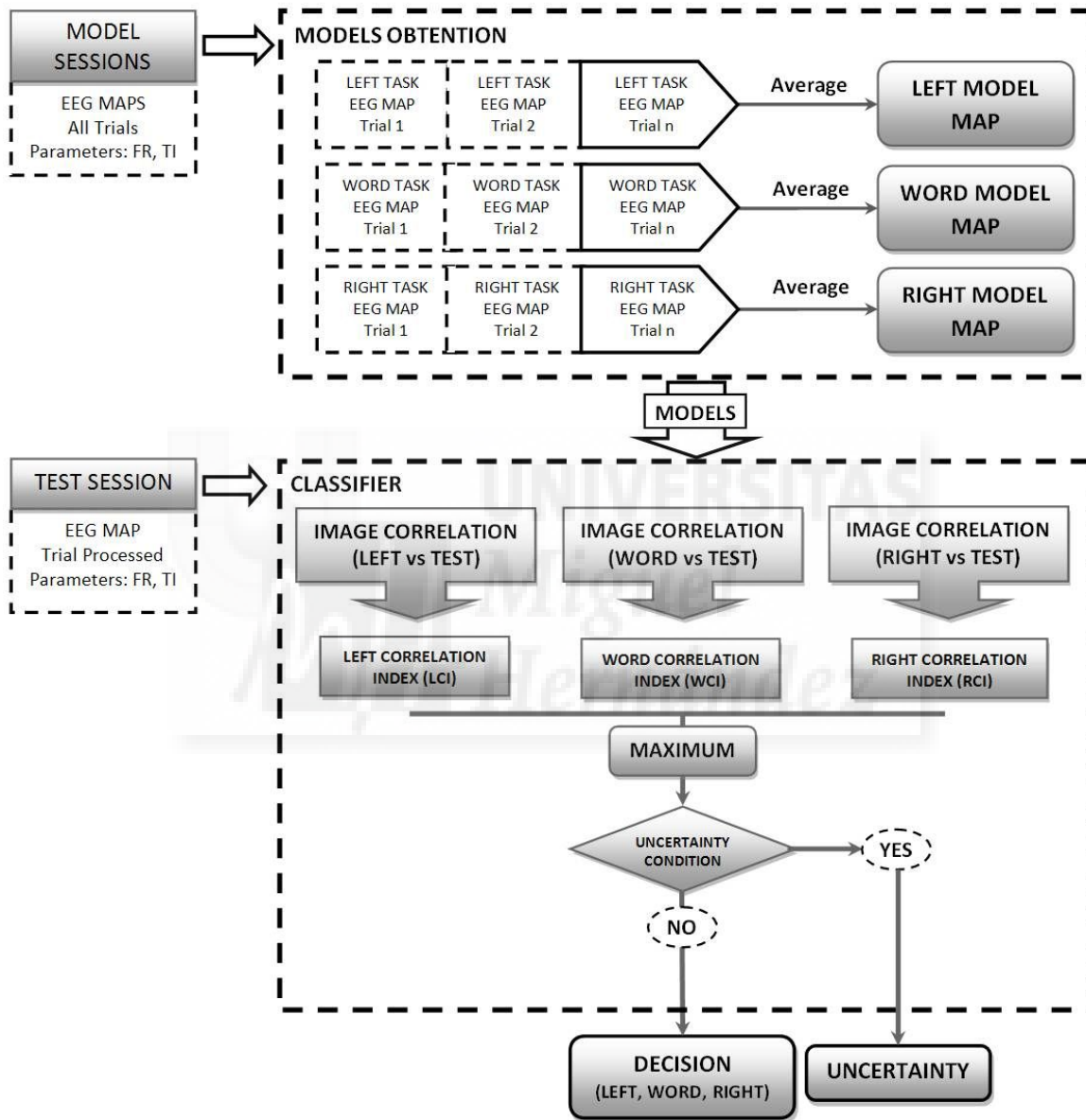


Figure 3.1: Classification algorithm. FR: optimal frequency. TI: time interval.

The *normalized cross-correlation* has been used to solve these limitations. The similarity between the EEG maps will be obtained as shown in (3.1):

$$\gamma(u, v) = \frac{\sum_{x,y}[f(x, y) - \bar{f}_{u,v}][m(x - u, y - v) - \bar{m}]}{\{\sum_{x,y}[f(x, y) - \bar{f}_{u,v}]^2 \sum_{x,y}[m(x - u, y - v) - \bar{m}]^2\}^{0.5}} \quad (3.1)$$

where  $f(x, y)$  is the EEG map of the trial to be classified,  $m(x, y)$  is EEG map of the model,  $\bar{m}$  is the mean of the EEG map of the model and  $\bar{f}_{u,v}$  is the mean of the EEG map of the trial which is going to be classified.

The resulting matrix  $\gamma(u, v)$  contains the correlation coefficients of each point of the output image  $(u, v)$ , which can range in value from -1 to 1. To obtain a unique correlation coefficient, the highest value of the matrix is selected as the images change in shape and position. This is made to work with a more reliable correlation parameter.

When a particular session of data is tested (Figure 3.1), each trial is compared with the models using the *normalized cross-correlation* algorithm. After this comparison, an index of correlation for each task is obtained. The maximum value of the index is selected obtaining the corresponding class. Afterwards, an uncertainty condition is evaluated. To that end, the indexes of correlation previously obtained are compared. An uncertainty threshold is subtracted to the maximum value, if one or both of the remaining two indexes are still above this limit, the trial is rejected and classified as uncertainty. If not, the mental task with the maximum correlation value remains. The computational load of this operation is around 200 ms which makes it suitable for real-time BMI applications.

### 3.2.2 Classifier Parameters

As it has been mentioned before, the selection of the parameters of the classifier (frequency, time interval and uncertainty threshold) is a very important factor. The accuracy of the final classifier depends substantially on this selection of parameters. To obtain the best success rate on the final classification, an optimization protocol is proposed in Figure 3.2. The protocol follows a specific order:

1. The optimal frequency is studied. Only the best one is selected.

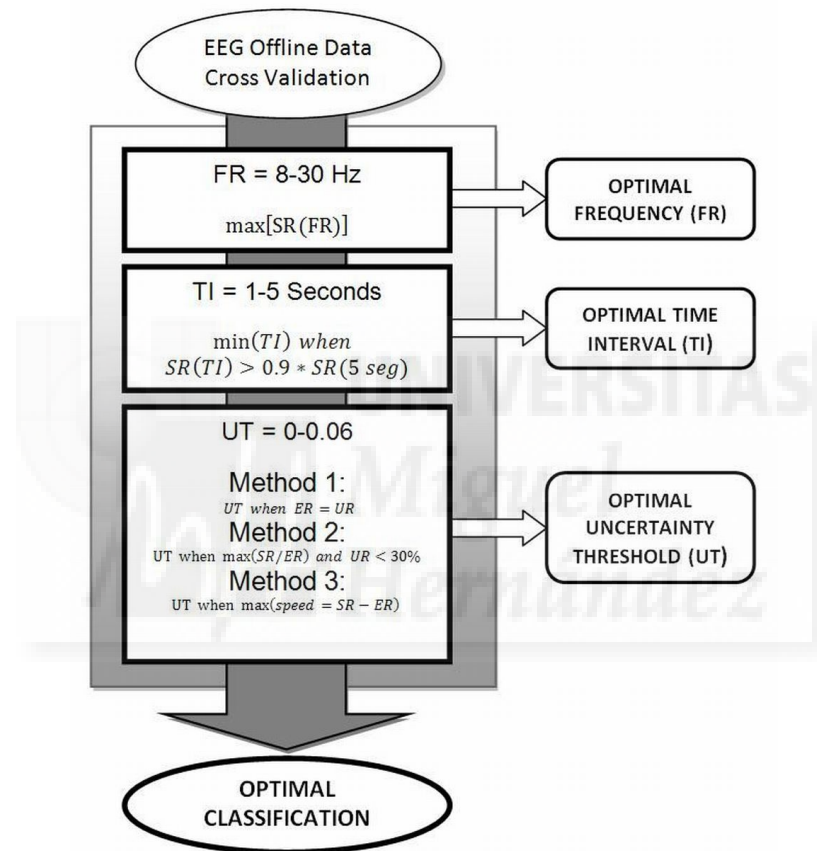


Figure 3.2: Optimization protocol. SR: success rate. UR: uncertainty rate. ER: error rate.

2. Using the frequency chosen, the suitable time interval is studied.
3. Once the first two parameters are selected, the best uncertainty threshold is obtained.

The parameters are studied in order of importance. In other words, changes in each parameter studied should not affect the previous one.

#### **Frequency:**

When creating the EEG maps for each mental task, it is desirable to obtain the maximum difference between each of them. It has been proved that the motor activity is mainly produced in the Mu band (8-12 Hz), so a better accuracy is expected if the image correlation classifier is used to classify motor imagery tasks. If not, different frequencies should be analyzed to obtain the best success rate. To obtain the optimal frequency, the classifier is applied using a cross-fold validation for all the frequencies at its disposal. The frequency with the highest success rate is then selected. The initial time interval used is 5 seconds to obtain the highest accuracy of the classifier.

#### **Time interval:**

The processing time interval is inversely proportional to accuracy. It is expected that with a bigger amount of data, the brain activity will provide more information and the classification will improve. However, in BMIs, this processing time is critical as they work in real time. The range of time has been defined between 1-5 seconds to show the different accuracies and select the more suitable time interval for each subject. A limit of a 10% of success rate loss has been defined when selecting this time interval (Figure 3.2). This has been done to assure an acceptable accuracy in the classifier.

#### **Uncertainty:**

The final parameter to optimize is the uncertainty threshold. This threshold is used to reject trials that cannot be clearly classified. The uncertainty rate affects the global speed of the BMI system and the accuracy of the classifier. When the uncertainty is high the reliability increases but the speed is lower. On the other hand, if the uncertainty is

low the speed increases, but the error is higher. In order to select the suitable threshold, three different methods have been implemented (Figure 3.2):

- Method 1: the uncertainty threshold is selected when the uncertainty rate is the same as the error rate. This method seeks the same proportion between error and uncertainty.
- Method 2: the proportion between success rate and error rate is obtained. A maximum of 30% uncertainty rate is fixed. This method seeks a higher uncertainty rate and, as a result, a higher reliability on the classification.
- Method 3: the uncertainty threshold where the maximum difference between the success rate and the error rate (maximum speed) occurs is selected. This method seeks a lower uncertainty rate but a higher speed on the classification.

### 3.3 Analysis of the EEG Mapping Classifier

The classifier has been tested with the data provided by IDIAP Research Institute for BCI Competition 2003. These data are based on the performance of mental tasks related to motor imagery. The optimization protocol previously described has been used to select the optimal parameters of the classifier. After studying this optimization, the final results are presented using the selected parameters. For each subject, the protocol explained in the previous section has been tested using a 4-fold cross-validation (three sessions used for training and one for test) and an average success rate of the four combinations has been obtained. The success rate using the predefined model sessions from BCI Competition (1 to 3) and the predefined test session (4) are also shown and compared with the results of the BCI Competition III-Set V [112]. These results have led to the publication of two conference papers [6, 7] and a journal article [8].

#### 3.3.1 EEG Data Used

The data set V of “mental imagery, multi-class” provided by IDIAP Research Institute for BCI Competition 2003 has been used to test the classifier [113]. This data set

contains recordings from 3 subjects without motor impairment during 4 non-feedback sessions (3 for training and 1 for test). The subjects made these experiments in 4 sessions on the same day, each one lasting 4 minutes and with 5-10 minutes breaks between them. For each session, the subjects performed three different tasks:

1. Imagination of repetitive self-paced left hand movements (“left” mental task).
2. Imagination of repetitive self-paced right hand movements (“right” mental task).
3. Generation of words beginning with the same random letter (“word” mental task).

The data are provided in two ways: raw EEG signals with a sampling rate of 512 Hz, and precomputed features. To obtain these features the raw EEG potentials were first spatially filtered with a surface Laplacian and then, every 62.5 ms (16 times per second), the power spectral density (PSD) in the band 8-30 Hz was estimated over the last second of data with a frequency resolution of 2 Hz.

The electrodes used to register the EEG signals are the 8 centro-parietal of the International 10/10 System [60]: C3, Cz, C4, CP1, CP2, P3, Pz and P4 (Figure 3.3, left). The final EEG sample is a 96-dimensional vector (8 channels with 12 frequency components).

The EEG mapping consists of the geometrical representation of the activity of these 8 electrodes. To that end, a grid of 99x99 pixels has been created performing an interpolation of the PSD values of the electrodes that have been represented on the grid in their approximate real position. To that end, the inverse distance interpolation method has been used [114], creating a smooth surface. In Figure 3.3, right, an example of EEG map can be seen. The axes show the normalized position of the electrodes over the scalp (X and Y) and the values are scaled between 0 and 1 to improve the differences on the image. Each EEG map shows a particular frequency and mental task.

### 3.3.2 Frequency Study

To obtain the optimal frequency for each subject, the classifier has been used with an initial time interval of five seconds, obtaining the success rate for each frequency between 8 and 30 Hz with a resolution of 2 Hz. The EEG maps are created for each



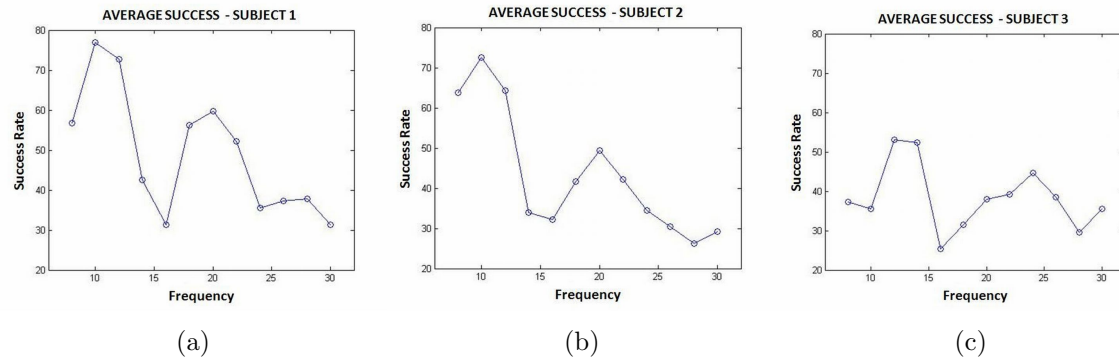


Figure 3.4: Average success rate after cross-validation for different frequencies.



Table 3.1: EEG Mapping success rate (%) with a time interval of 5 seconds.

Fold	Subject 1	Subject 2	Subject 3
<b>123+4</b>	85.71	73.80	64.28
124+3	79.06	85.71	40.47
134+2	78.57	66.66	65.85
234+1	64.28	64.28	41.46
Average	76.91	72.61	53.02
<b>BCI Competition Winner</b>	79.60	70.30	56.00

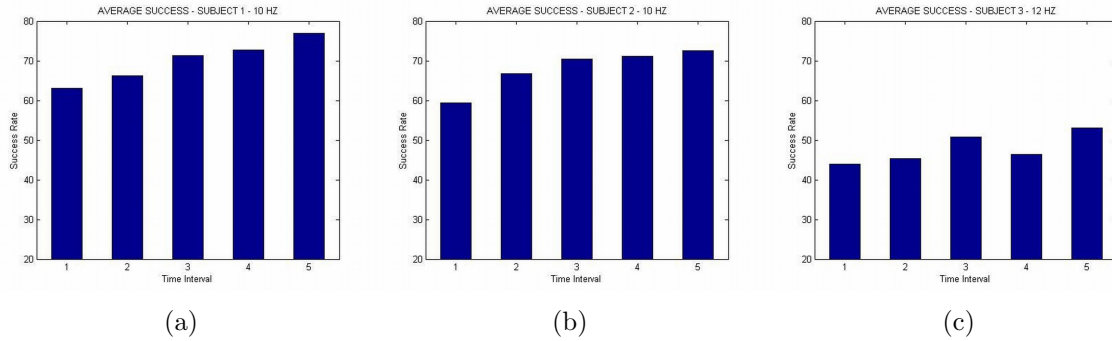


Figure 3.5: Average success rate after cross-validation for different time intervals with the selected frequencies.

direct comparison between these results and the BCI Competition ones. However, it is remarkable that the success rates of the first row (123+4) are substantially above the ones obtained by the winner of the competition [112].

### 3.3.3 Time Interval Study

The processing time interval is a very important factor in real time systems such as a BMI. The main goal is to reduce as much as possible the length of the trials processed in a real-time application. After defining the optimal frequency for each subject, the time interval has been studied. To that end, the selected frequency is used to obtain the success rate of the classifier for different time intervals: 1, 2, 3, 4 and 5 seconds. The results obtained show a small reduction of the success rate each second reduced (Figure 3.5). The processing time interval is selected by taking into account a reliability limit of reduction that is fixed as a 10% of maximum success rate loss. Using this limit, the time interval selected is 3 seconds for Subject 1, 2 seconds for Subject 2 and 3 seconds for Subject 3, obtaining a success rate of 71.38%, 66.82% and 50.87% respectively.

### 3.3.4 Uncertainty Study

Once the first two parameters (frequency and time interval) are selected, an uncertainty threshold is introduced in order to reduce the error. The main goal of this uncertainty

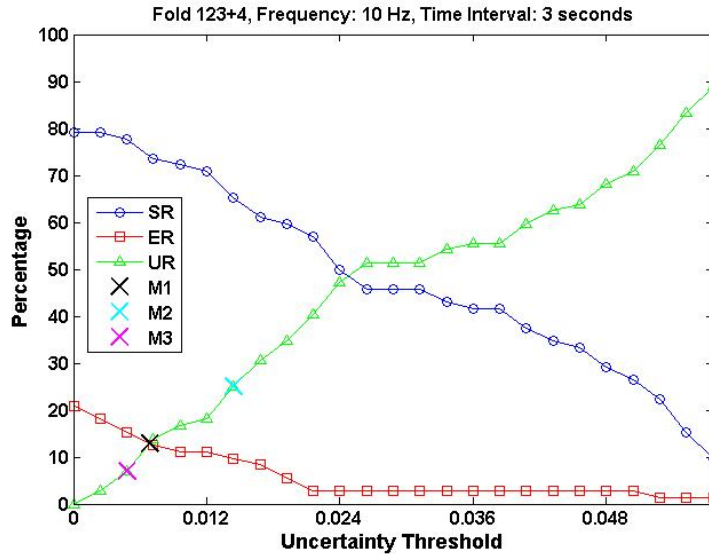


Figure 3.6: Subject 1 - Evolution of the success (SR), error (ER) and uncertainty rate (UR) for different uncertainty thresholds and selection of thresholds using the three methods proposed (M1, M2 and M3).

threshold is to reject trials which cannot be clearly classified. In this way, the success rate of the classifier decreases but also the error rate. If the proportion of reduction is greater for the error rate than for the success rate, the introduction of the uncertainty threshold will increase the global success rate of the system.

Three different methods to obtain the uncertainty threshold have been described in Section 3.2.2. The use of a particular method will be more suitable depending on the final application of the BMI, as the proportion of uncertainty affects the speed and accuracy of the system. Figures 3.6, 3.7 and 3.8 show examples for each of the subjects. The uncertainty threshold ranges between 0 and 0.06 with a resolution of 0.0025. The success, error and uncertainty rates are calculated for the whole range of thresholds and for each method. A cross marks the final uncertainty threshold obtained after applying the criterium for each method. This procedure has been followed four times using the same 4-fold cross-validation already described in the previous studies of frequency and time interval and the average of the four thresholds obtained has been carried out to calculate a unique uncertainty threshold for each subject and method.

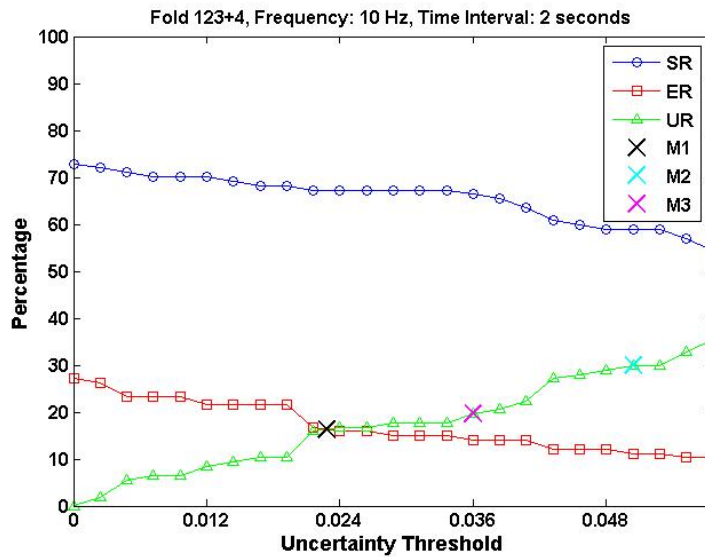


Figure 3.7: Subject 2 - Evolution of the success (SR), error (ER) and uncertainty rate (UR) for different uncertainty thresholds and selection of thresholds using the three methods proposed (M1, M2 and M3).

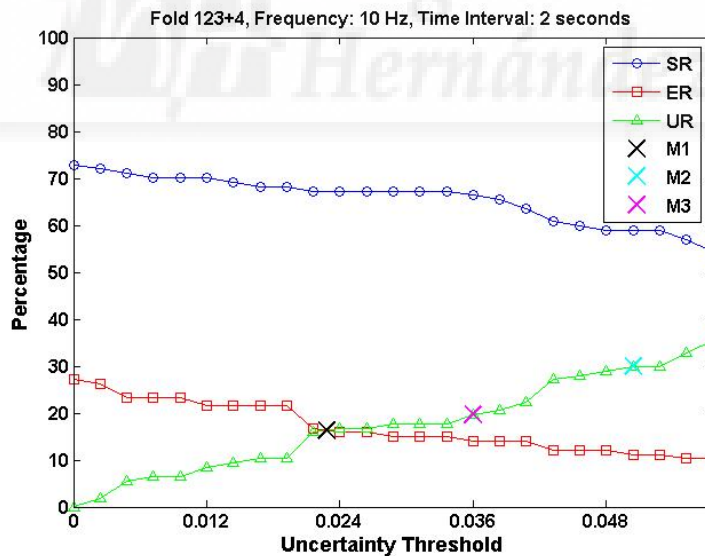


Figure 3.8: Subject 3 - Evolution of the success (SR), error (ER) and uncertainty rate (UR) for different uncertainty thresholds and selection of thresholds using the three methods proposed (M1, M2 and M3).

Tables 3.2, 3.3 and 3.4 show the results obtained for Subject 1, 2 and 3 using the three methods. It also shows the results without using uncertainty thresholds, i.e.,  $UT = 0$ . The first three columns present the success, uncertainty and error rate, and the fourth column presents the global success rate, where  $GSR = SR/(SR + ER)$ . The uncertainty rate affects the speed of the BMI applied to a global system. In other words, the accuracy improves by reducing the speed of the application controlled by the BMI. The selection of the uncertainty estimation method will depend on the characteristics of the final application controlled, particularly in terms of speed and reliability.

The results indicate that the introduction of uncertainty in the classifier substantially increases the global success rate. In fact, the improvement is about a 5% for all subjects and methods. This seems quite remarkable, as the success rate was already quite high in at least two subjects (71.38% and 66.82%). The results for the three methods are slightly different but this difference is still remarkable. As it has been already stated, depending on the final application of the BMI, a method may be more useful than another. In particular, methods 1 and 2 are quite similar and have low error but high uncertainty. These methods will be useful in applications where reliability is more critical. On the other hand, method 3 has a worse performance in terms of accuracy but is better for applications where the speed of decision is more important. The results obtained may also change depending on the subject. This general optimization protocol is applied to make the selection of the most suitable method possible for each subject and final application.

### 3.3.5 Discussion and Conclusions

The results of success rate for each subject have been presented after optimizing the three parameters of the classifier based on EEG mapping analysis (Table 3.5). The study of frequencies shows that the motor activity is mainly focused in the Mu band (8-12 Hz), although the Beta band (16-31 Hz) is also activated. Only the main frequency (the one where success rate is higher) has been selected. The use of other frequencies may be useful in future improvements of the classifier where EEG maps of different frequencies can be compared to support the classification. With a processing time interval of 5 seconds, it was shown that the success rate improves for all subjects

Table 3.2: Subject 1, results with uncertainty (Frequency: 10 Hz, Time Interval: 3 seconds). SR: success rate (%). UR: uncertainty rate (%). ER: error rate (%). GSR: global success rate (%). UT: uncertainty threshold.

		SR	UR	ER	GSR
METHOD 1	123+4	66.66	23.61	9.72	87.27
	124+3	61.64	16.43	21.92	73.77
	134+2	60.56	23.94	15.49	79.63
	234+1	45.07	28.16	26.76	62.75
	<b>AVERAGE</b>	<b>58.48</b>	<b>23.03</b>	<b>18.47</b>	<b>76.00</b>
METHOD 2	123+4	61.11	30.55	8.33	88.00
	124+3	60.27	21.91	17.08	77.92
	134+2	60.56	25.35	14.08	81.14
	234+1	45.07	29.57	25.35	64.00
	<b>AVERAGE</b>	<b>56.75</b>	<b>26.84</b>	<b>16.21</b>	<b>77.78</b>
METHOD 3	123+4	73.61	12.50	13.88	84.14
	124+3	65.75	12.32	21.91	75.01
	134+2	69.01	8.45	22.53	75.39
	234+1	54.92	11.26	33.8	61.90
	<b>AVERAGE</b>	<b>65.82</b>	<b>11.13</b>	<b>23.03</b>	<b>74.08</b>
NO THRESHOLD	123+4	79.17	0.00	20.83	79.17
	124+3	73.97	0.00	26.03	73.97
	134+2	73.24	0.00	26.76	73.24
	234+1	59.15	0.00	40.85	59.15
	<b>AVERAGE</b>	<b>71.38</b>	<b>0.00</b>	<b>28.62</b>	<b>71.38</b>

Table 3.3: Subject 2, results with uncertainty (Frequency: 10 Hz, Time Interval: 2 seconds). SR: success rate (%). UR: uncertainty rate (%). ER: error rate (%). GSR: global success rate (%). UT: uncertainty threshold.

		SR	UR	ER	GSR
METHOD 1	123+4	63.55	22.42	14.01	81.94
	124+3	77.57	12.15	10.28	88.30
	134+2	47.66	22.42	29.90	61.45
	234+1	36.44	20.84	32.71	52.70
	<b>AVERAGE</b>	<b>56.31</b>	<b>19.46</b>	<b>21.73</b>	<b>72.16</b>
METHOD 2	123+4	63.55	22.42	14.01	81.94
	124+3	77.57	12.15	10.28	88.30
	134+2	47.66	22.42	29.90	61.45
	234+1	36.44	30.84	32.71	52.70
	<b>AVERAGE</b>	<b>56.31</b>	<b>21.96</b>	<b>21.73</b>	<b>72.16</b>
METHOD 3	123+4	66.35	19.62	14.01	82.57
	124+3	78.50	11.21	10.28	88.42
	134+2	49.53	20.56	29.90	62.36
	234+1	40.18	27.10	32.71	55.12
	<b>AVERAGE</b>	<b>58.64</b>	<b>19.62</b>	<b>21.73</b>	<b>72.97</b>
NO THRESHOLD	123+4	72.90	0.00	27.10	72.90
	124+3	84.11	0.00	15.89	84.11
	134+2	58.88	0.00	41.12	58.88
	234+1	51.40	0.00	48.60	51.40
	<b>AVERAGE</b>	<b>66.82</b>	<b>0.00</b>	<b>33.20</b>	<b>66.82</b>

Table 3.4: Subject 3, results with uncertainty (Frequency: 12 Hz, Time Interval: 3 seconds). SR: success rate (%). UR: uncertainty rate (%). ER: error rate (%). GSR: global success rate (%). UT: uncertainty threshold.

		SR	UR	ER	GSR
METHOD 1	123+4	36.61	39.43	23.94	60.46
	124+3	31.42	32.85	35.71	46.80
	134+2	42.85	37.14	20.00	68.18
	234+1	37.14	30.00	32.85	53.06
	<b>AVERAGE</b>	<b>37.01</b>	<b>34.86</b>	<b>28.13</b>	<b>56.82</b>
METHOD 2	123+4	38.02	38.02	23.94	61.36
	124+3	31.42	31.42	32.14	49.43
	134+2	42.85	35.71	21.42	66.67
	234+1	37.14	30.00	32.85	53.06
	<b>AVERAGE</b>	<b>37.36</b>	<b>33.79</b>	<b>27.59</b>	<b>57.52</b>
METHOD 3	123+4	45.97	23.94	30.98	59.74
	124+3	31.42	24.28	44.28	41.51
	134+2	45.71	27.14	27.14	62.75
	234+1	38.57	24.28	37.14	50.94
	<b>AVERAGE</b>	<b>40.42</b>	<b>24.91</b>	<b>34.89</b>	<b>53.67</b>
NO THRESHOLD	123+4	56.34	0.00	43.66	56.34
	124+3	40.00	0.00	60.00	40.00
	134+2	58.57	0.00	41.43	58.57
	234+1	48.57	0.00	51.43	48.57
	<b>AVERAGE</b>	<b>50.87</b>	<b>0.00</b>	<b>49.13</b>	<b>50.87</b>

Table 3.5: Optimal parameters of the image correlation classifier for each subject. Global Success Rate (%) after cross-validation (GSR 1) and for the combination 123+4 (GSR 2). FR: Optimal frequency. TI: Time interval. UT: Uncertainty threshold.

	FR	TI	Method	UT	GSR 1	GSR 2
Subject 1	10 Hz	3 seconds	1	0.0146	76.00	87.27
			2	0.0169	77.78	88.00
			3	0.0069	74.08	84.14
Subject 2	10 Hz	2 seconds	1	0.0409	72.16	81.94
			2	0.0419	72.16	81.94
			3	0.0381	72.97	82.57
Subject 3	12 Hz	3 seconds	1	0.0469	56.82	60.46
			2	0.0462	57.52	61.36
			3	0.0394	53.67	59.74

in comparison to BCI Competition results [112]. However, these results take into account a smaller processing interval so a smaller time interval is desirable. The study of this reduction has shown that only a maximum processing time interval of 3 seconds is necessary (2 seconds in one case) to perform a robust classification. This reduction makes possible the use of this kind of classifier in real-time BMIs. The reduction of success rate is substantially compensated by the introduction of an uncertainty threshold which rejects trials that cannot be clearly classified. Three methods were defined to obtain these uncertainty thresholds. All the methods (explained in Section 3.2.2) prove that, with the introduction of uncertainty, the proportion of error rate reduction is greater than the proportion of success rate reduction. The global success rate has been calculated showing that the improvement of success rate is nearly a 5% in all cases. The results for GSR 2, which uses the same combination of sessions shown in BCI Competition, are higher than the results obtained in [112]. Nevertheless, each method has its own characteristics which make them more or less suitable depending on the final application of the BMI. Methods 1 and 2 are slower but more accurate,

while Method 3 is faster but a bit less accurate.

This section has shown the application of the EEG mapping classifier to a BCI database (BCI Competition 2003). The time interval of processing has been reduced and an uncertainty threshold has been introduced showing an important improvement of the success rates. The suitability of three different methods to obtain this threshold has been discussed and the results suggest that each method may be suitable depending on the final application in terms of speed and reliability. The final success rates improve the results of previous classifiers and encourage us to introduce new improvements in this kind of classification. The findings of this study suggest that this EEG mapping method may be suitable for classification of more than three mental tasks as the image models obtained for each task show big differences between them. The next section will be centered in testing the classifier in a real-time BMI environment.

## 3.4 Real-Time Application

In this section, the EEG mapping classifier is tested in real time. For this purpose, the EEG maps are obtained after a suitable processing of the raw EEG data registered from 4 healthy subjects who participated in the experiments. Two mental tasks related to motor imagery have been classified, including an uncertainty state to prevent errors in classification. To measure the accuracy and reliability of the EEG mapping classifier, the subjects have performed several bidimensional trajectories in order to control the cursor position in a visual interface using the BMI. An in-depth analysis of the frequency and uncertainty threshold chosen for each subject has been performed to optimize the method and to obtain a better performance of the classification. These results have led to the publication of a journal article [9].

### 3.4.1 Materials and Methods

#### 3.4.1.1 Register

To register the EEG signals, the gUSBamp device (g.Tec, Austria) has been used (Figure 3.9). This device has 16 channels. The signal is registered with a sample frequency of

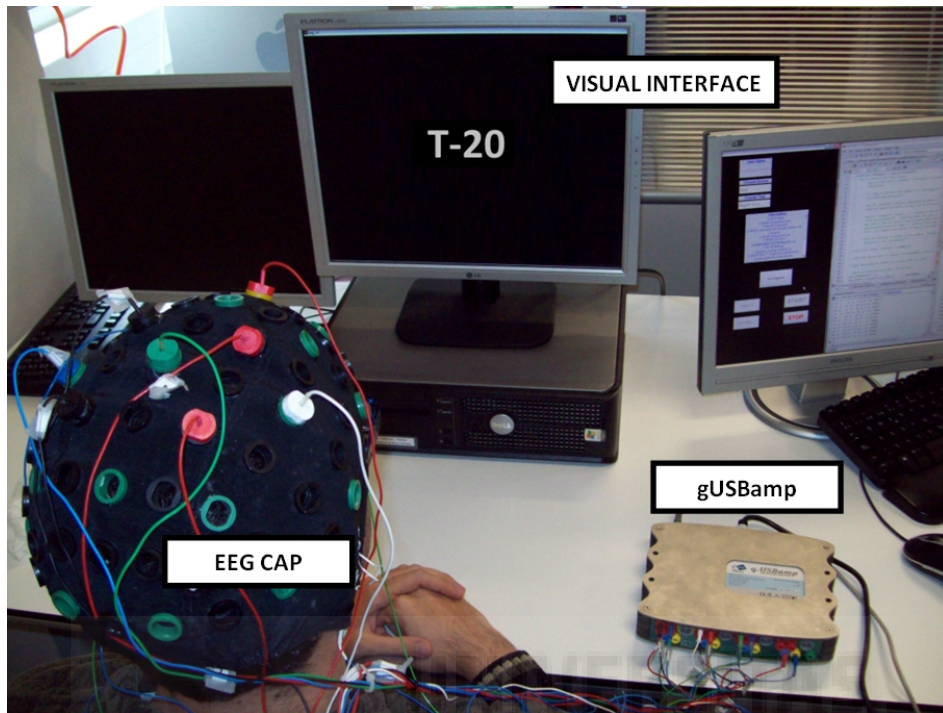


Figure 3.9: Real-time Brain-Machine Interface environment.

1200 Hz and two filters are applied: a bandpass filter between 0.1 and 100 Hz, and a Notch filter of 50 Hz to remove the perturbation of the electrical network. These filters are internally included in the device.

The software used for registering the EEG signals has been developed in Matlab (Mathworks Inc.) using the API (Application Programming Interface) provided by the device (gUSBamp). Previous studies indicate that the imagination of a movement generates the same mental process as the performance of the movement itself [64]. Therefore, the imagination of motor movements is expected to generate a sufficient modulation of the Mu band making possible an accurate future classification. The volunteers have performed two different mental tasks:

- Imagination of low circular movements of the left arm (“left” mental task).
- Imagination of low circular movements of the right arm (“right” mental task).

The selection of the electrodes on the scalp is based on an extension of the International 10/10 System [60]. This selection is mainly located on the motor cortex, which

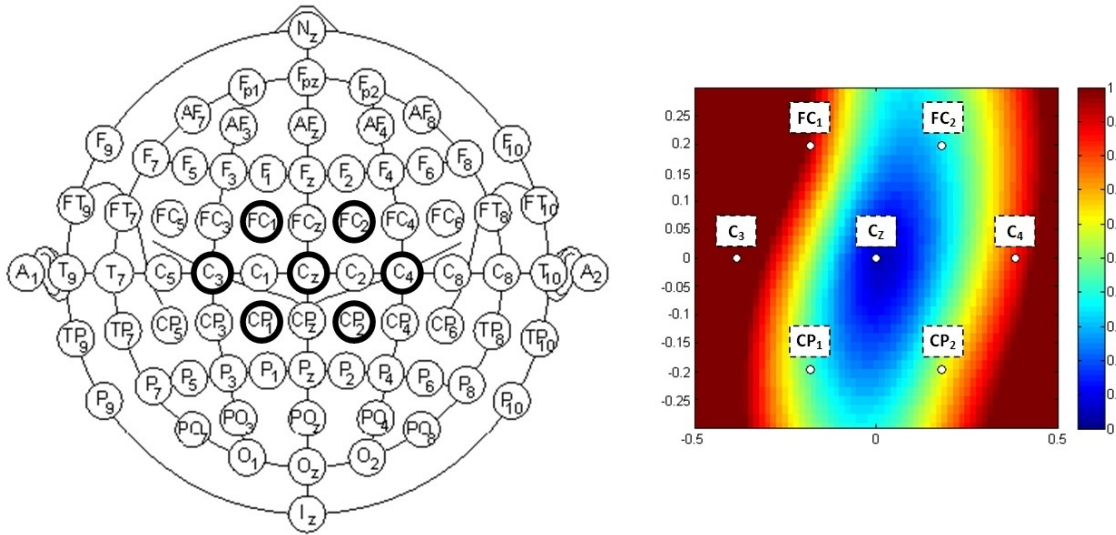


Figure 3.10: Electrodes location on the motor cortex (left). Example of EEG map (right). The scale is normalized between 0 and 1 as it can be seen on the scale bar. Each electrode is placed in its particular position and the value generates the map.

is the area of motor activation (Figure 3.10, left). Seven electrodes have been chosen to register the EEG signals: FC1, FC2, C3, Cz, C4, CP1 and CP2. The main goal of this selection is to obtain a more specific area of the motor cortex activity to improve the classification.

### 3.4.1.2 Processing

Once the EEG signals are registered, first a preprocessing of the signals must be performed to improve the quality of the signals. As it has been mentioned, the amplifier has its own filters. So, in this case, only a Laplacian smoothing filter is applied as seen in [115]. It consists of subtracting, on each electrode, the contribution of the surrounding electrodes by taking into account the distance to the main electrode:

$$V_i^{LAP} = V_i^{ER} - \sum_{j \in S_i} g_{ij} V_j^{ER} \quad (3.2)$$

where:

$$g_{ij} = \left( \frac{1}{d_{ij}} \right) / \sum_{j \in S_i} \left( \frac{1}{d_{ij}} \right) \quad (3.3)$$

According to this formulation,  $S_i$  is the set of electrodes that surround the main electrode. In our case, all the surrounding electrodes in the selected set, while  $d_{ij}$  is the distance between the main electrode  $i$  to the surrounding electrodes  $j$ . After the preprocessing, the extraction of the features of the EEG signals is done using an algorithm based on the frequency domain. The algorithm used is the Fast Fourier Transform (FFT), which decomposes the input signal into different frequencies. After studying experimentally the data the range of frequencies between 8 and 30 Hz (with a resolution of 2 Hz) have been considered. This means that for each electrode, 12 frequency features are obtained centered in the selected frequencies.

### 3.4.1.3 EEG Mapping Classifier

To classify the different mental tasks, the EEG mapping classifier explained in the previous section has been used. The classifier is based on the correlation of EEG maps. The EEG maps corresponding to the models of each mental task (right and left) are created. These models are compared to the EEG maps obtained from the registered signal which is classified. Each EEG map shows a particular frequency and task (Figure 3.10). A total of 12 frequencies have been obtained but only the most suitable frequency is selected for each subject. As it will be explained in the adjustment of the classifier, to obtain the proper frequency and the models (left and right) from this frequency, offline data are tested for each frequency by performing a cross-validation. The models with the best success rate are selected to be used in the remaining tests. The EEG maps are obtained for a window of 5 seconds and classified each 0.5 seconds.

The two models (left and right) are compared with the trials that need to be classified using a *normalized cross-correlation* [110]. When a particular session of data is tested, each trial is compared with the previously obtained models using this method (see Section 3.2.1). After this comparison, an index of correlation for each task is obtained. The maximum value of the index is selected obtaining the corresponding class. Afterwards, two uncertainty conditions are evaluated:

- The first uncertainty condition is applied by introducing a fixed threshold to both indexes of correlation (left and right). If the models do not fulfill this condition, the trial is rejected as uncertain. In other words, the correlation between the models and the trial classified should be enough to consider that the data is correctly registered and does not correspond to noise and other issues related to the incorrect operation of the amplifier and to prevent errors in classification. This threshold has been experimentally fixed to a minimum of 90 % of correlation between the models and the trials classified.
- The second uncertainty condition is applied by introducing a threshold between both indexes of correlation (left and right). If both are too similar, the trial is rejected as uncertainty. This second threshold prevents wrong classifications. This uncertainty threshold is selected when the uncertainty rate is the same as the error rate after performing a cross-validation between sessions. This method seeks the same proportion between error and uncertainty in the overall classification.

Finally, to obtain the final decision of the BMI, a simple statistical operation has been performed to reduce errors. The final decision is calculated as the mode of the last five outputs provided by the BMI. This is also done to reduce errors while performing changes of mental tasks.

#### 3.4.1.4 Classifier Adjustment Protocol

The uncertainty thresholds, the suitable frequency and the models for each subject are selected after performing a particular protocol:

1. First, five offline sessions are registered. The offline sessions consist of asking the subjects to think about both tasks in a particular sequence. In this case, the subjects do not have visual feedback to show a real-time classification accuracy. From these sessions, the models (left and right) are obtained and tested using a 5-fold cross-validation between sessions, where the most suitable frequency is selected. The classifier is tested for each of the 12 frequencies obtained after processing the EEG signals (8-30 Hz with a resolution of 2 Hz). The most significant one,

i.e. the one with the best success rate (normally contained in the Mu band), is selected. The models for left and right tasks corresponding to this frequency are kept for future sessions.

2. Afterwards, the classifier is updated by performing sets of three online sessions. After each set, a new model is obtained. Now, the subjects obtain a continuous visual feedback of the tasks performed. This improves the accuracy of the classification and allows obtaining better models. These online sessions are repeated until the final success rate is accurate enough.
3. Finally, the proper uncertainty thresholds are selected from the last set of online sessions.

After performing this protocol, the two EEG mapping models obtained for both mental tasks are ready to be used in a real-time application. In our case, this real-time application consists of a visual interface where the subject controls the cursor position using the BMI in order to perform several trajectories. This application adequately shows the performance of a real-time classification and can be translated to more complex tasks in future works.

#### **3.4.1.5 Visual Interface and Trajectory Application**

A visual interface to perform both training and trajectory sessions has been designed. It is mainly divided into three sections: offline, online and trajectory interfaces. The appearance of the visual interface during a training session is shown in Figure 3.11. For the offline sessions, a similar timing paradigm as the one described in [116] is used to register the data. First, a cross is shown for three seconds, then the mental task to think about is shown for two seconds and finally there is a period between eight and ten seconds to perform the mental task (Figure 3.12). The cross is shown to relax between each task. Both left and right tasks are repeated randomly 8 times per session. For the online sessions, the same paradigm is used, but in this case, the subject is able to see the performance of the classification during the third period (8-10 seconds). To that end, an arrow moves left or right every time the classification is correct. After the task is shown, the arrow appears on the center of the screen pointing the corresponding direction (left

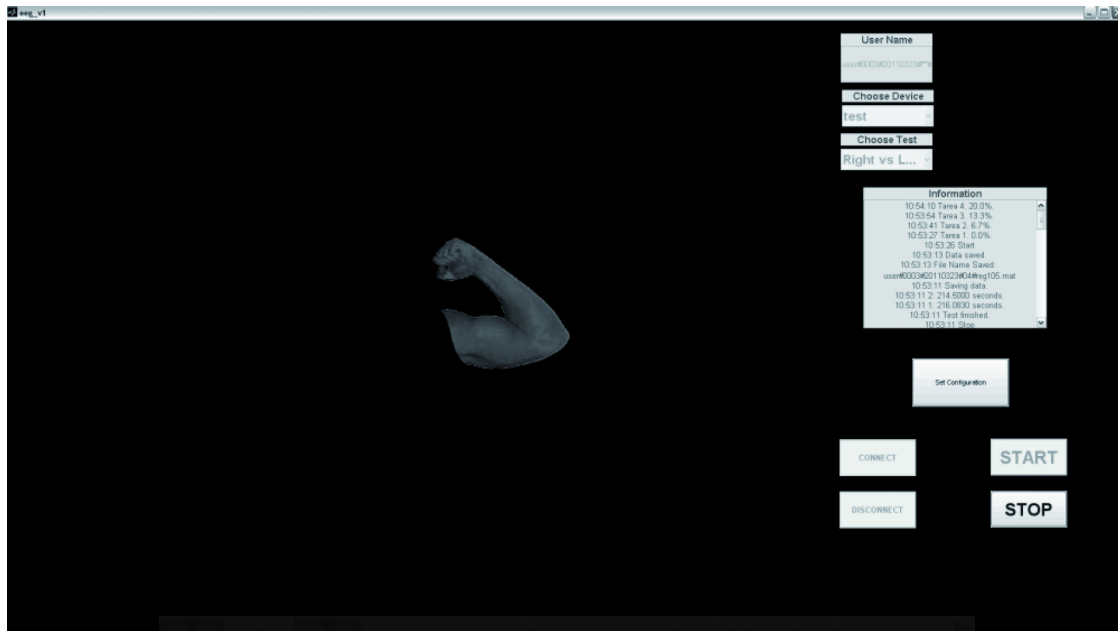


Figure 3.11: Visual interface for BMI training.

or right, depending on the task). For each processed trial (each 0.5 seconds) the arrow moves to the corresponding direction if the classification is successful, if not, the arrow does not move.

Finally, the trajectory screen consists of two targets placed on a grid as shown in Figure 3.13. The trajectory starts at the top point and goes downwards automatically until reaching the bottom border. The subject is asked to think right or left (moving the cursor right or left) to pass through the targets. The targets are aimed at encouraging the subjects and the final accuracy is measured by obtaining the distance in pixels to the center of each target. This means, that a 100% accuracy is obtained when passing through the center and decreases with the distance until reaching an accuracy of 0% (50 pixels away from the center). Score is also measured after dividing each target into three different areas (different colors). The outer section scores 1 point, the medium section scores 5 points and, finally, the inner section scores 10 points. This numerical score is calculated later and it is not shown to the subjects. This kind of scoring system is quite qualitative, as BMI systems are still far from being able to perform very accurate trajectories, but it has been proved to be very useful to stimulate competitiveness

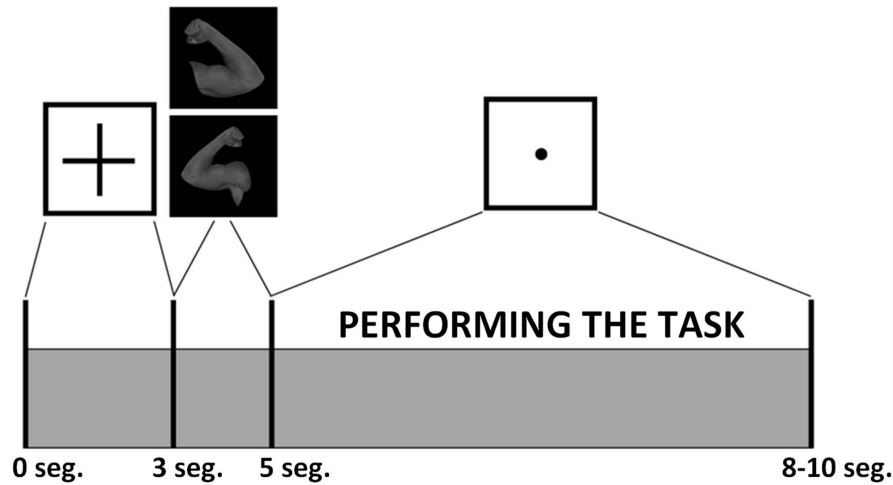


Figure 3.12: Offline BMI register timing paradigm.



Figure 3.13: Several trajectories performed by the volunteers using BMI based on EEG Mapping.

between subjects.

### 3.4.2 Results and Discussion

Four able-bodied volunteers have taken part on the experiments. The volunteers are four men, all healthy and with ages between 25 and 39 years old (mean  $30.2 \pm 6.4$ ). All of them are familiarized with biomedical technologies. Two of the subjects have experience using BMIs, while the others are naive in this kind of devices. The experiments took place in an separate room to prevent distractions. As it has been explained before, the volunteers have performed 5 offline sessions (4 minutes each) and, then, sets of 3 online

sessions (4 minutes each) to completely adjust the EEG mapping models. Afterwards, 10 trajectories (around 1 minute each) have been performed and score and accuracy have been measured. The total time of the tests (including resting periods) is about one hour and half.

In Table 4.2, the offline and online results obtained are shown. First, the average results of the offline cross-validation for each subject are shown. These results do not include uncertainty. Then, the results obtained for the last set of online sessions for each subject are shown (final adjustment). As it can be seen, the offline results are still far from being useful to accurately classify the signals. However, the models obtained in these sessions are used for the online training by introducing a visual feedback where the volunteer can see if the classification is performed correctly. The success rate improves in the online training for Subjects 1 and 2. Particularly, for Subject 1, the success rate is above 80%. For Subjects 3 and 4, error decreases as well (more uncertainty). Figure 3.14 shows the evolution of the online results for both tasks (left and right) obtained by Subject 1. As it can be seen, the volunteer obtains a very high success rate for the right mental task and during the tests he/she is able to get used to the system and to improve the success rate for the left mental task and even more for the right mental task.

As mentioned before, the application designed consists of a grid where two targets are shown. The subject is able to perform motor imagery mental tasks (right and left) to reach the targets. First, the volunteer continuously performs a right mental task in order to move the cursor and reach the first target and then continuously performs a left mental task to reach the last one. Figure 3.13 shows three different trajectories. The first one is a perfect trajectory where the subject is able to score in both targets. The second one shows a typical example of trajectory where the subject has difficulties when performing a particular mental task (in this case, the imagination of left arm movement). Finally, the third one shows a quite satisfactory trajectory in terms of accuracy and intention. However, in terms of score, the subject is not able to reach the second target.

The results of accuracy and score are shown in Table 3.7. As it can be seen, the score results are poor. As it has been previously mentioned, giving score is aimed

Table 3.6: Training results with the BMI based on EEG Mapping.

	<b>Test</b>	<b>Success</b>	<b>Uncertainty</b>	<b>Error</b>
Subject 1	Offline	52.0 %	-	48.0 %
	Online 1	76.0 %	12.0 %	12.0 %
	Online 2	72.0 %	16.0 %	12.0 %
	Online 3	80.8 %	3.8 %	15.4 %
Subject 2	Offline	46.2 %	-	53.9 %
	Online 1	65.4 %	0.0 %	34.6 %
	Online 2	56.0 %	16.0 %	28.0 %
	Online 3	64.0 %	0.0 %	36.0 %
Subject 3	Offline	52.0 %	-	48.0 %
	Online 1	42.3 %	19.2 %	38.5 %
	Online 2	40.0 %	8.0 %	52.0 %
	Online 3	56.0 %	12.0 %	32.0 %
Subject 4	Offline	57.7 %	-	42.3 %
	Online 1	54.5 %	12.0 %	33.5 %
	Online 2	56.0 %	16.0 %	28.0 %
	Online 3	52.0 %	16.0 %	32.0 %

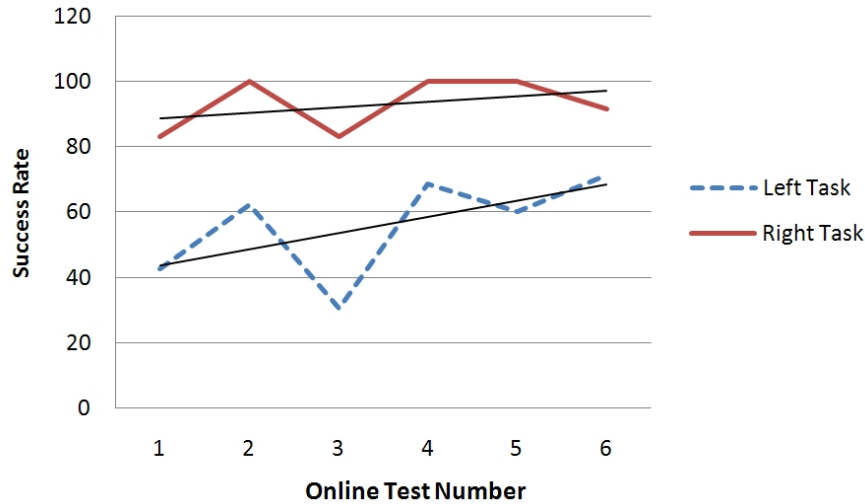


Figure 3.14: Evolution of the success rate for left and right mental tasks during the online training for Subject 1.

at encouraging the volunteers. BMI systems are not accurate enough to obtain precise trajectories. However, Subjects 1 and 2 clearly achieve better scores than the remaining two. The accuracy percentage calculated is a more realistic measure of the general performance of the BMI. For Subjects 1 and 2, accuracy in both targets are similar and high. These volunteers are able to totally control the trajectory with an acceptable error. Subjects 3 and 4 are able to obtain good results with the first target (perform a right mental task), but sometimes fail to reach the second one (perform a left mental task). This means that the success rate is high for right and poor for left. In general, all four volunteers are able to control the trajectories, particularly Subjects 1 and 2, who obtain very good results.

### 3.4.3 Conclusions

In this section, a non-invasive BMI based on the correlation of EEG maps has been tested to perform applications in real-time. To that end, a visual application to perform trajectories has been designed. Two targets are shown on a grid and the volunteers are asked to reach the targets by performing tasks related to motor imagery (in this case, the imagination of the movement of the left and right arm). The classifier has

Table 3.7: Tests results with the BMI based on EEG Mapping.

	Score target 1	Score target 2	Total score	Accuracy target 1	Accuracy target 2	Average accuracy
Subject 1	4.6	2.5	7.1	76.0 %	73.0 %	74.5 %
Subject 2	4.6	5.7	10.3	78.0 %	84.0 %	81.0 %
Subject 3	4.6	1.1	5.7	73.3 %	31.3 %	52.3 %
Subject 4	2.3	3.3	5.5	59.3 %	28.7 %	44.0 %
<b>Mean</b>	<b>4.0</b>	<b>3.2</b>	<b>7.2</b>	<b>71.7 %</b>	<b>54.2 %</b>	<b>63.0 %</b>

been improved from previous works by introducing two uncertainty conditions. Four able-bodied volunteers tested the application. The accuracy and score obtained prove that this BMI is ready to be used in more complex applications for people with a severe motor disability that could help them in their daily life.

In future works, the main goal will be to adapt this BMI to more useful and meaningful environments, such as the control of a robot arm to perform grasping operations of daily objects and the control of web browser. The next section will show the application of this classifier to the control of an assistive planar robot.

### 3.5 Control of an Assistive Planar Robot

In this section, the EEG mapping classifier has been applied to a real world scenario. The BMI based on the correlation of EEG maps described in previous sections has been used to control a pneumatic planar robot arm in an assistive application. The BMI system follows the same training protocol explained in the previous section. After training it, the BMI has been used to control the robot arm. The application designed consists of moving the end effector of the robot in a plane in order to reach a particular target. The subject sits in front of a screen located in the robot environment. A visual interface shows the different movement options. The first strategy is based on a hierarchical control where the subject can decide the axis and the direction of movement.

The second strategy is based on a directional control, where the subject can continuously decide the direction of the movement and the command is generated continuously. Both strategies are tested by performing trajectories to reach several goals on a plane. The results show that the subject is able to successfully reach the goals and suggest that the system is capable of performing more complex tasks in a realistic environment, for example, grasping daily objects with a gripper. These results have led to the publication of two conference papers [10, 11].

### 3.5.1 Materials and Methods

The BMI based on the correlation of EEG maps has been used to control the PuPArm [117, 118] (see Figure 3.15), a force-controlled planar robot designed and developed by the nBio research group at the Miguel Hernández University of Elche (Spain) (for more details see Appendix A). To control the assistive planar robot (PuPArm) with the BMI, two different control strategies have been defined. The first one is a hierarchical control where the subject can choose the axis and direction of the movement obtaining 4 possible commands (up, down, left and right). The second one is a directional control where the subject can continuously control the direction of the movement using a wheel-designed interface that generates periodical commands to move the robot in the selected direction.

#### 3.5.1.1 Hierarchical Control

The first control strategy is a hierarchical approach where the subject is able to select the axis and direction of the movement of the end effector using a hierarchical interface. With this control strategy, the subject can move to any of the four possible directions (up, down, left or right) a predefined distance of 10 cm. The decisions (direction) are sent via UDP to the computer that controls the planar robot and the robot is controlled via USB through Simulink. The output command from the BMI is translated to an absolute position by increasing the position in 10 cm on the selected direction. This position is sent to the robot controller, where the current position is updated and the torque command is generated, moving the robot to the desired direction.

Each decision is taken using the BMI following a hierarchical control protocol (Figure 3.16). Two decision menus are shown to the subject using a visual interface. With the first one, the axis of movement is chosen. Afterwards, another menu asks for the direction of the movement depending on the axis previously selected. The visual interface shows a cursor that is moved with the BMI (left or right) to select one of the options (Figure 3.17, left). The minimum BMI commands sent to reach an option are 10 and time taken to select one of the options is around 5.4 seconds (5 seconds of decisions and 0.4 seconds to change menus), so the minimum time taken to perform a movement is around 10.8 seconds.

The hierarchical strategy has been chosen to allow a more precise and slower control of the end effector which can be critical in future grasping applications.

### 3.5.1.2 Directional Control

The second control strategy allows the subject to continuously control the direction of the movement and to generate commands every 5 seconds. As it can be seen in Figure

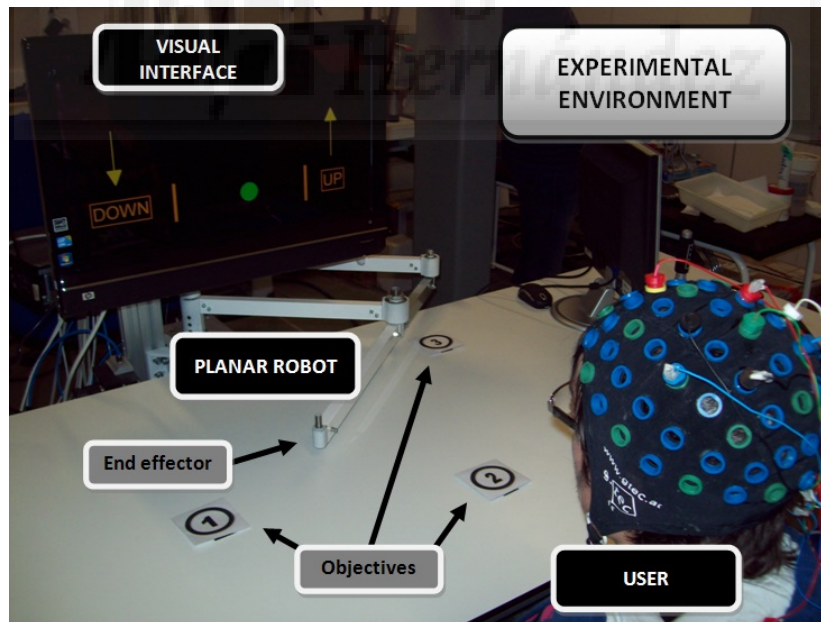


Figure 3.15: Experimental environment of the planar robot. The subject sits in front of the robot arm and a screen provides visual feedback.

3.17, right, a wheel is shown to the subject where an arrow points to the direction of the movement of the end effector. The subject can rotate the arrow right or left using the BMI as far as the left and right limits allow it. These limits have a range of 60 degrees and the arrow moves 5 degrees anytime a mental task is classified (each 0.5 seconds). Every 5 seconds, the robot moves in the direction pointed by the arrow and the wheel is updated showing new limits, but in this case drawing them equidistant to the final position of the arrow. This way, it is possible to rotate the arrow  $360^\circ$  after several decisions. Each final command moves the end effector 5 cm to the selected direction.

As before, the decisions are sent via UDP to the computer that controls the planar robot via a similar Simulink scheme. The output command from the BMI is translated to an absolute position by increasing the position in X and Y to obtain a movement of 5 cm in the selected direction. Then, this position is sent to robot controller where the current position is updated and the torque command is generated.

The directional strategy has been chosen to allow a faster and less restricted control of the robot end effector.

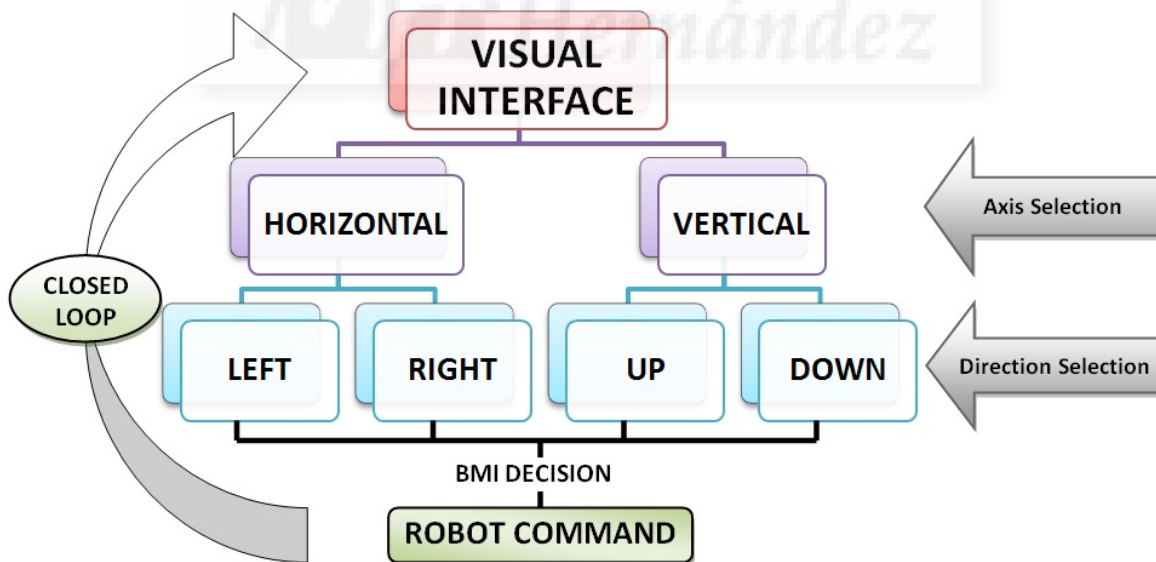


Figure 3.16: Hierarchical control protocol. The subject decides both axis and direction to perform a single movement.

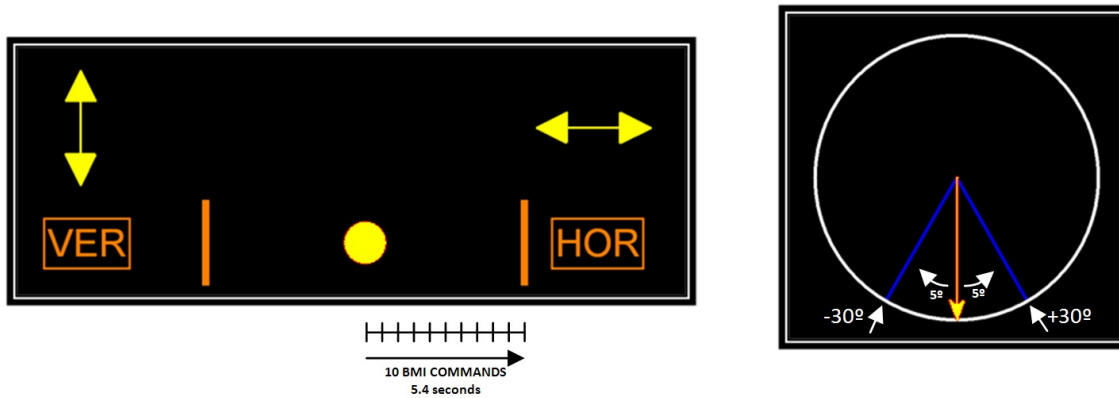


Figure 3.17: Hierarchical control interface (left). Directional control interface (right).

### 3.5.2 Results and Discussion

An assistive application has been designed to control the planar robot with the BMI and test both control strategies. The application consists of reaching three goals on a table. The end effector of the PuPArm is placed over the start position (Figure 3.15) and then, the subject takes control of the robot and moves it to the desired goal.

One able-bodied volunteer has taken part on the experiments. The volunteer was a man, healthy and with an age of 25 years old. Before performing the tests, the volunteer had already performed a previous training session (which is not reported in the previous section) where the classifier was adjusted showing an average success rate

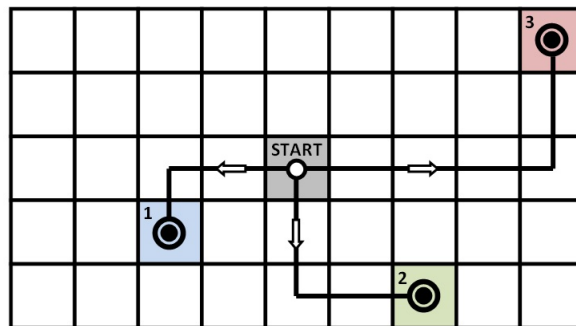


Figure 3.18: Example of test with the hierarchical control protocol (expected trajectory).

of 76.3%, with 10.6% uncertainty and 13.1% error. From this results it can be seen that the EEG mapping classifier is accurate enough to perform real-time applications like the one proposed in this section.

For each goal and control strategy, the volunteer has performed three trajectories with the planar robot. For the hierarchical control strategy, the volunteer is asked to reach exactly the position where each goal is marked. In Figure 3.18, an example of a perfect trajectory for each goal is shown. The minimum movement decisions taken to reach the objectives 1, 2 and 3 are 3, 4 and 6, respectively. In this case, the movements are predefined by the range of movement selected for the robot (10 cm). However, for the directional control strategy, the volunteer has to move as close as possible to the goals, as the output commands for this strategy depend on the position pointed by the arrow.

In Table 3.8, the results obtained are shown. For the hierarchical approach, time taken to reach each objective is measured, as well as decision errors made on each trajectory along with the number of movement decisions taken to reach the objective. The average time taken in each decision (two decisions per movement) is also shown. For the directional approach, time taken to reach the goals is measured and error taken is also shown. In Figure 3.19, the trajectories obtained for each goal are shown.

Table 3.8: Experimental results using the BMI based on EEG Mapping to control the planar robot.

Target	Test	HIERARCHICAL CONTROL			DIRECTIONAL CONTROL		
		Errors/Decisions	Decision time(s)	Test time(s)	Error (mm)	Test time(s)	
1	1	0/3	11.7	76.7	19.0	41.2	
	2	0/3	16.4	98.7	21.0	141.2	
	3	1/5	9.2	93.2	29.0	56.3	
	Avg		<b>12.4</b>	<b>89.5</b>	<b>23.0</b>	<b>79.5</b>	
2	1	1/6	9.1	110.2	88.0	41.2	
	2	1/6	9.6	115.7	35.0	36.2	
	3	2/8	8.8	142.2	67.0	36.2	
	Avg		<b>9.2</b>	<b>122.7</b>	<b>63.3</b>	<b>37.8</b>	
3	1	1/8	6.4	103.2	14.0	71.2	
	2	0/6	6.8	86.2	30.0	71.2	
	3	0/6	10.7	129.7	111.0	91.2	
	Avg		<b>8.0</b>	<b>106.4</b>	<b>51.6</b>	<b>77.8</b>	
	Total Avg		<b>9.8</b>	<b>106.2</b>	<b>45.9</b>	<b>65.1</b>	

With the hierarchical control strategy, the results obtained in terms of decision success are quite high (88.2 %), as the subject generally makes no more than one wrong movement decision in a single trajectory (except from one case). Any wrong decision needs to be solved in the following movement affecting the final time taken to reach the objective. However, the introduction of the hierarchical control solves the lower reliability of a pure BMI and allows the subject to achieve every objective in a quite reasonable time. The average time taken to reach the furthest goal (objective 3) is 106.4 seconds. Contrary to expectations, the second goal takes more time than the third (122.7 seconds). This is due to the hierarchical control protocol, where the decisions taken to achieve this objective imply a greater number of mental task changes. This has been proved to be more difficult for the subject. It is also interesting to note that in all nine cases of these experimental tests, the subject is capable of reaching the objectives and the average time to take a decision (9.8 seconds) which makes this system sufficiently fast and reliable.

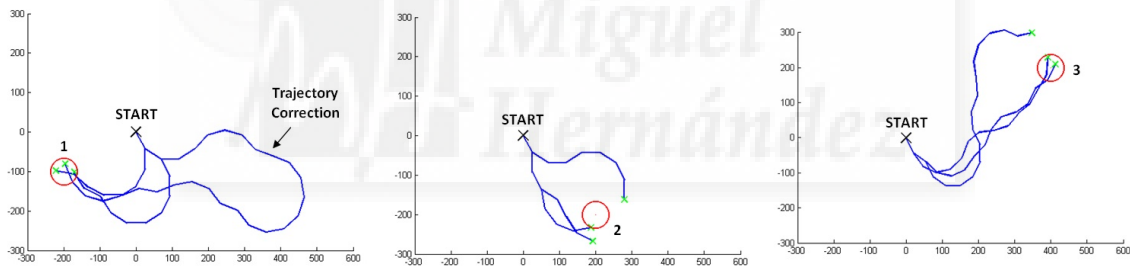


Figure 3.19: Results with the directional control strategy for goals 1, 2 and 3 (scale in mm). The goals are marked with a circle and the start and final position are marked with a cross.

With the directional control strategy, the precision is accurate enough in most of the cases. As it can be seen in Figure 3.19, the subject is able to reach 6 of 9 goals, which means a correct approaching in a 66% of the cases. The maximum error measured is 11.1 cm. In this sense, for future experiments, the improvement of this precision will be important when undertaking grasping operations in a real environment. As it can be observed, time taken to reach the goals dramatically decreases compared to

the hierarchical control, so the directional control has been proved to be a quite fast approaching method. In fact, the average time taken of all 9 tests is 65.1 seconds, around a 40% faster than the hierarchical control (106.2 seconds). It is also remarkable that the volunteer is able to correct a wrong trajectory (see Figure 3.19, left). As it can be seen, all the trajectories start with the same initial angle (the arrow points down) which reflects an initial bias of the interface that could be corrected with additional control commands.

In terms of usability and comfortability, the volunteer has pointed out that the concentration taken to perform the BMI mental tasks is lower for the directional control as relaxation is possible when the movement direction is on the way of the goal. The higher speed of this strategy is also an important advantage for the subject. On the other hand, the volunteer thought that the hierarchical approach was more reliable. As commented before, this fact can be relevant in a realistic application to grasp daily objects.

### 3.5.3 Conclusions

In this section, two control strategies to move a planar robot with a Brain-Machine Interface based on the correlation of EEG maps have been tested by performing 2D movements to reach several goals. The first strategy consists on a hierarchical control where the subject can choose both the axis and direction of the movement. With the second strategy, the subject is able to continuously control the direction of the movement to approach the goals. The results obtained show that the hierarchical control strategy is more reliable but slower than the directional one, which is less precise but more comfortable for the subject. Moreover, the volunteer has been able to reach the goals with both strategies which suggests that this system could successfully work in more complex applications.

In future works, a more realistic environment will be designed to perform grasping tasks of daily objects. In this sense, a pneumatic gripper will be attached at the robot end effector. The EEG mapping classifier will be enhanced by studying different mental tasks and different electrodes positioning to adapt it to a greater range of subjects. The control strategies will be also be improved to reduce positioning error, when necessary,

and time taken to perform the movements of the end effector.

## 3.6 Conclusions

In this chapter, a novel method of classification for spontaneous motor imagery BMIs based on a normalized cross-correlation of EEG maps has been presented. An optimization protocol has been applied to adjust the parameters of the classifier for each subject. This protocol takes into account not only the final accuracy of the classifier but also the speed of the classification. To that end, the time interval of processing has been reduced and an uncertainty threshold has been introduced showing an important improvement of the success rates. The suitability of three different methods to obtain this threshold has been discussed and the results suggest that each method may be suitable depending on the final application in terms of speed and reliability. The final success rates improve the results of previous classifiers and encourage us to introduce new improvements in this kind of classification. The findings of this study suggest that this EEG mapping method may be suitable for the classification of more than three mental tasks as the image models obtained for each task show big differences between them.

A non-invasive BMI based on the correlation of EEG maps has been tested to perform applications in real-time. To that end, a visual application to perform trajectories has been designed. Two targets are shown on a grid and the volunteers are asked to reach the targets by performing tasks related to motor imagery (in this case, the imagination of the movement of the left and right arm). The classifier has been improved from previous works by introducing two uncertainty conditions. Four able-bodied volunteers tested the application. The accuracy and score obtained prove that this BMI is ready to be used in more complex applications for people with a severe motor disability that could help them in their daily life.

The EEG Mapping classifier has been applied to a real world scenario. Two control strategies to move a planar robot with a Brain-Machine Interface based on the correlation of EEG maps have been tested by performing 2D movements to reach several goals. The first strategy consists on a hierarchical control where the subject can choose

both the axis and direction of the movement. With the second strategy, the subject is able to continuously control the direction of the movement to approach the goals. The results obtained show that the hierarchical control strategy is more reliable but slower than the directional one, which is less precise but more comfortable for the subject. Moreover, the volunteer is able to reach the goals with both strategies which suggests that this system could successfully work in more complex applications.



## UPPER LIMB MOVEMENT DECODING FROM LOW FREQUENCY EEG SIGNALS

### 4.1 Introduction

Currently, one of the main challenges of BMIs is to characterize and decode upper limb kinematics from brain signals. Up to now, decoding approaches are mainly centered on intracortical recordings, usually performed in non-human primates, where arrays of microelectrodes are implanted directly in the motor cortex. In some studies, the motor cortical activity of monkeys was used to perform reaching and grasping activities with a robot arm [30], or to perform three dimensional movements that included force grasping for self-feeding using a mechanical device [31]. Invasive approaches have been successfully used in people with motor disabilities to perform reaching and grasping tasks [32, 33]. Less invasive procedures such as electrocorticography (ECoG) have been used to decode two-dimensional arm trajectories [119] and different types of grasping [120]. Despite its potential, invasive approaches require surgery, what limits its use. In this respect, non invasive methods can compensate the drawbacks of intracortical recordings. In this sense, some studies have used magnetoencephalographic (MEG) signals to predict hand movements to perform 2D trajectories [121]. Also, this kind of signals have been used in combination with electroencephalographic (EEG) signals to discriminate between different center-out movements [122]. Regarding EEG signals, their low signal-to-noise ratio challenges the kind of trajectory decoders that can be

built.

Recent works suggest that it is possible to decode hand or arm kinematics (position and velocity) from slow cortical potentials, i.e., EEG signals oscillations below 2 Hz [77]. To that end, multidimensional linear regression models are applied to the data. In this work, the volunteers were asked to perform random selections of eight targets in a 3D environment. The results showed that better correlations between velocity and EEG recordings were found when the users performed linear hand-reaching movements. In other works, the use of low frequency components ( $<2\text{Hz}$ ) showed the best correlation results when performing continuous and rhythmic right arm movements [123]. In this case, volunteers were asked to perform natural arm movements with a variable speed. From these studies it was concluded that decoding performance is at least partially related to the type of movement performed.

Decoding methods based on the analysis of low frequency EEG components have gone some way towards a deeper knowledge of motor neural correlates. However, there is certain controversy about how the decoding performance is assessed. A very recent study holds that this methodology has the risks of overestimating the decoding performance due to the mathematical properties of linear regression between signals in the same frequency range (in this case, slow arm movements and slow cortical potentials) [124]. This study states that, in fact, the results do not show higher accuracies than chance level and the correlation is not sensitive to scaling. In a previous work, the use of multidimensional linear regression was proposed as the decoding method to control a cursor reporting that it is possible to accomplish a two-dimensional control of this cursor with performance levels comparable to those of invasive BMI systems [125]. In their study, the decoding models had to be recalibrated to include a scaling factor due to the fact that the correlation metric is invariant to scale. The controversy of how these results are assessed is still a matter of discussion [125, 126, 127], so it is necessary to gather further evidence of the real possibilities of decoding arm trajectories from EEG slow cortical potentials. Some studies have suggested the introduction of electromyographic information (EMG) into this decoding procedure [128] or even a simplification of it using the new conceptual approach of muscle synergies [129].

In this chapter, we first assess the real possibilities of using linear regression methods

to decode upper limb kinematics from EEG signals (Section 4.2). To that end, we compare several results obtained by applying linear regression techniques to decode upper limb kinematics from EEG signals using a center-out reaching approach. The difference between real arm movement and imagined arm movement has been computed using the decoding approach presented in [77], which consists of a multidimensional linear regression model. First, the correlation between the decoded and the performed kinematics has been obtained. The results show that real arm movement decoding is significantly above chance levels which were calculated from random and shuffled EEG data. However, imagined arm movements are not significantly above chance levels and, in fact, below real arm movements. Passive movements have been then performed using the same protocol to study the influence of movement artifacts in the decoding. The results show non-significant decoding correlations and prove that decoding accuracy during movement is due purely to a neural correlation and not related to muscle artifacts. Finally, all the tests have been recomputed to obtain a discrete classification of reached targets and allow obtaining the same conclusions with a very high classification accuracy. From these findings, it can be concluded that the discrete classification of reached targets from decoding approaches may be a more suitable real-time methodology than a direct decoding of hand position.

Additionally we analyze the influence in the decoding of the performed arm movement in terms of velocity, trajectory and variability (Section 4.3). To that end, the decoding correlation has been studied by performing upper limb movements with different speeds and trajectories. Low frequency components of the EEG signals have been decoded with linear models to obtain the position of the hand during performed trajectories using a planar robot. A visual interface, showing a disc moving in a 2D environment, has been used as feedback. The volunteers are asked to follow the disc, which moves randomly on the screen with a constant speed, by controlling a cursor with the planar robot. The disc size is changed in each session to evaluate the influence of movement accuracy. Finally, concentration and ergonomic aspects are also taken into account. To that end, volunteers are asked to fill a comprehensive survey of the tests that includes questions about tiredness, comfort, frustration, entertainment and difficulty. This survey allows solving different small issues during the experimental tests

and improves ergonomics of the robot arm and the tests in general.

Finally, the discrete classification of reached targets has been applied in real time (Section 4.4). In the experiments, subjects are asked to reach two targets on a screen by moving the computer mouse. First, the decoding models have been obtained from fast training runs where both mouse trajectories and EEG signals are recorded. Then, these models have been applied to decode the mouse cursor trajectories and, afterwards, the direction of movement has been classified and compared to the actual performed trajectories. The results obtained show significant classification rates of horizontal movements. This work is aimed at obtaining an accurate way of decoding hand movement intention that could be applied on the control of an exoskeleton in future rehabilitation tasks.

## 4.2 Continuous and Discrete Decoding of Upper Limb Kinematics from EEG Signals in Center-Out Reaching Tasks

In this section, we compare several results obtained by applying linear regression techniques to decode upper limb kinematics from EEG signals using a center-out reaching approach. The experimental tests are based on a center-out protocol where a cursor moves from a central position to several targets equally distributed around it. The difference between real arm movement and imagined arm movement was computed using a decoding approach consisting of a multidimensional linear regression model. Passive movements were also performed using the same protocol to study the influence of movement artifacts in the decoding. Finally, we also evaluated the discrete classification of reached targets. To that end, the decoding has been computed to obtain the trajectory of the cursor for each movement and then, the angle of movement (or momentum) has been calculated to classify the direction of the movement, i.e., the reached target. The results obtained in this section have led to the preparation of a journal article [12].

### 4.2.1 Materials and Methods

### 4.2.2 Experimental Tests

The experimental tests are based on a center-out protocol in which subjects sat in front of a computer screen where a cursor moves from a central position to several targets equally distributed around it (see Figure 4.1, top). EEG signals were recorded along with the position and velocity of the cursor. Three different tests were performed. The first one took place in the Defitech Foundation Chair in Non-Invasive Brain-Machine Interface (CNBI) at the École Polytechnique Fédérale de Lausanne (EPFL) in Switzerland. The remaining tests took place in the Brain-Machine Interface Systems Lab at the Miguel Hernández University in Elche (Spain).

- *Motor imagery center-out*: the cursor is moved automatically to reach 8 different targets that are randomly highlighted on the screen. Each time the cursor reaches a target, it returns to the central position and a new target is highlighted. Subjects are asked to follow the cursor with their eyes while imagining hand or finger movements on a plane. The cursor takes 4 seconds to reach each target and 4 seconds to return to the central position without any waiting period in between. 5 runs of 5 minutes (around 37 reached targets) each were performed by 5 able-bodied subjects (A1-A5), all male ( $26.4 \pm 0.9$  year-old). EEG signals were acquired using a Biosemi ActiveTwo amplifier with a sample frequency of 2048 Hz. 64 electrodes were placed following the 10/10 International System. Ground and reference electrodes were replaced by the Common Mode Sense (CMS) active electrode and the Driven Right Leg (DRL) active electrode.
- *Real center-out movement*: in this case, the subjects control the cursor movement using a planar robot (see Figure 4.1, top). The planar robot arm used is the PuPArm, a force-controlled robot designed and developed by the nBio research group at the Miguel Hernández University of Elche (Spain) [117, 118] (for more details see Appendix A). As before, the goal is to reach the target that is randomly highlighted on the screen. The subject must reach it and then return to the central position. Each time a target is reached or the cursor enters the central position,

a waiting period of 400 ms is introduced. Each subject executed 10 runs in which 40 targets were highlighted (around 3 minutes per run). 5 able-bodied subjects (B1-B5), all male ( $26.4 \pm 3.1$  year-old) performed the tests. The equipment used was the gUSBamp (g.Tec, GmbH, Austria) with a sample frequency of 1200 Hz. 16 electrodes were recorded distributed over the central and parietal cortex, where a higher activity related to arm movements is expected. The reference was placed on the right earlobe and ground was placed on the AFz position.

- *Passive center-out movement*: subjects are asked to passively grasp the planar robot end effector while the researcher operates the robot. The experimental tests are the same as with the real center-out movement. Subjects carried out 5 runs in which 40 targets were highlighted (around 3 minutes per run). 5 able-bodied subjects (C1-C5), all male ( $25.2 \pm 2.6$  year-old) performed the tests.

#### 4.2.2.1 Preprocessing

First, cursor kinematics were resampled to match EEG signals. EEG signals were visually inspected to reject blinks, and frontal channels were discarded to diminish ocular artifacts. For this reason, the same 16 electrodes were considered for the analysis of all conditions: FC5, FC1, FC2, FC6, C3, Cz, C4, CP5, CP1, CP2, CP6, P3, Pz, P4, PO3 and PO4. According to previous literature, information related to Slow Cortical Potentials (SCPs) is localized above 0.1 Hz [130]. As a consequence, EEG signals were band-pass filtered with a zero-phase 4th-order Butterworth filter between 0.1-2 Hz. For comparison purposes they were also filtered between 8-12 Hz, 14-30 Hz and 0.1-40 Hz, to estimate the amount of information present in each frequency band performing a similar analysis to the one shown by Antelis et al. [124]. Cursor kinematics (position and speed) were also low-pass filtered with a zero-phase 4th-order Butterworth filter below 2 Hz. Finally, EEG data from each electrode  $i$  were standardized by subtracting, for each time sample ( $t$ ), the mean ( $\bar{V}_i$ ) of the signal and dividing the result by the standard deviation ( $SD_{V_i}$ ) as shown in (4.1).

$$EV_i[t] = \frac{V_i[t] - \bar{V}_i}{SD_{V_i}} \quad (4.1)$$

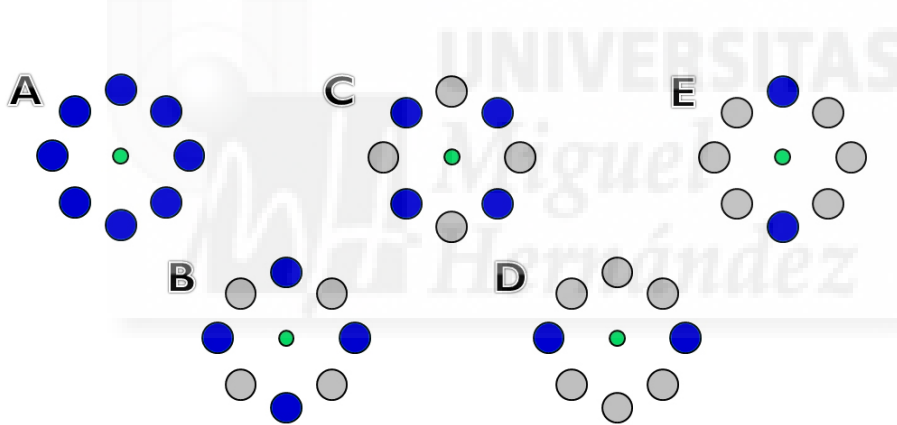
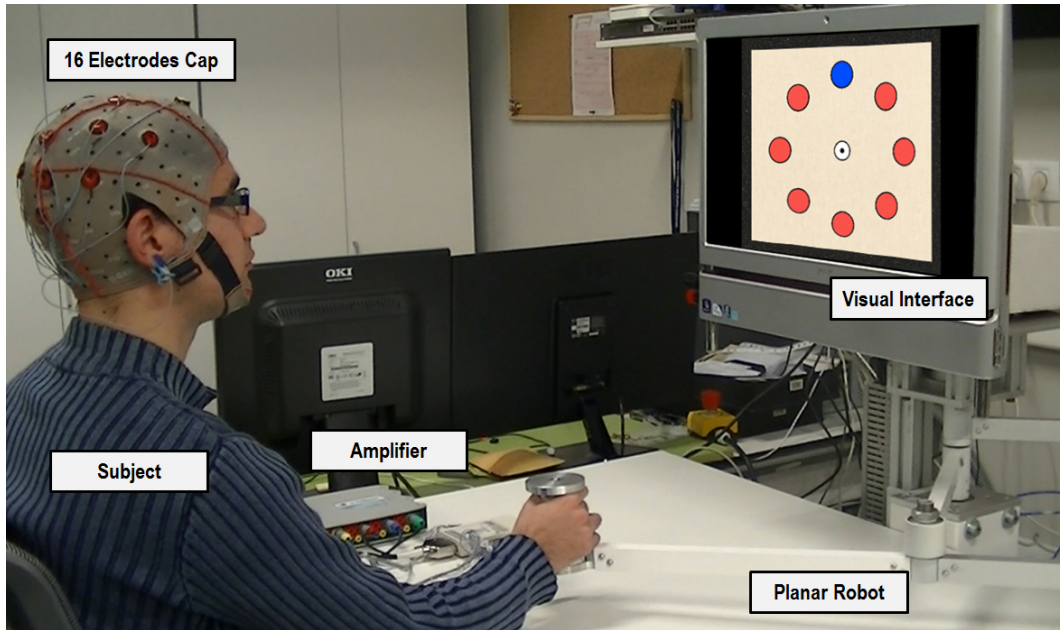


Figure 4.1: Top, experimental setup. The subject performs the center-out movements in front a screen showing the cursor and target locations. The subject is asked to reach the highlighted targets with the planar robot or follow the automatic movement of the cursor while performing motor imagery of hand or finger movements on a plane. Bottom, different configuration of possible targets have been analyzed to compare the performance of target decoding. Configuration A covers all the targets shown. For configurations B and C, 4 targets are taken into account in the analysis. Finally, configurations D and E correspond to a discrimination between two opposite target directions.

### 4.2.2.2 Decoding

A multidimensional linear regression has been applied to decode kinematics from EEG signals,

$$x[t] = a + \sum_{n=1}^N \sum_{k=0}^L b_{nk} S_n[t-k] \quad (4.2)$$

where  $x[t]$  is the kinematics state (position and velocity) at time  $t$  and  $S_n$  is the signal from channel  $n$ .  $L$  corresponds to the number of lags and  $N$  to the number of channels. The decoding parameters,  $a$  and  $b$ , were estimated using a cross-fold validation for each condition. The values for the parameters  $L$  and  $N$  are:  $L = 10$  (around 80 ms of signal) and  $N = 16$  (central and occipital electrodes uniformly distributed).

To simplify the process, the matrix form of (4.2) has been used as follows:

$$X[4 \times 1] = A[4 \times NF] * Z[NF \times 1] + R[4 \times 1] \quad (4.3)$$

where  $X$  is the kinematic state  $[PxPyVxVy]'$ ,  $A$  is the transformation matrix,  $Z$  is the features array,  $R$  is the scale matrix (independent term of the linear regression) and  $NF$  is the number of features used which depends on the time lag  $L$  and the number of channels  $N$  ( $NF = L * N + 1$ ).

### 4.2.2.3 Analysis

The decoding performance has been analyzed in two ways. First, by obtaining the Pearson correlation coefficient between the decoded and the performed trajectories (continuous decoding) and finally, by classifying the direction of each movement and compare it with the actual reached target (discrete decoding).

- **Continuous Decoding:**

For the continuous decoding, the matrices  $A$  and  $R$  in (4.3) have been obtained using a ten-fold cross validation. For each fold, the training data has been used to compute the decoding matrices that are then applied to the test data to obtain the decoded kinematics. We computed the Pearson correlation coefficient between the real and decoded kinematics for each fold and then computed the average to obtain

the final decoding accuracy. The results have been compared for different ranges of frequencies (0.1-2 Hz, 8-12 Hz, 14-30 Hz and 0.1-40 Hz). Additionally, shuffled and random data have been used as input to assess if the decoding accuracy was above chance levels. Shuffled data have been obtained by randomly mixing target labels of real data and the associated kinematics to keep the temporal structure of the EEG signals. Random data have been obtained by generating a uniform noise with the same size of real input data. Both shuffled and random data have been filtered and standardized in the same way as the actual experimental data. Random and shuffled data decoding coefficients have been computed 100 times to avoid chance effects due to the stochastic nature of the process.

- **Discrete Decoding:**

For the discrete decoding analysis, the success rate of reaching a particular target has been obtained for the frequency range (0.1-2 Hz). Only SCPs have been analyzed as the continuous decoding shows non-significant results in other bands (see Section 4.2.3.1). To that end, EEG signals and kinematics have been manually segmented into blocks for each center-out movement and labeled with the corresponding target. First, the trajectory of the cursor has been decoded for each movement block (from the decoded X and Y positions) and then, the angle of movement (or momentum) has been calculated and compared to the angular position of each target to classify the direction of the movement, i.e., the reached target. This classification has been performed using a ten-fold cross-validation for 5 different target configurations (see Figure 4.1, bottom). The movement workspace is divided into sectors depending on the configuration of targets. For example, for two targets, the workspace is divided into two sectors and the estimated angle is assigned to the nearest target. As before, shuffled and random data was used to estimate chance levels.

## 4.2.3 Results

### 4.2.3.1 Continuous Decoding

The Pearson correlation coefficient has been obtained after computing a cross-fold validation between all sessions for each subject. Figure 4.2 shows the Pearson correlation coefficient obtained while performing imagined and real center-out movements when decoding signals in the frequency band 0.1-2 Hz. Motor imagery decoding (Figure 4.2A) did not yield high correlation coefficients for any of the subjects. However, most subjects showed a high correlation in the X velocity component, with small deviations. In general, the correlation for the decoded X velocity component (averaged between all subjects) is clearly higher than the rest ( $0.265 \pm 0.103$  versus  $0.055 \pm 0.160$  for X position,  $0.037 \pm 0.115$  for Y position and  $0.054 \pm 0.121$  for Y velocity). On the other hand, real center-out movement showed higher decoding correlations (Figure 4.2B). Particularly, subjects B3 and B5 obtain the best decoding accuracy with some components reaching a value of 0.5.

Figure 4.3 shows an example of 30 seconds kinematic reconstruction (2D position and velocity) for one of the subjects performing real movements. In this particular example, decoding coefficients above 0.5 show a very accurate reconstruction of the performed trajectories (X Position and Y Position). When the decoding correlation decreases (X Velocity, Y Velocity), the reconstructed signal preserves its tendency but reduces its accuracy.

To estimate the significance of our findings, the decoding models have been tested with random and shuffled data and compared with the results for motor imagery and real movement (Figure 4.4). For motor imagery, only X Velocity yielded results above chance level ( $p < 0.001$ ) (Figure 4.4A). This suggests that the SCPs do not convey enough information to decode kinematic information from motor imagery. On the other hand, the results show that real movement is decoded significantly above chance level for any component ( $p < 0.001$ , Wilcoxon Sum-Rank Test)(Figure 4.4B). Interestingly, decoded X velocity from imagined movements shows no significant difference when compared to the corresponding X velocity component for real movements (Figure 4.4C). The reason for the higher accuracy of the X Velocity component is not clear. For the

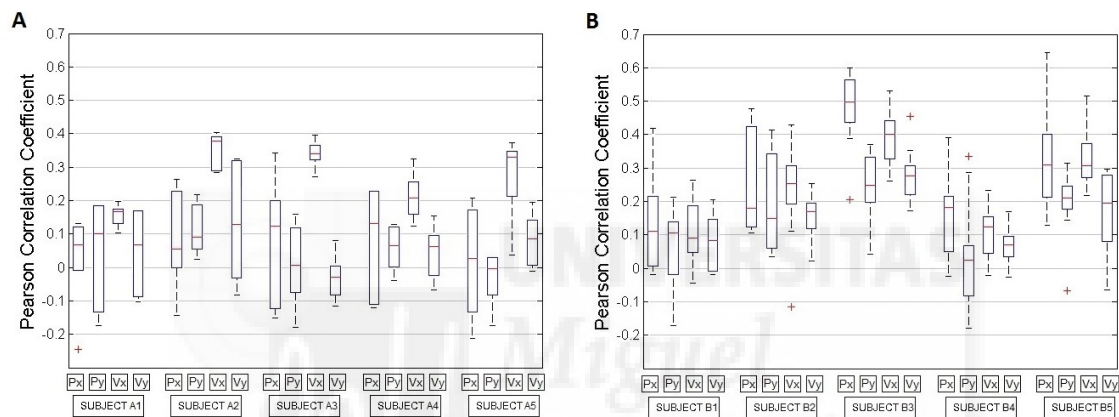


Figure 4.2: Continuous decoding of center-out trajectories for motor imagery center-out (A) and real center-out movement (B) for the frequency band 0.1-2 Hz. The boxplot represents the Pearson correlation coefficient obtained after computing a cross-fold validation between all sessions. For each subject (1-5) the graph shows results for position (Px and Py) and velocity (Vx and Vy).

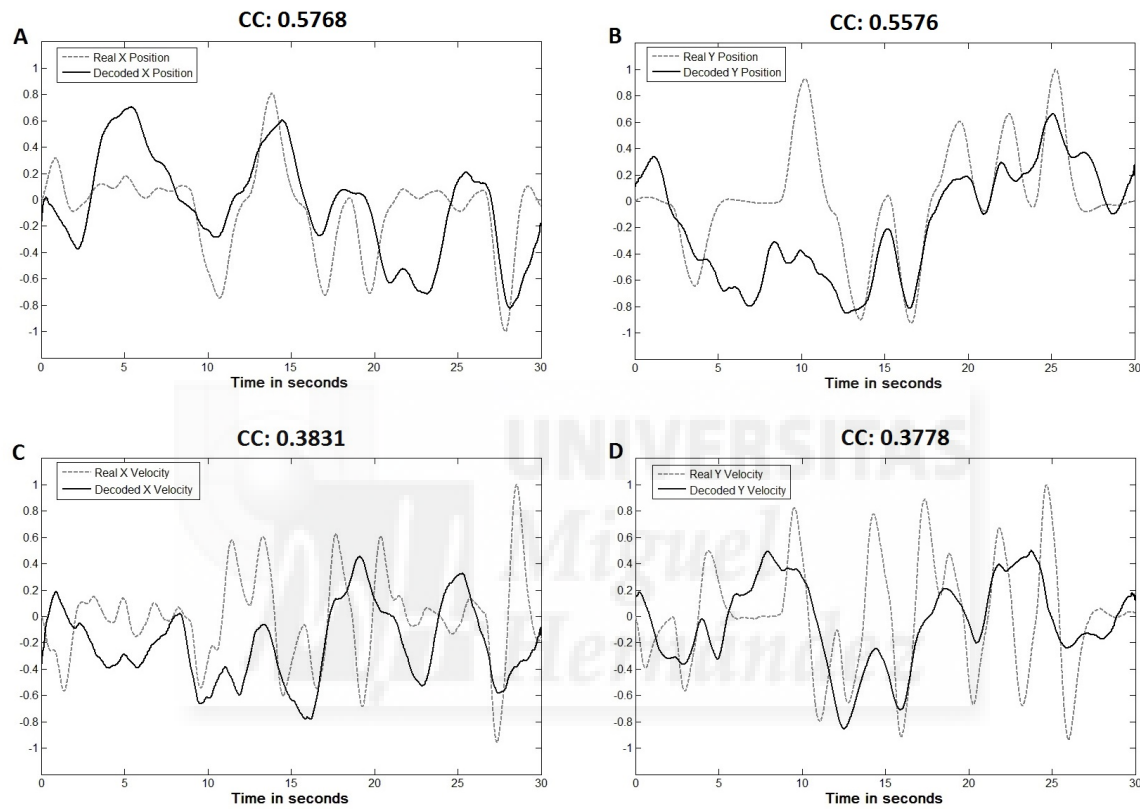


Figure 4.3: Continuous decoding of kinematics using the linear regression decoding method (Subject 3 - Real Center-out Movement). The grey dotted line represents the real performed movement. The continuous black line represents the decoded kinematics (A: X Position, B: Y Position, C: X Velocity, D: Y Velocity). The correlation coefficient (CC) obtained from the correlation of both signals is also shown.

remaining components, decoding from real movements is always significantly higher than motor imagery ( $p < 0.001$ ) (Figure 4.4C). These findings differ from previous reports [124], where the correlations and normalized errors of the results of real models were not statistically different from shuffled and random models.

Previous studies have claimed that upper limb kinematics are better reconstructed from low frequency EEG signals [77, 123, 124]. We test this hypothesis by analyzing the decoding performance using the signal in four different frequency bands: 0.1-2 Hz (SCPs), 8-12 Hz (alpha band), 14-30 Hz (beta band) and 0.1-40 Hz (Figure 4.5). The results were computed for four different sets of data: motor imagery center-out, real center-out movement, random data and shuffled data.

In agreement with these studies, our analysis showed that decoding correlations of higher frequency bands were not significantly above zero and that the low frequency band (0.1-2 Hz) yielded the best decoding accuracies. Decoding performance using SCPs was slightly but not significantly above results obtained with a larger frequency band (0.1-40 Hz) that includes the irrelevant higher frequencies.

#### 4.2.3.2 Discrete Decoding

Figure 4.6 shows the success rate of targets correctly classified after computing a cross-fold validation between all sessions recorded for imagined and real center-out movement (4.6A and 4.6B, respectively). For each subject the graph shows the five different target configurations proposed (Figure 4.1, bottom). The success rate obtained from motor imagery is quite low (averaged:  $14.05 \pm 4.81$  for configuration A,  $27.67 \pm 8.40$  for configuration B,  $29.9 \pm 9.93$  for configuration C,  $61.52 \pm 15.25$  for configuration D and  $55.61 \pm 18.43$  for configuration E). On the other hand, the results from real movement yield important improvements for all the configurations (averaged:  $29.00 \pm 11.82$  for configuration A,  $51.30 \pm 19.24$  for configuration B,  $52.30 \pm 20.53$  for configuration C,  $79.60 \pm 15.90$  for configuration D and  $75.60 \pm 17.04$  for configuration E). As expected, these discrete results show certain similarities with the corresponding continuous results. Unsurprisingly, subjects B3 and B5, who obtained the best decoding accuracies in the continuous approach, also had the highest success rates. The success rate obtained in the classification of two targets (configurations D and E) is particularly remarkable

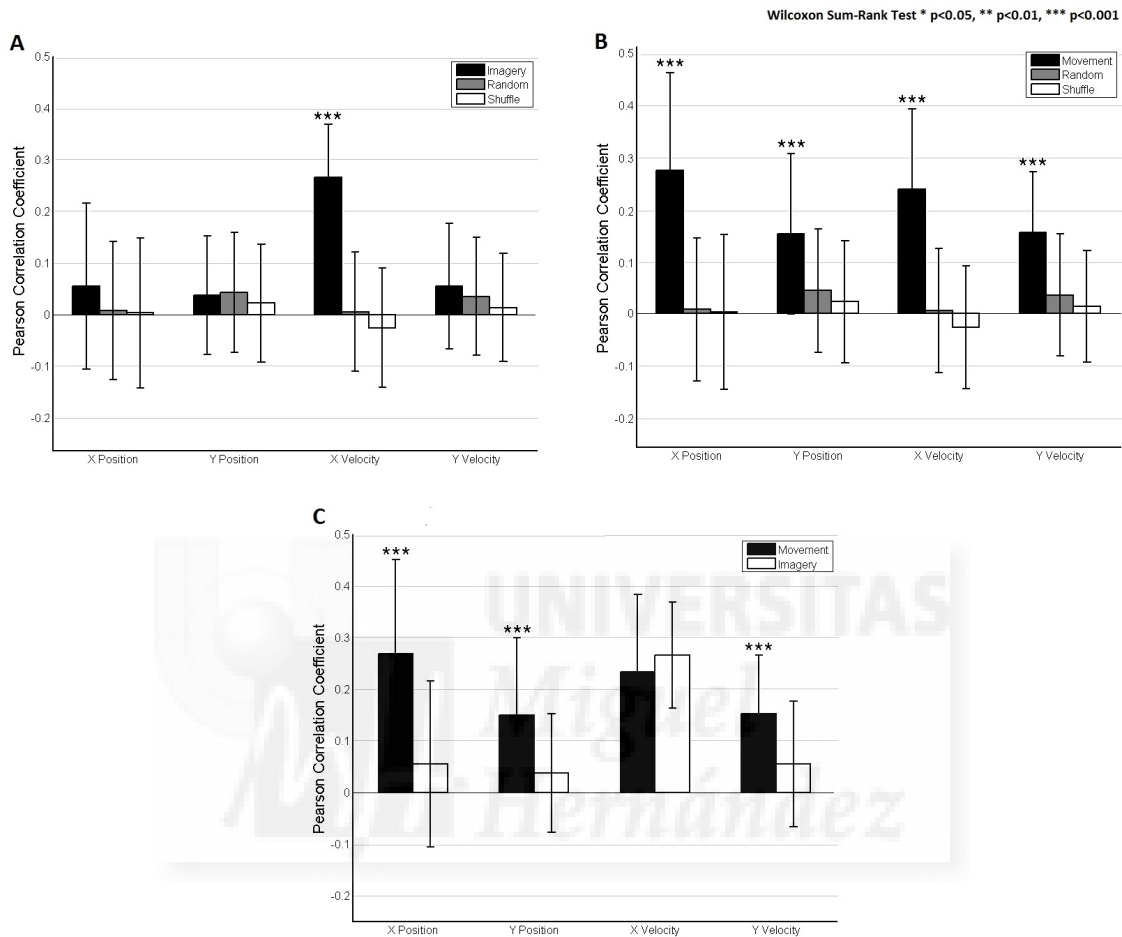


Figure 4.4: Continuous decoding of center-out trajectories comparing different experimental data: motor imagery center-out, real center-out movement, shuffled data and random data. The Pearson correlation coefficient is obtained after computing a cross-fold validation between all sessions and then averaged between subjects. Each graph shows results for position ( $P_x$  and  $P_y$ ) and velocity ( $V_x$  and  $V_y$ ). Graph A reflects differences of motor imagery center-out versus random and shuffled data. Graph B reflects differences of real center-out movement versus random and shuffled data. Finally, graph C reflects differences of real center-out movement versus motor imagery center-out. The stars represent significant differences with respect to random and shuffle conditions.

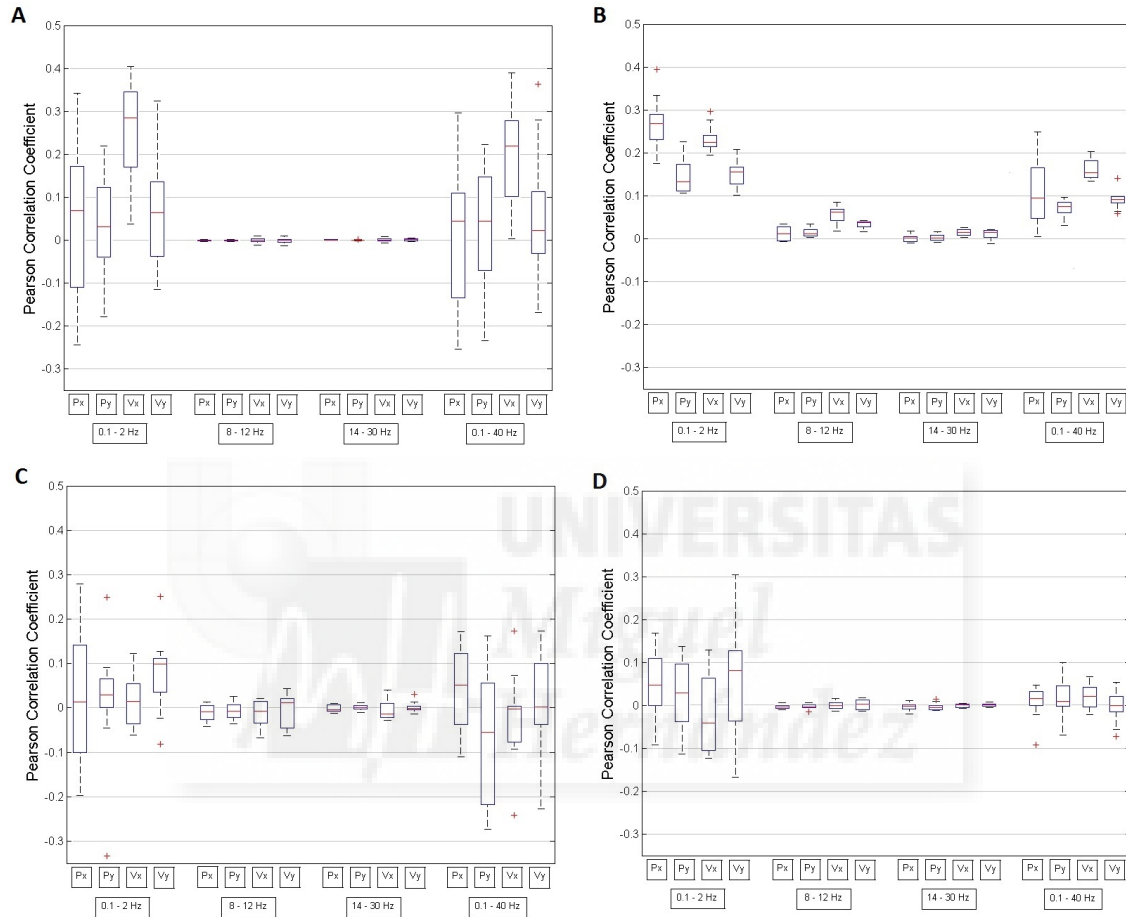


Figure 4.5: Comparison between different frequency bands: 0.1-2 Hz (low frequencies), 8-12 Hz (alpha band), 14-30 Hz (beta band) and 0.1-40 Hz. The boxplot represents the Pearson correlation coefficient obtained after computing a cross-fold validation between all sessions for each subject and then averaged between subjects. Position (Px and Py) and velocity (Vx and Vy) are shown for different experimental data: motor imagery center-out (A), real center-out movement (B), shuffled data (C) and random data (D).

(subject B3,  $93.00 \pm 6.75$  and subject B5,  $89.00 \pm 11.00$  for configuration D; and subject B3,  $88.00 \pm 11.35$  and subject B5,  $87.00 \pm 9.48$  for configuration E).

Theoretically, chance level for configuration A (8 targets) should be a 12.5%, for configurations B and C (4 targets) a 25% and for configurations D and E (2 targets) a 50%. However, as the number of sessions is small, these levels may not be representative. As a consequence, discrete decoding has been computed for shuffled data and random data the same way as in the continuous decoding and compared with motor imagery and real movement results (Figure 4.7). The results show that motor imagery is significantly above chance level (Figure 4.7A) for configurations C ( $p < 0.001$ , Wilcoxon Sum-Rank Test), D ( $p < 0.001$ ) and E ( $p < 0.001$  compared to random data and  $p < 0.05$  compared to shuffled data). Real movement is significantly above chance level for all configurations ( $p < 0.001$ , Wilcoxon Sum-Rank Test)(Figure 4.7B). These new findings show differences with the continuous approach, indicating neural correlates of motor imagery movement directions when a small number of targets are classified (configurations C, D and E). The reduction of targets and, as a consequence, trials computed to obtain the decoding models may be a cause of this significance. On the other hand, significance levels between motor imagery and real movement indicate that success rate is clearly higher when performing the real center-out movement for all configurations (Figure 4.7C). In this case, X Velocity, which showed similar decoding correlations for both experiments in the continuous decoding, is not used for the discrete decoding and, subsequently, the difference between real movement and motor imagery increases.

### 4.2.3.3 Decoding passive movement

Although the results obtained from the decoding of real center-out movement are significantly above chance level, it cannot be concluded with complete certainty that this is not caused by the influence of muscle artifacts while reaching each of the targets and that the neural correlation between EEG signals and upper limb movements is, in fact, non-existent. To discard this possibility, a third set of experiments was undertaken. During these experiments, subjects were asked to repeat the same protocol used for the real center-out movement experiments but, in this case, they had to passively grasp the planar robot end effector and their arm was moved by the experimenter. This new data

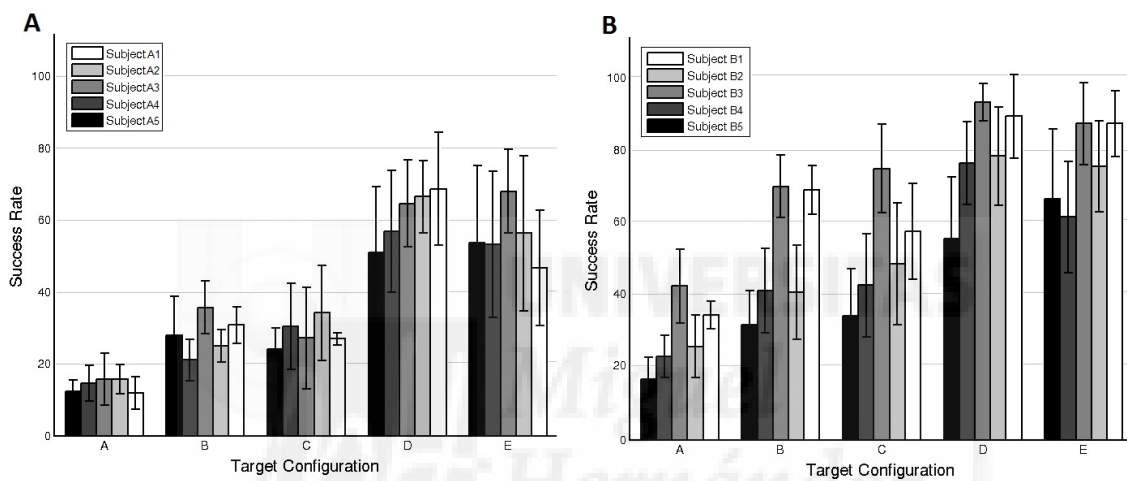


Figure 4.6: Discrete decoding of center-out trajectories for motor imagery center-out (A) and real center-out movement (B). The barplot represents the success rate of targets correctly classified obtained after computing a cross-fold validation between all sessions. For each subject (1-5) the graph shows results of five different target configurations (as shown in Figure 4.1).

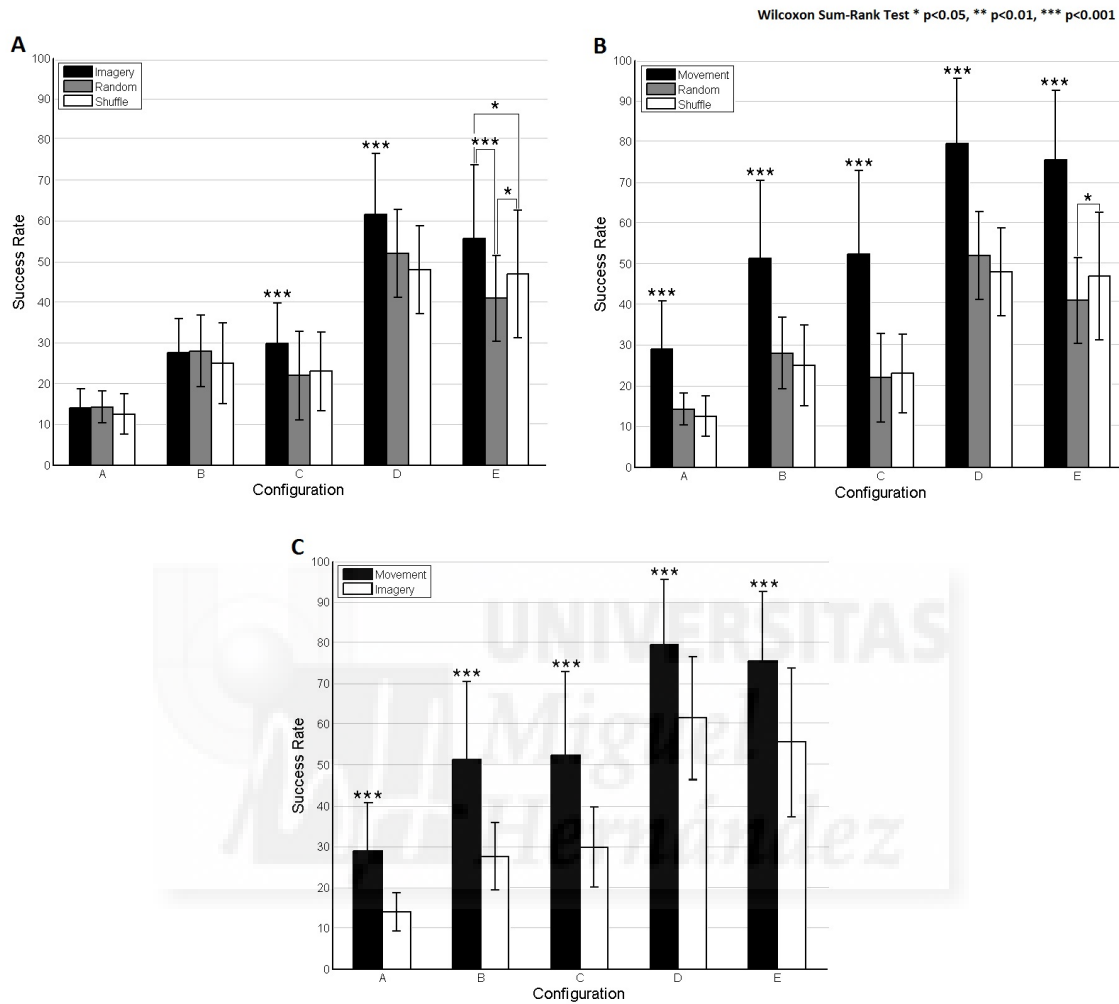


Figure 4.7: Discrete decoding of center-out trajectories comparing different experimental data: motor imagery center-out, real center-out movement, shuffled data and random data. The success rate of targets correctly classified is obtained after computing a cross-fold validation between all sessions and then averaged between subjects. Each graph shows results of five different target configurations: A-E (see Figure 4.1). Graph A reflects differences of motor imagery center-out versus random and shuffled data. Graph B reflects differences of real center-out movement versus random and shuffled data. Finally, graph C reflects differences of real center-out movement versus motor imagery center-out.

set was then analyzed the same way as the previous data (decoding of low frequency components 0.1-2 Hz) and it is expected to have non-significant decoding accuracies, both with the continuous and the discrete approach.

Figure 4.8A shows the Pearson correlation coefficient obtained while performing passive center-out movements (continuous approach) and Figure 4.8B shows the success rate of targets correctly classified (discrete approach). The results obtained from this set of data were not above chance level for both continuous and discrete approaches and corroborate our initial assumptions, indicating EEG slow cortical potentials carry significant information to decode real center-out movements. The significance of neural activity during active center-out movements is analyzed in Figure 4.9 showing that the decoding accuracy is always significantly above the levels of passive movement for all the components (X Position, Y Position, X Velocity and Y Velocity) ( $p < 0.001$ , Wilcoxon Sum-Rank Test, Figure 4.9A) and the success rate is significantly above the levels of passive movements for all the configurations ( $p < 0.001$ , Wilcoxon Sum-Rank Test, Figure 4.9B).

#### 4.2.4 Discussion and Conclusions

This section contributes to the assessment of feasibility of using linear regression methods to decode upper limb kinematics from EEG signals. Previous work states that it is possible to decode hand or arm kinematics (position and velocity) from slow cortical potentials, i.e., EEG signals below 2 Hz [77, 123, 131, 132]. However, these results may have been misinterpreted due to the inherent properties of linear regression methods, particularly, when comparing EEG signals with the same frequency range as the decoded kinematics [124]. To confirm or reject this conclusion, we have applied a similar methodology to center-out movement and center-out motor imagery experimental data in a two dimensional space and we have analyzed the significance of the results.

As previously reported [77, 124, 125], low frequency bands (0.1-2 Hz) concentrate most of the information extracted from upper limb kinematics decoding, this is consistent with the properties of linear regression. However, our findings indicate that decoding accuracies obtained from real center-out movements are significantly above chance levels and do not depend on muscle artifacts produced during the reaching

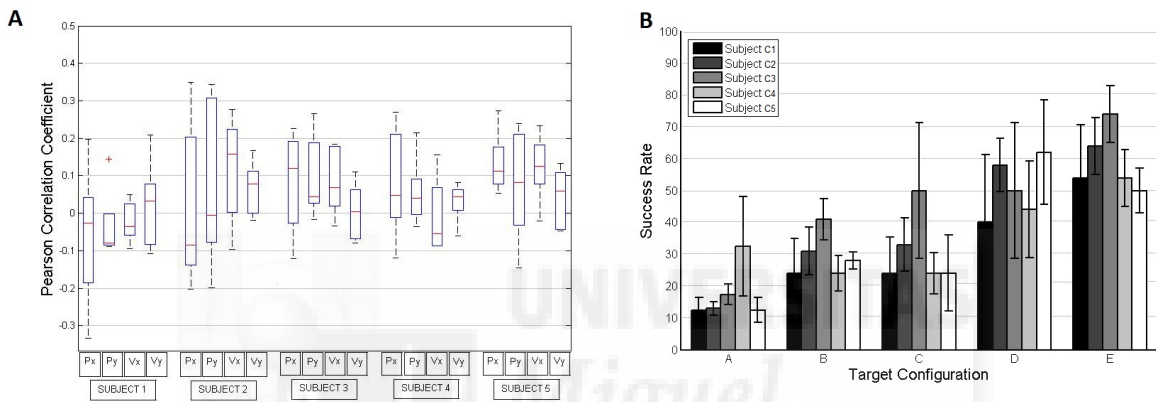


Figure 4.8: Continuous (A) and discrete (B) decoding of center-out trajectories for passive center-out movement. (A) represents the Pearson correlation coefficient obtained after computing a cross-fold validation between all sessions. For each subject (1-5) the graph shows results for position (Px and Py) and velocity (Vx and Vy). (B) represents the success rate of targets correctly classified obtained after computing a cross-fold validation between all sessions. For each subject (1-5) the graph shows results of five different target configurations (see Figure 4.1).

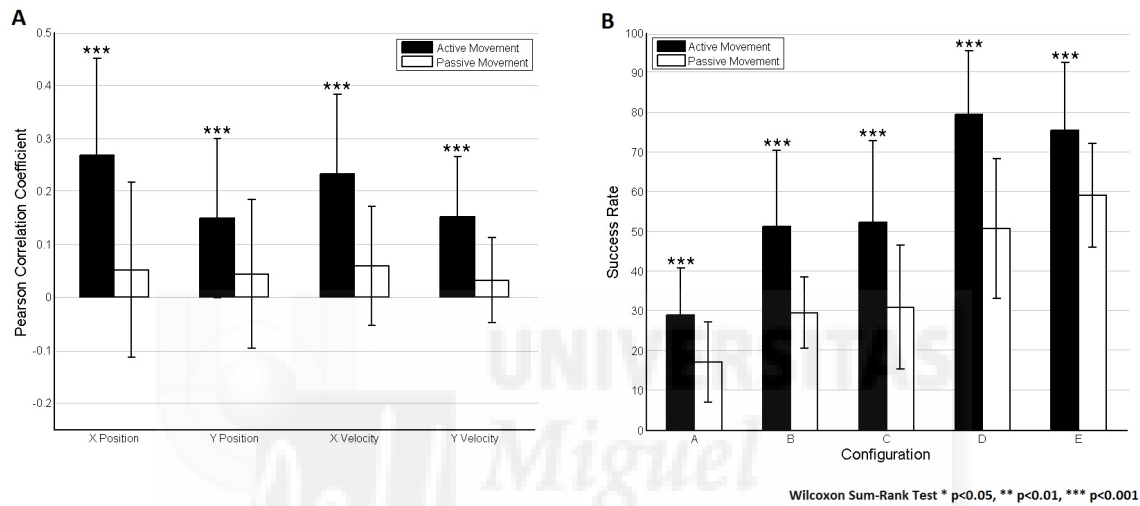


Figure 4.9: Continuous (A) and discrete (B) decoding of center-out trajectories comparing active center-out movement and passive center-out movement. For the continuous decoding, the Pearson correlation coefficient is obtained after computing a cross-fold validation between all sessions and then averaged between subjects. The results for position (Px and Py) and velocity (Vx and Vy) are displayed. For the discrete decoding, the success rate of targets correctly classified is obtained after computing a cross-fold validation between all sessions and then averaged between subjects. The results of five different target configurations (see Figure 4.1) are displayed.

movements. Indeed, our results show that it is not possible to decode passive movements using EEG slow cortical potentials. On the other hand, motor imagery, shuffled and random conditions show that individual correlation values are high but not above chance (likely due to the properties of the correlation metric which is invariant to scale and has a non-linear nature [124]). This implies that decoding performance of active arm movements is significantly above motor imagery center-out trajectories. The low decoding performance of motor imagery center-out trajectories may be due to the potential confound of having smooth pursuit in the motor imagery condition. In fact, the motor imagery condition is subject to an important limitation as subjects do not undertake any training process which could eventually improve decoding as they learn to better modulate their EEG. Nevertheless, the presence of significant information in horizontal imagined movement opens an encouraging possibility of improving this decoding accuracy in future reoriented experiments.

The decoding accuracies are quite low compared to what is reported in other recent works [125], where the authors state that it is possible to accomplish a two-dimensional real time control of a cursor with performance levels comparable to those of invasive BMI systems. These findings are still subject of controversy [126, 127] and it is suggested that, in fact, the results obtained are closer to chance levels than what it is actually claimed. In any case, direct two-dimensional control appears to be difficult to achieve with acceptable accuracy levels using continuous decoding methods. For this reason, in this work we have proposed a simplification of the method by computing a discrete classification of reached targets. This kind of approach has been recently explored in several works [122, 133, 134]. In our case, the results have shown high success rates for different target configurations, presenting a clear coherence with the previously obtained decoding accuracies. These results are quite encouraging and suggest that an online application of this methodology may provide an accurate identification of upper limb movement intention. By reducing the dimensionality of the classification output, this discrete approach presents promising advantages in future neurorehabilitation procedures, where EEG slow cortical potentials could be exploited to classify arm movement directions [135] and even detect movement onset [136]. Regarding rehabilitation assistance, this simplification should not affect its application as rehabilitation

therapy is often based on repetitive movements [137].

### 4.3 Analysis of Movement Variability in Upper Limb Kinematics Decoding from EEG Signals

In this section, the influence of arm movement variability in the decoding performance has been analyzed. To that end, the decoding correlation has been studied by performing upper limb movements with different speeds and trajectories. To that end, low frequency components of the EEG signals have been decoded with linear models to obtain the position of the hand during performed trajectories using a planar robot. A visual interface, showing a disc moving in a 2D environment, has been used as feedback. The volunteers are asked to follow the disc, which moves randomly on the screen with a constant speed, by controlling a cursor with the planar robot. The disc size has been changed in each session to evaluate the influence of movement accuracy. Finally, concentration and ergonomic aspects have been also taken into account. To that end, volunteers have been asked to fill a comprehensive survey of the tests that included questions about tiredness, comfort, frustration, entertainment and difficulty. This survey allows solving different small issues during the experimental tests to improve ergonomics of the robot arm and the tests in general. The results obtained in this section have led to the preparation of a journal article [13]

#### 4.3.1 Materials and Methods

##### 4.3.1.1 Subjects

Five healthy volunteers (all male and right-handed) with ages between 25 and 30 years (mean  $27.8 \pm 2.0$ ) took part in the experiments. All volunteers are engineering students or researchers and are familiar to the technologies applied in this work. Written consent according to the Helsinki declaration was obtained from each subject.

### 4.3.1.2 Experimental Paradigm

The volunteers were asked to follow a disc that moved randomly on the screen with a constant speed by controlling a black cursor with a planar robot arm (Figure 4.10). To that end, the disc randomly changed its orientation each 100 ms (10 degrees clockwise or anti-clockwise) and moved forward a particular amount of pixels. In previous works, it was proved that subjects do not fixate on the moving object but on the movement starting and finishing points [138]. However, in these tests, subjects were specifically asked to fixate on the cursor movement. To control the cursor a planar robot arm the volunteer had to move the end effector of a planar robot inside a workspace of 225x150 mm. The planar robot arm used is the PuPArm, a force-controlled robot designed and developed by the nBio research group at the Miguel Hernández University of Elche (Spain) [117, 118] (for more details see Appendix A). 4 different speeds were defined (approximately 20, 30, 40 and 50 mm/second). For each speed, 3 sessions, with a different disc size (5, 7.5 and 10 pixels/diameter), were performed. The order of sessions was not randomized. Each session consisted of five runs of continuous movements during 45 seconds. After each round, a success percentage, representing the time the volunteer was able to stay inside the disc, was shown and a resting period of 4 seconds was included between runs. The total time of the experiment was about 1 hour. All volunteers sat in front of a computer screen in an isolated room to avoid disturbances during the recordings.

### 4.3.1.3 EEG Recordings and Preprocessing

For the recordings, a cap with 16 sintered Ag/AgCl ring electrodes has been used (g.GAMMAcap and g.LADYbird models, g.Tec). The electrodes were placed over the scalp with the following distribution: FC5, FC1, FC2, FC6, C3, Cz, C4, CP5, CP1, CP2, CP6, P3, Pz, P4, PO3 and PO4, according to the International 10/10 System. The electrodes were chosen around motor and premotor cortex, the area where more information was expected to appear. Moreover, frontal electrodes, which can be influenced by ocular artifacts, were not selected. The signal was recorded and amplified through a gUSBamp (g.Tec, GmbH, Austria) with a sampling rate of 1200 Hz and then band-pass filtered between 0.01 and 200 Hz with a zero-phase high-order Chebyshev

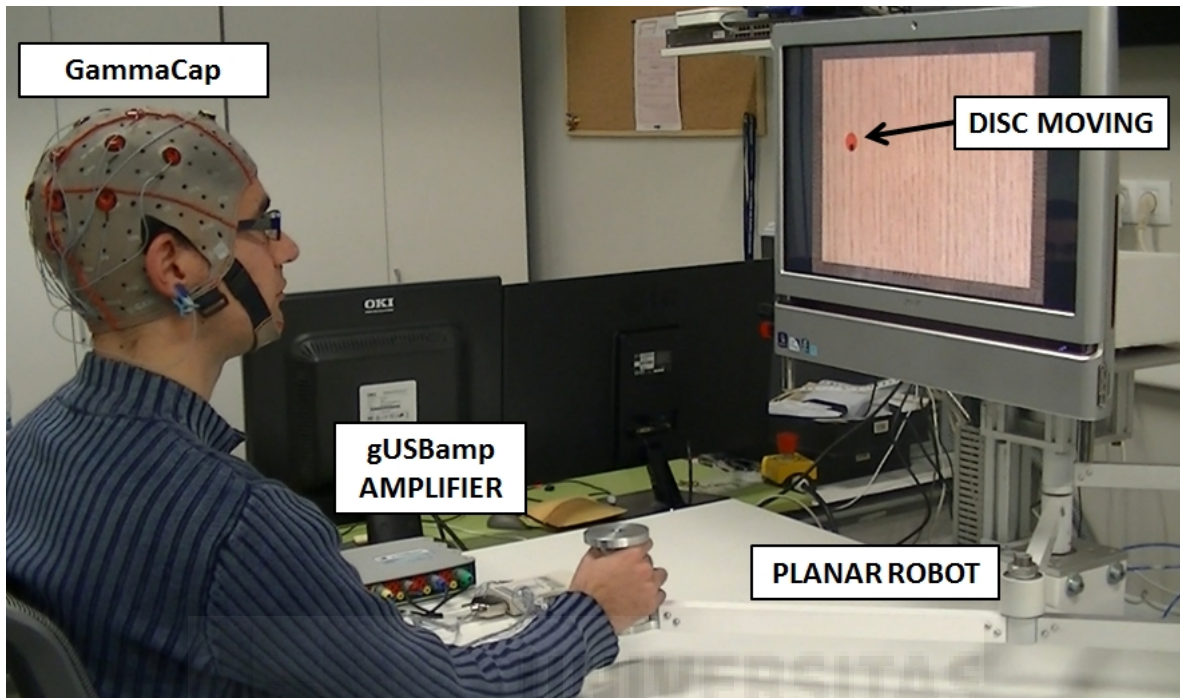


Figure 4.10: Experimental environment showing the subject performing the tracking movements in front a screen. The subject should follow the red circle by controlling a black cursor with the planar robot.

filter. Then, a zero-phase Butterworth low-pass filter was applied to eliminate frequencies higher than 2 Hz. Finally, EEG data from each electrode were standardized as shown in previous sections (Section 4.2.2.1). This standardization was computed for each performed round.

#### 4.3.1.4 Data Decoding Procedure

To decode the position of the upper limb, the same procedures already used in Section 4.2.2.2 have been applied. In this case, only X and Y positions have been decoded. The resulting decoded hand positions have been compared to the original hand positions. To that end, the Pearson correlation coefficient has been obtained for each axis after performing a 5-fold cross validation between all 5 runs for each session. Additionally, shuffled and random data have been used as input to assess if the decoding accuracy

was above chance levels. Shuffled data have been obtained by randomly mixing trials of real data. Random data have been obtained by generating a uniform noise with the same size of real input data. Both shuffled and random data have been filtered and standardized in the same way as the actual experimental data. Random and shuffled data decoding coefficients have been computed 100 times to avoid chance effects due to the stochastic nature of the process.

#### 4.3.1.5 Participant Survey

After and during the rest periods between tests, all volunteers were asked to fill a comprehensive survey of the experiments. Regarding the whole experimental procedure, volunteers were asked about tiredness, comfort, frustration, entertainment and difficulty. They were also asked about particular aspects of the recording system, the planar robot and the graphical interface. Finally, they included their general impressions and suggestions about the tests.

#### 4.3.2 Results

In Figure 4.11, an example of the bidimensional reconstruction of a trajectory is shown (up-left). The gray path represents the original disc trajectory, while the black path shows the one performed by the subject with the planar robot. For the X-axis and the Y-axis (right), the subject is able to follow the original disc trajectory with a small delay. Table 4.1 shows the tracking accuracy measured during the performed trajectory. This percentage represents the amount of time the volunteer is able to stay inside the disc during each round. The average tracking accuracy ( $\mu$ ) for each speed and disc size and the standard deviation ( $SD$ ) is also presented. From Table 4.1 it can be observed a natural decreasing in the tracking accuracy when the speed increases and the disc gets smaller. This relationship is generally similar for all subjects. However, Subject 5 shows a very low tracking accuracy compared to the rest of subjects likely biased by his ability to control the planar robot arm.

Table 4.2 shows the Pearson correlation coefficients obtained for each volunteer after performing the hand position decoding. The results are shown for each speed and disc

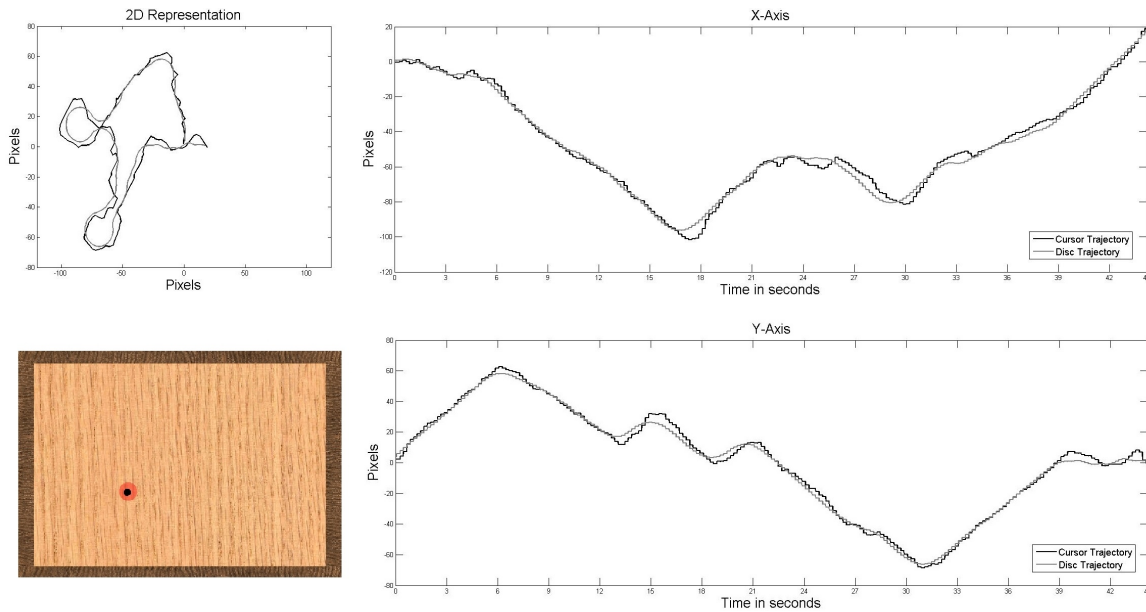


Figure 4.11: Example of the trajectory followed by the subject. 2D Representation of the trajectory (top-left). X and Y axis trajectories (right). Appearance of the visual interface (bottom-left)

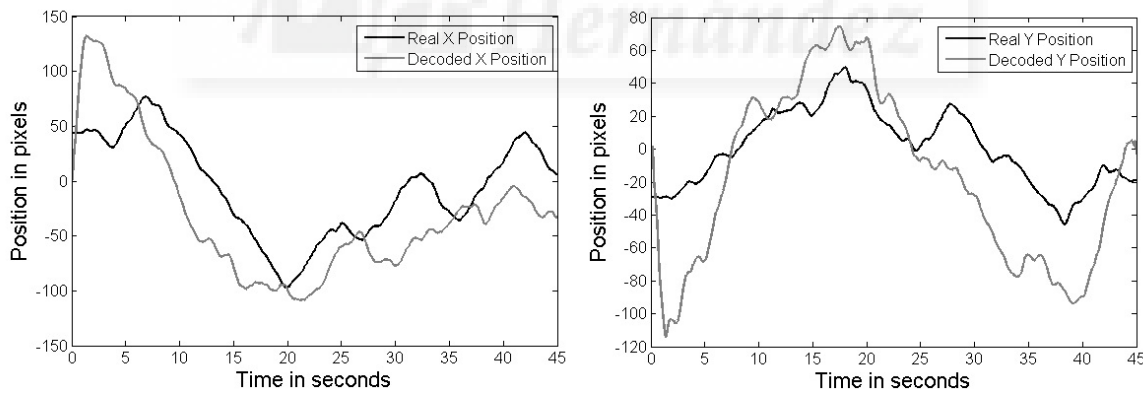


Figure 4.12: Example of a decoded trajectory for subject 4. Horizontal axis (left) and vertical axis (right).

size regarding X-axis and Y-axis. The mean ( $\mu$ ) and standard deviation ( $SD$ ) is also presented for each axis and speed, showing a decrease in the decoding performance for faster trajectories. In Figure 4.12, an example of decoded trajectories is shown. The

decoded X and Y position is shown for Subject 4 with the minimum speed (20 mm/s) and the smallest disc size. Figure 4.13 shows a graphical representation of the averaged Pearson correlation coefficients for the different disc sizes and speeds. It also presents the results for random and shuffled conditions. From these results, it can be observed that there is a significant difference between the two chance conditions (random and shuffled) and the different movement conditions. A negative correlation between speed and decoding performance is also deduced from this analysis.

Figure 4.14 shows the volunteers general perception of the experimental tests. Each category was given a score from 1 (low) to 5 (high). The radial representation of these scores for each volunteer is shown (in grey) as well as the average radial representation (in black). Five general aspects are studied: tiredness, comfort, frustration, entertainment and difficulty. Volunteers found that the tests had a reasonable level of tiredness ( $2.8 \pm 0.4$ ). The evolution of the tests was not very frustrating ( $2.8 \pm 1.3$ ), except from Subject 5 which had serious difficulties when following the disc for the first set of experiments. Also, the tests had an important increasing difficulty ( $3.2 \pm 0.4$ ). There was a general agreement regarding comfort ( $3.0 \pm 0.0$ ) and all the subjects found the experiments quite entertaining ( $3.8 \pm 0.4$ ). The volunteers were also asked about hardware and software issues. Each category was given a score from 1 (low) to 5 (high). The use of the EEG cap showed an average satisfaction of  $3.2 \pm 0.4$ , which was below the average satisfaction obtained from the planar robot and the graphical interface ( $3.8 \pm 0.4$  and  $3.8 \pm 0.4$ , respectively).

After the experimental tests, volunteers were asked about their general opinion. All the volunteers agreed about the suitability of the graphical interface, although they suggested some visual modifications that could be made to improve contrast during the disc and cursor movements. Regarding resting periods between runs and task duration, all volunteers agreed that the time protocol was satisfactory. Finally, after explaining the purpose of the experimental procedure, the general opinion among the volunteers was favorable in terms of usefulness.

Table 4.1: Accuracy percentages (%) for different disc speeds (mm/s) and sizes (diameter in pixels).

SPEED	SIZE	S1	S2	S3	S4	S5	AVG
20	10	99.29	99.56	97.69	99.47	87.38	96.68±5.25
	7.5	96.71	96.89	96.62	97.69	73.29	92.24±10.60
	5	93.24	82.22	84.53	87.29	42.44	77.94±20.27
30	10	96.00	97.87	95.38	94.67	63.24	89.43±14.69
	7.5	90.76	84.71	88.89	88.89	50.27	80.70±17.15
	5	73.78	59.56	70.93	68.98	27.51	60.15±19.01
40	10	28.31	45.64	38.31	37.11	45.91	39.59±6.29
	7.5	22.36	16.18	33.38	25.42	37.47	26.96±8.53
	5	16.00	6.09	15.38	9.38	15.91	12.55±4.55
50	10	28.22	27.11	35.11	31.96	29.73	30.43±3.19
	7.5	21.33	13.29	24.00	15.64	17.64	18.38±4.31
	5	9.60	4.22	12.36	6.13	9.24	8.31±3.18

Table 4.2: Pearson correlation coefficients after decoding hand trajectories performed with the planar robot for different disc speeds (mm/s) and sizes (diameter in pixels).

		<b>S1</b>		<b>S2</b>		<b>S3</b>	
<b>SPEED</b>	<b>SIZE</b>	<b>X-AXIS</b>	<b>Y-AXIS</b>	<b>X-AXIS</b>	<b>Y-AXIS</b>	<b>X-AXIS</b>	<b>Y-AXIS</b>
20	10	0.38	0.37	0.38	0.38	0.13	0.20
	7.5	0.34	0.40	0.22	0.39	0.41	0.22
	5	0.35	0.40	0.44	0.41	0.37	0.37
30	10	0.19	0.20	0.22	0.17	0.19	0.31
	7.5	0.38	0.25	0.30	0.20	0.49	0.29
	5	0.26	0.24	0.32	0.27	0.37	0.13
40	10	0.18	0.19	0.20	0.11	0.13	0.26
	7.5	0.17	0.27	0.15	0.15	0.15	0.20
	5	0.22	0.17	0.08	0.12	0.15	0.18
50	10	0.16	0.10	0.21	0.14	0.14	0.12
	7.5	0.15	0.11	0.21	0.18	0.17	0.16
	5	0.12	0.10	0.06	0.16	0.10	0.10

		<b>S4</b>		<b>S5</b>		<b>MEAN±STD</b>	
<b>SPEED</b>	<b>SIZE</b>	<b>X-AXIS</b>	<b>Y-AXIS</b>	<b>X-AXIS</b>	<b>Y-AXIS</b>	<b>X-AXIS</b>	<b>Y-AXIS</b>
20	10	0.29	0.29	0.30	0.14	0.30±0.10	0.27±0.10
	7.5	0.26	0.45	0.13	0.25	0.27±0.11	0.34±0.10
	5	0.34	0.54	0.25	0.23	0.35±0.07	0.39±0.11
30	10	0.36	0.29	0.22	0.14	0.24±0.07	0.22±0.08
	7.5	0.28	0.35	0.23	0.19	0.34±0.10	0.25±0.07
	5	0.43	0.29	0.27	0.26	0.33±0.07	0.24±0.06
40	10	0.16	0.09	0.10	0.10	0.15±0.04	0.15±0.07
	7.5	0.29	0.19	0.12	0.16	0.18±0.07	0.19±0.05
	5	0.14	0.19	0.16	0.22	0.15±0.05	0.17±0.03
50	10	0.23	0.17	0.26	0.25	0.20±0.05	0.16±0.06
	7.5	0.23	0.15	0.20	0.29	0.20±0.03	0.18±0.07
	5	0.26	0.28	0.14	0.22	0.13±0.08	0.17±0.08

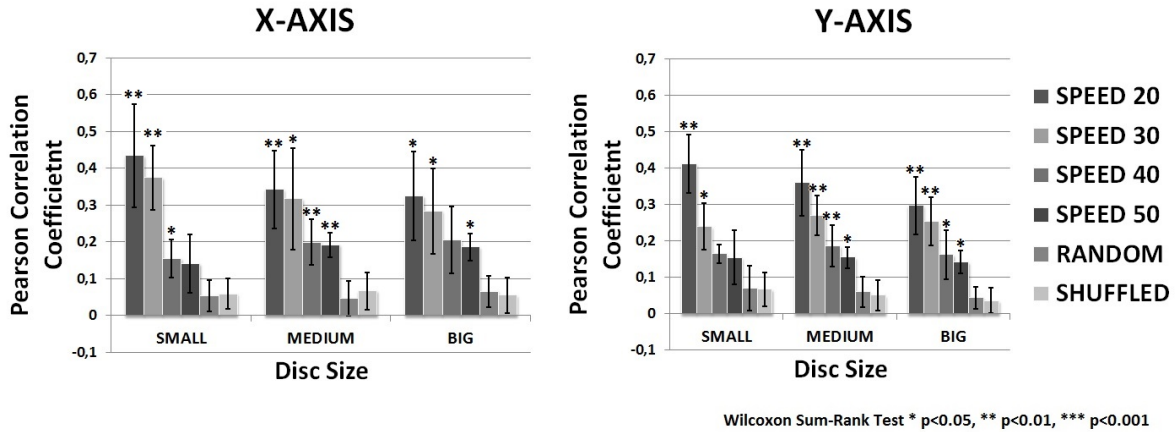


Figure 4.13: Decoding performance regarding speed (mm/s) and disc size (small, medium, big). The stars represent significant differences with respect to random and shuffled conditions.

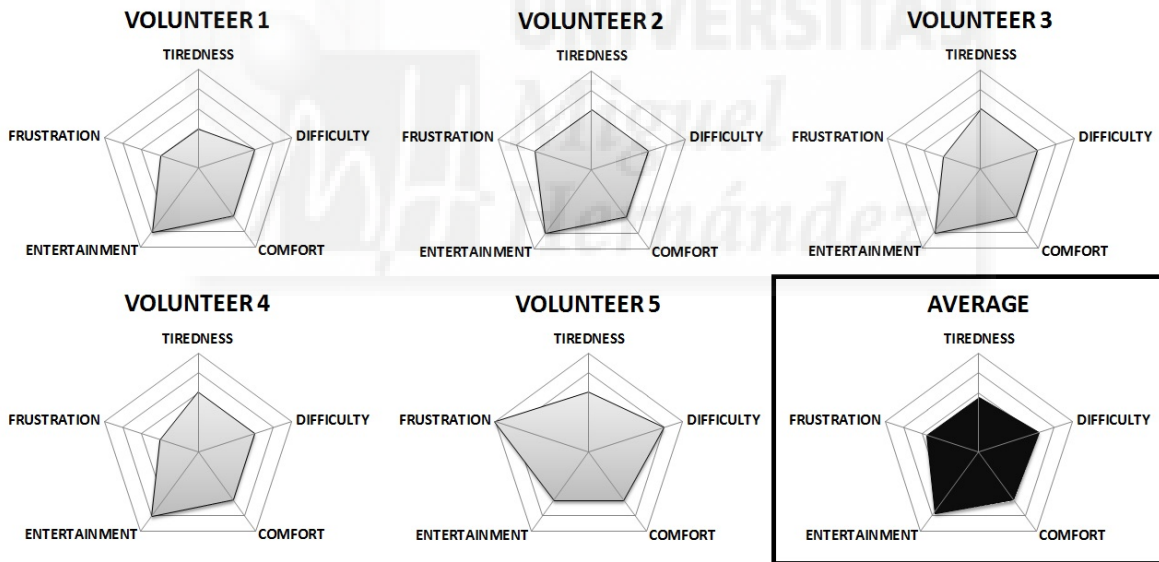


Figure 4.14: Radial representation of the volunteers general impressions. In black, average impression of the experimental tests.

### 4.3.3 Discussion

The significance of the decoding performances has been analyzed from the results presented in Figure 4.13. To that end, random and shuffled conditions have been compared

to the average decoding coefficients obtained for different disc sizes. This analysis has shown that decoding performance of slower speeds (20 and 30 mm/s) is always significantly above chance ( $p < 0.05$ , Wilcoxon Sum-Rank Test) for both axes and for all disc sizes. In the case of faster trajectories (40 and 50 mm/s), this occurs for several of the experimental conditions mainly when the speed is 40 mm/s. For the remaining conditions, decoding performance was not significantly above chance, which suggests that the stability of the decoding performance over the folds during the cross-validation process is not sufficient to obtain significant results. Nevertheless, a consequence of this non-significance may be the small number of samples introduced in the statistical analysis so further research should be undertaken to assess the effects of performing a larger set of trajectories to validate this significance.

The presence of significant decoding correlations in most of the experimental conditions differs from what is claimed in [124], where decoding performance of upper-limb movements was not above chance, and suggest that kinematic parameters of hand movement can be inferred from neural information through linear regression models. Nonetheless, the improvements obtained when reducing movement speed may be caused by the inherent properties of the correlation metric [124]. According to the results, movement speed has an influence over the decoding performance. In fact, higher speeds cause a decrease in the decoding correlation coefficients for both axis. This significant relationship between both variables (movement speed and tracking accuracy) was found after performing a two-way ANOVA analysis ( $p < 0.05$ ) using the decoding correlation as the dependant variable.

It is also relevant how decoding accuracy and tracking accuracy are strongly related. In fact, the average Pearson correlation coefficient obtained between tracking success rates and the corresponding decoding rates for all volunteers is quite high (0.83 for S1, 0.77 for S2, 0.72 for S3, 0.74 for S4 and 0,78 for S5), which means that a better tracking of the disc while performing the movements with the robot arm is translated, generally, into a better decoding performance. From these analysis, we conclude that the stability of movement may explain the good correlation between tracking accuracy and decoding performance. This is consistent with the results obtained in [77, 123], where continuous and linear movements obtained a better decoding performance.

The participant survey performed during and after the experimental tests has helped to evaluate human factors during the execution of hand movements with the planar robot arm. The results presented in Figure 4.14 have shown a general agreement in terms of usability and satisfaction. This results, however, may be biased by the previous experience of all participants with this kind of interfaces. Moreover, the fact that disc speed and size are not randomized over the different runs may influence decoding performance due to tiredness or familiarization with the task. Further experimental research should focus in enlarging the number of subjects with naive participants and randomizing speed and size conditions to obtain a better evaluation of the decoding performance.

#### 4.3.4 Conclusions

In this section, we reported the influence of speed, trajectory and movement variability in hand kinematics decoding by performing bidimensional trajectories with a planar robot arm. To that end, five healthy volunteers were asked to follow a disc, which moved aleatory on the screen with a constant speed, by controlling a cursor with the planar robot. The results obtained show better decoding accuracies when performing steady and regular movements. The study has gone some way towards enhancing our understanding of the neural mechanisms during upper limb movement and it serves as a first step to apply this kinematics decoding technique to control assistive robotics in a more natural way, as well as opening new possibilities in rehabilitation procedures with exoskeletons.

In future works, real time testing is needed to show if this decoding is feasible in upper limb decoding applications. Also, brain signals variability of final patients, particularly people suffering from stroke, should be studied to prove the viability of this method in rehabilitation procedures. This research will serve as a base for future studies regarding upper limb kinematics decoding where further research to eliminate artifact influence and improve accuracy should be undertaken.

## 4.4 Real-Time Decoding of Arm Movements from EEG Signals

In this section, a discrete decoding of horizontal arm movements has been performed. In the experiments, subjects are asked to reach two targets on a screen by moving the computer mouse. First, the decoding models are obtained from fast training runs where both mouse trajectories and EEG signals are recorded. Then, these models are applied to decode the mouse cursor trajectories and, afterwards, the direction of movement is classified and compared to the actual performed trajectories. The results obtained have led to the submission of a conference paper [14].

### 4.4.1 Materials and Methods

The system architecture is shown in Figure 4.15. Subjects perform mouse movements to control a cursor on the screen. First, EEG signals are registered and preprocessed. Afterwards, the cursor kinematics are decoded and the direction of movement is classified and displayed on the screen which acts as visual feedback.

#### 4.4.1.1 Experimental Procedure

Five healthy subjects (all male and right-handed) with ages between 23 and 31 years old ( $26.8 \pm 3.3$ ) performed the experiments. The experimental tests were performed in front of a computer screen as shown in Figure 4.16. Subjects were asked to perform one training run and then five online runs of the decoding protocol. During the training, subjects control the cursor movement using a computer mouse. The goal is to reach the target that is randomly highlighted on the screen. The subject must reach it and then return to the central position. Each time a target is reached or the cursor enters the central position, a waiting period of 400 ms is introduced. Subjects perform 10 movements and both cursor position and EEG signals are recorded simultaneously. The same protocol is followed during the five online runs, but in this case subjects perform 40 movements and each time a target is reached, a message with the classification is shown (LEFT or RIGHT).

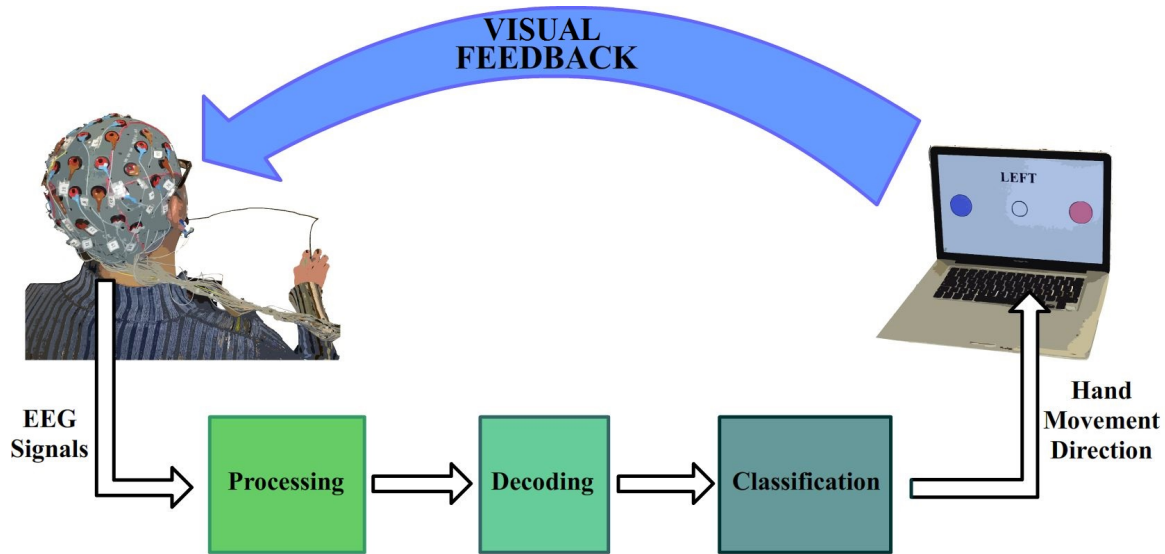


Figure 4.15: System architecture to decode horizontal hand movements. EEG Signals are registered and processed. Afterwards, from the decoded trajectories the movement direction is classified.

#### 4.4.1.2 Register and Preprocessing

EEG signals were registered with the gUSBamp amplifier of g.Tec using a gGammaCap of 16 electrodes with a distribution chosen according to the International 10/10 System: Fz, FC5, FC1, FCz, FC2, FC6, C3, Cz, C4, CP5, CP1, CP2, CP6, P3, Pz and P4. EEG signals were manually analyzed to reject blinks, and frontal channels were discarded to diminish ocular artifacts. Both EEG signals and cursor kinematics were low-pass filtered with a 2th-order Butterworth filter below 2 Hz. Finally, EEG data from each electrode were standardized as shown in previous sections (Section 4.2.2.1). This standardization was computed for all the data session for the training run and in windows of 1 second during the online runs.

#### 4.4.1.3 Decoding Method and Classification of Targets

A multidimensional linear regression has been applied to decode kinematics from EEG signals according to the method described in Section 4.2.2.2. To classify the direction of movement in real time, the decoding method is applied on the training run to obtain

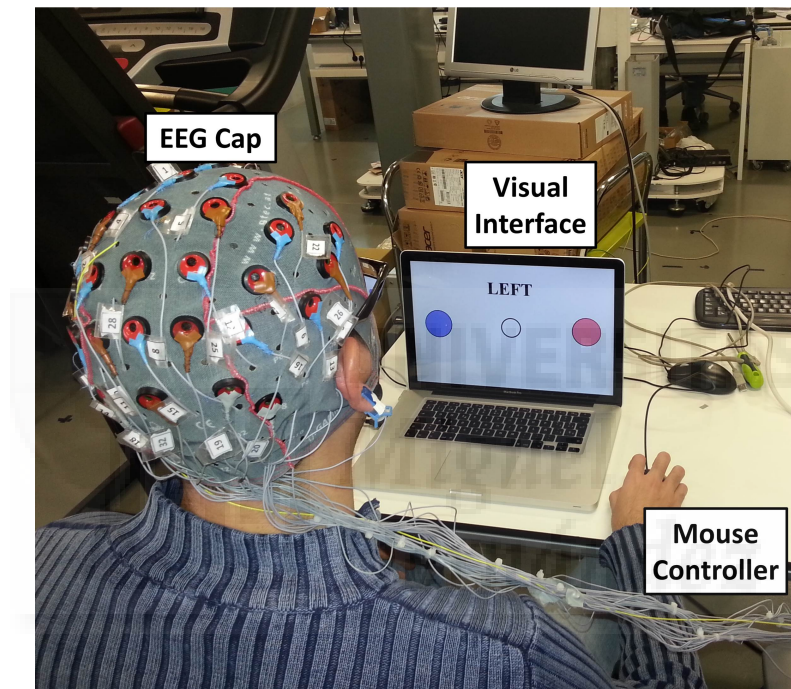


Figure 4.16: Experimental environment where the subject performs horizontal trajectories with the computer mouse. In the computer screen two targets are randomly highlighted and the subject must reach them by moving the computer mouse. The online classification is indicated on the top of the screen (LEFT or RIGHT message).

the transformation matrices  $A$  and  $R$  that will act as the decoding model. This model is applied in real time during the performance of the online runs. To that end, 1 second windows of EEG data are analyzed every time a target is reached and the decoded trajectory is obtained. Afterwards, the angle (or momentum) of this trajectory is computed and left or right direction is assigned depending on the decoded angle.

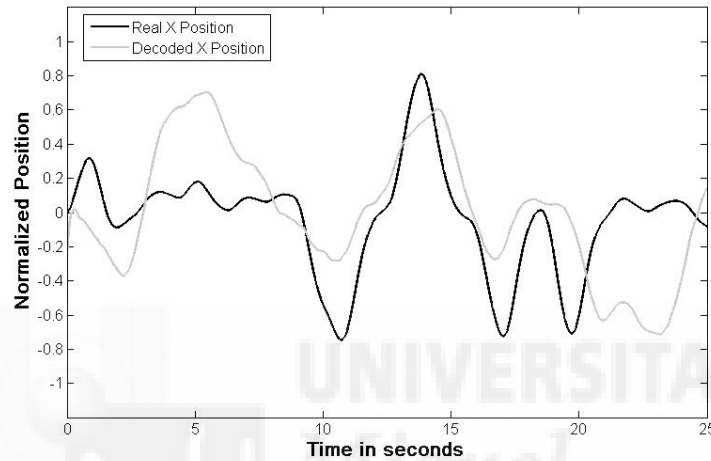


Figure 4.17: Example of the decoded X position during horizontal hand movements.

Additionally, random data was used to compute the significance of our findings. To that end, decoding models have been obtained with a random uniform noise and then applied to the online runs by performing 400 horizontal movements. In this case, the input data were always a random uniform noise.

#### 4.4.2 Results and Discussion

Figure 4.17 shows an example of the decoded X position of the mouse cursor compared to the actual trajectory. From this graph, it is apparent that the decoded signal follows the original one but it may not be accurate enough to obtain a proper real time control of the cursor. For this reason, the methodology proposed in this section tries to increase the reliability of the decoding by reducing the number of classified outputs to only two.

Table 4.3 shows the success rate (%) obtained for the classification of 2 targets. Subjects 2 ( $71.5 \pm 12.1$ ) and 5 ( $80.0 \pm 10.6$ ) obtain the best results. For Subject 4, the success

Table 4.3: Success rate (%) obtained for the classification of two targets.

RUN	S1	S2	S3	S4	S5
1	55.0	87.5	47.5	62.5	70.0
2	52.5	80.0	62.5	60.0	65.0
3	62.5	57.5	52.5	70.0	87.5
4	55.0	75.0	52.5	60.0	85.0
5	40.0	57.5	62.5	60.0	92.5
AVG	<b>53.0±7.3</b>	<b>71.5±12.1</b>	<b>55.5±6.0</b>	<b>62.5±3.9</b>	<b>80.0±10.6</b>

rate decreases ( $62.5 \pm 3.9$ ). The remaining subjects obtained success rates slightly above a 50% ( $53.0 \pm 7.3$  for Subject 1 and  $55.5 \pm 6.0$  for Subject 3). These findings have been compared to chance levels as reported in Figure 4.18. The success rates obtained for Subjects 1 and 3, although above the averaged chance level, are not significant. On the other hand, for the rest of the subjects, we found significant correlations during the online experiments which suggest interesting applications of this decoding technique.

In view of these results, some improvements can be applied to obtain accurate classification rates for all the subjects. The introduction of an uncertainty threshold could increase the success rate. In this case, the system would become slower but much more reliable which is a key aspect in rehabilitation robotics. Also, the decoding parameters  $L$  and  $N$  could be particularized for different subjects to obtain higher decoding correlations.

### 4.4.3 Conclusions

In this section, we have presented a methodology to decode horizontal hand movements from low frequency EEG components. To that end, multidimensional linear regression models have been applied to obtain the decoded trajectories of the computer mouse and then, the direction of the movement is classified according to the angle or momentum of the trajectory. The results for the classification of two directions are significantly higher than chance levels for most of the subjects which implies that this online classification

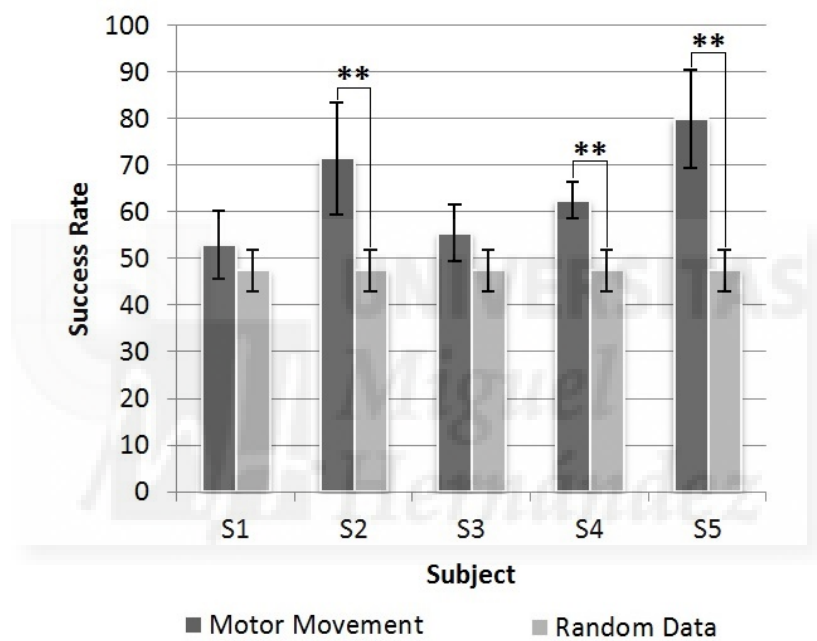


Figure 4.18: Average classification rates for each subject compared to chance level rates. Wilcoxon Sum-Rank Test ( $*p < 0.05$ ,  $**p < 0.01$ ,  $***p < 0.001$ ).

could be applied in future rehabilitation procedures with an upper limb exoskeleton.

Moreover, the reliability of the system can be improved by introducing some modifications in the methodology such as uncertainty thresholds to improve the robustness of classification and an in-depth analysis of the decoding parameters. In future works, the extension of this methodology to a larger number of directions should improve the possibilities of application to more complex rehabilitation procedures. Also, other assistive applications that require the classification of discrete states could be benefited from the proposed methods.

## 4.5 Conclusions

In this chapter, the decoding of upper limb movements from low frequency EEG components has been studied. First, the decoding performance of center-out reaching tasks has been analyzed to assess the real possibilities of using linear regression methods to decode upper limb kinematics from EEG signals. The results show that low frequency bands (0.1-2 Hz) concentrate most of the information extracted from upper limb kinematics decoding, confirming the properties of linear regression. Additionally, our current findings indicate that decoding accuracies obtained from real center-out movements are significantly above chance levels and do not depend on muscle artifacts produced during the reaching movements. Motor imagery, shuffled and random conditions show that individual correlation values are high but not above chance (likely due to the properties of the correlation metric). Although active arm movements are significantly above motor imagery center-out trajectories, the presence of significant information in horizontal imagined movement opens an encouraging possibility of improving this decoding accuracy in future reoriented experiments. These results are, however, subject to an important limitation, as a direct two-dimensional control appears to be difficult to achieve with acceptable accuracy levels using continuous decoding methods. For this reason, in this chapter we have proposed a simplification of the method by computing a discrete classification of reached targets. The results have shown high success rates for different target configurations, presenting a clear coherence with the previously obtained decoding accuracies. By reducing the dimensionality of the classification out-

put, this discrete approach presents promising advantages in future neurorehabilitation procedures, where it could be applied to classify arm movement onset and direction.

In a second section, the influence of speed, trajectory and movement variability in hand kinematics decoding has been reported by performing bidimensional trajectories with a planar robot arm. To that end, five healthy volunteers were asked to follow a disc, which moved aleatory on the screen with a constant speed, by controlling a cursor with the planar robot. The results obtained show better decoding accuracies when performing steady and regular movements. The study has gone some way towards enhancing our understanding of the neural mechanisms during upper limb movement and it serves as a first step to apply this kinematics decoding technique to control assistive robotics in a more natural way, as well as opening new possibilities in rehabilitation procedures with exoskeletons.

Finally, the decoding methodology has been used to decode horizontal hand movements in real-time. To that end, multidimensional linear regression models have been applied to obtain the decoded trajectories of the computer mouse and then, the direction of the movement has been classified according to the angle or momentum of the trajectory. The results for the classification of two directions are significantly higher than chance levels for most of the subjects which implies that this real-time classification could be applied in future rehabilitation procedures with an upper limb exoskeleton. The success rate obtained in the real-time classification of horizontal movement directions using decoding techniques is, up to a certain point, below the results obtained from classical motor imagery classification such as the EEG mapping methodology proposed in Chapter 3. Nevertheless, motor imagery techniques may be less suitable for rehabilitation purposes as they do not take into account human ergonomic factors resulting in a less intuitive and more unnatural control of external devices, such as a prosthetic arm.



## CONCLUSIONS AND FUTURE WORK

### 5.1 Conclusions

This thesis has led to several contributions in the field of Brain-Machine Interfaces. It also provides tools in order to assess the suitability and benefits of applying these methodologies in rehabilitation and assistive applications with motor disabled subjects. This thesis has also gone some way towards enhancing our understanding of neural-motor correlations and provides new knowledge for future research.

This thesis presents **a novel classification method of mental tasks based on the correlation of EEG maps**. This classifier has been successfully tested in non-invasive spontaneous Brain-Machine Interfaces. These studies have provided the following contributions:

- A novel classification method for spontaneous motor imagery BMIs based on a normalized cross-correlation of EEG maps has been presented. An optimization protocol has been applied to adjust the parameters of the classifier for each subject. This protocol takes into account not only the final accuracy of the classifier but also the speed of the classification. To that end, the time interval of processing has been reduced and an uncertainty threshold has been introduced showing an important improvement of the success rates. The suitability of three different methods to obtain this threshold has been discussed and the results suggest that each method may be suitable depending on the final application in terms

of speed and reliability. The final success rates improve the results of previous classifiers and encourage us to introduce new improvements in this kind of classification. The findings of this study suggest that this EEG mapping method may be suitable for classification of more than three mental tasks as the image models obtained for each task show big differences between them.

- A non-invasive BMI based on the correlation of EEG maps has been tested to perform applications in real-time. To that end, a visual computer application to perform trajectories has been designed. Two targets are shown on a grid and the volunteers are asked to reach the targets by performing tasks related to motor imagery (in this case, the imagination of the movement of the left and right arm). The classifier has been improved from previous works by introducing two uncertainty conditions. Four able-bodied volunteers tested the application. The accuracy and score obtained prove that this BMI is ready to be used in more complex applications for people with a severe motor disability that could help them in their daily life.
- The EEG Mapping classifier has been applied to a real world scenario. Two control strategies to move a planar robot with a Brain-Machine Interface based on the correlation of EEG maps have been tested by performing 2D movements to reach several goals. The first strategy consists on a hierarchical control where the subject can choose both the axis and direction of the movement. With the second strategy, the subject is able to continuously control the direction of the movement to approach the goals. The results obtained show that the hierarchical control strategy is more reliable but slower than the directional one, which is less precise but more comfortable for the subject. Moreover, the volunteer is able to reach the goals with both strategies which suggests that this system could successfully work in more complex applications.

In addition, this thesis gives **additional evidence** with respect to the **decoding of upper limb kinematics in humans from low frequency EEG components**. These studies have provided the following contributions:

- This thesis assesses the real possibilities of using linear regression methods to decode upper limb kinematics from EEG signals. Low frequency bands (0.1-2 Hz) concentrate most of the information extracted from upper limb kinematics decoding, confirming the properties of linear regression. Additionally, our current findings indicate that decoding accuracies obtained from real center-out movements are significantly above chance levels and do not depend on muscle artifacts produced during the reaching movements. Motor imagery, shuffled and random conditions show that individual correlation values are high but not above chance (likely due to the properties of the correlation metric). Although active arm movements are significantly above motor imagery center-out trajectories, the presence of significant information in horizontal imagined movement opens an encouraging possibility of improving this decoding accuracy in future reoriented experiments. These results are, however, subject to an important limitation, as a direct two-dimensional control appears to be difficult to achieve with acceptable accuracy levels using continuous decoding methods. For this reason, in this work we have proposed a simplification of the method by computing a discrete classification of reached targets. The results have shown high success offline rates for different target configurations, presenting a clear coherence with the previously obtained decoding accuracies. By reducing the dimensionality of the classification output, this discrete approach presents promising advantages in future neurorehabilitation procedures, where it could be applied to classify arm movement onset and direction.
- The influence of speed, trajectory and movement variability in arm kinematics decoding has been reported by performing bidimensional trajectories with a planar robot arm. To that end, five healthy volunteers were asked to follow a disc, which moved aleatory on the computer screen with a constant speed, by controlling a cursor with the planar robot. The results obtained show better decoding accuracies when performing steady and regular movements. The study has gone some way towards enhancing our understanding of the neural mechanisms during upper limb movement and it serves as a first step to apply this kinematics decoding technique to control assistive robotics in a more natural way, as well as

opening new possibilities in rehabilitation procedures with exoskeletons.

- A methodology to decode horizontal hand movements in real-time from low frequency EEG components has been presented. To that end, multidimensional linear regression models have been applied to obtain the decoded trajectories of the computer mouse and then, the direction of the movement is classified according to the angle or momentum of the trajectory. The results for the classification of two directions are significantly higher than chance levels for most of the subjects which implies that this real-time classification could be applied in future rehabilitation procedures with an upper limb exoskeleton.

## 5.2 Future Works

The results obtained in this thesis encourage us to undertake more ambitious goals. In future works, more realistic environments can be designed to perform grasping tasks of daily objects by applying EEG mapping classification to the control of a robot arm. The EEG mapping classifier will be enhanced by studying different mental tasks and different electrodes positioning to adapt it to a greater range of users. The control strategies will be also improved to reduce positioning error, when necessary, and time taken to perform the movements of the end effector.

Regarding decoding procedures, brain signals variability of final patients, particularly people suffering from stroke, should be studied to prove the viability of this method in rehabilitation procedures. This research will serve as a base for future studies regarding upper limb kinematics decoding where further research to eliminate artifact influence and improve accuracy should be undertaken. Also, other decoding models, such as non-linear and adaptive approaches, may be applied to reduce, or even eliminate, the influence of the related arm movements. Moreover, the reliability of the discrete decoding can be improved by introducing some modifications in the methodology such as uncertainty thresholds to improve the robustness of classification and an in-depth analysis of the decoding parameters. In future works, the extension of this methodology to a larger number of directions should improve the possibilities of application to more complex rehabilitation procedures. Also, other assistive applications

that require the classification of discrete states could be benefited from the proposed methods.





## CONCLUSIONES Y TRABAJOS FUTUROS

### 6.1 Conclusiones

Esta tesis ha conducido a varias contribuciones en el campo de las Interfaces Cerebro-Máquina. También proporciona herramientas para evaluar la idoneidad y los beneficios de aplicar estas metodologías en aplicaciones asistivas y de rehabilitación en sujetos con discapacidad motora. Esta tesis ha supuesto además una mejora en el conocimiento actual de las correlaciones neuro-motoras y proporciona nuevos hallazgos para investigaciones futuras.

La tesis presenta **un nuevo método de clasificación de tareas mentales basado en la correlación de mapas EEG**. Este clasificador se ha probado con éxito en Interfaces Cerebro-Máquina no invasivas. Estos estudios han proporcionado las siguientes contribuciones:

- Se ha presentado un nuevo método de clasificación de tareas motoras para BMIs espontáneas basado en la correlación cruzada normalizada de mapas EEG. Se ha aplicado un protocolo de optimización para ajustar los parámetros del clasificador para cada sujeto. Este protocolo tiene en cuenta tanto la precisión final del clasificador como la velocidad de clasificación. Para ello, el intervalo de tiempo procesado se ha reducido y se ha introducido un umbral de incertidumbre que muestra una mejora importante en la tasa de acierto. Se ha discutido la idoneidad de tres métodos distintos utilizados para obtener este umbral y los resultados

sugieren que cada método puede ser adecuado dependiendo de la aplicación final en términos de velocidad y fiabilidad. Las tasas de acierto finales mejoran los resultados de clasificadores previos y nos animan a introducir nuevas mejoras en este tipo de clasificación. Los hallazgos de este estudio sugieren que el método de mapping EEG puede ser adecuado para la clasificación de más de tres tareas mentales puesto que los modelos obtenidos para cada tarea muestran grandes diferencias entre ellos.

- Se ha utilizado un sistema BMI no invasivo basado en la correlación de mapas EEG en aplicaciones en tiempo real. Para ello, se ha diseñado una aplicación visual de ordenador para la realización de trayectorias. En esta aplicación se muestran dos objetivos en la pantalla que los voluntarios deben alcanzar mediante la realización de tareas mentales relacionadas con la imaginación motora (en este caso, la imaginación del movimiento del brazo izquierdo y derecho). El clasificador se ha mejorado respecto a trabajos previos mediante la introducción de dos condiciones de incertidumbre. Cuatro usuarios sanos han probado la aplicación. La precisión y la puntuación obtenida demuestran que este BMI está listo para ser usado en aplicaciones más complejas que permitan ayudar a personas con una discapacidad motora severa en su vida diaria.
- Se ha aplicado el clasificador basado en mapas EEG a un escenario real. Se han probado dos estrategias de control para mover un robot planar mediante una Interfaz Cerebro-Máquina basada en la correlación de mapas EEG. Para ello, se han realizado movimientos 2D para alcanzar diversos objetivos. La primera estrategia consiste en un control jerárquico donde el sujeto puede elegir la dirección y el sentido del movimiento. Con la segunda estrategia, el sujeto es capaz de controlar de forma continua la dirección del movimiento para aproximarse a los objetivos. Los resultados obtenidos muestran que la estrategia de control jerárquico es más fiable pero más lenta mientras que la direccional, aunque menos precisa, es más confortable para el sujeto. Además, el voluntario ha sido capaz de alcanzar todos los objetivos con ambas estrategias lo que sugiere que el sistema puede funcionar en aplicaciones más complejas.

Adicionalmente, esta tesis proporciona **evidencias adicionales** respecto a la **decodificación de la cinemática del miembro superior en humanos a partir de componentes EEG de baja frecuencia**. Estos estudios han proporcionado las siguientes contribuciones:

- Esta tesis evalúa las posibilidades reales de usar métodos de regresión lineal para decodificar la cinemática del miembro superior a partir de señales EEG. Las bandas de baja frecuencia (0.1-2 Hz) concentran la mayoría de la información extraída de la decodificación de la cinemática del miembro superior, confirmando las propiedades de la regresión lineal. Adicionalmente, nuestros hallazgos indican que la precisión de la decodificación obtenida a partir de movimientos reales center-out es significativamente superior a niveles aleatorios y no se ve influida por artefactos musculares producidos durante los movimientos de alcance de objetivos. Las condiciones con datos reales de imaginación motora, datos aleatorios y datos mezclados muestran que los valores individuales de correlación son altos pero no superiores a la aleatoriedad (probablemente debido a las propiedades de la métrica de correlación). A pesar de que los movimientos activos del brazo son significativamente superiores a las trayectorias center-out con imaginación motora, la presencia de información significativa en los movimientos horizontales imaginados abre una posibilidad muy interesante de mejorar esta precisión de decodificación en experimentos futuros reorientados en este sentido. Estos resultados están, sin embargo, sujetos a una importante limitación, puesto que un control bidimensional directo parece difícil de lograr con niveles de precisión aceptables usando métodos de decodificación continua. Por esta razón, en este trabajo se ha propuesto la simplificación del método mediante la obtención de una clasificación discreta de los objetivos alcanzados. Los resultados muestran altas tasas de acierto offline para diferentes configuraciones de objetivos, presentando una clara coherencia con las precisiones de decodificación obtenidas previamente. Mediante la reducción de la dimensionalidad de las salidas clasificadas, esta aproximación discreta presenta ventajas prometedoras en procedimientos de rehabilitación futuros donde podría ser aplicada para clasificar el inicio y la dirección del movimiento del brazo.

- La influencia de la velocidad, la trayectoria y la variabilidad de movimiento en la decodificación de la cinemática del brazo se ha estudiado mediante la realización de trayectorias bidimensionales con un robot planar. Para ello, se solicitó que cinco voluntarios sanos siguieran un disco, que se movía aleatoriamente en la pantalla de un ordenador a una velocidad constante, mediante el control de un cursor con el robot planar. Los resultados obtenidos muestran una mejor precisión de decodificación cuando se realizan movimientos estables y regulares. Este estudio ha avanzado en la comprensión de los mecanimos neurales durante el movimiento del miembro superior y sirve como un primer paso para aplicar esta técnica de decodificación para controlar robótica asistiva de una manera más natural. Además, abre nuevas posibilidades en los procedimientos de rehabilitación con exoesqueletos.
- Se ha presentado una metodología para decodificar movimientos horizontales de la mano en tiempo real a partir de componentes EEG de baja frecuencia. Para ello, se han aplicado modelos de regresión lineal multidimensional para obtener las trayectorias decodificadas del ratón del ordenador y posteriormente, la dirección del movimiento se ha clasificado de acuerdo al ángulo o momento de la trayectoria. Los resultados de esta clasificación de dos direcciones son significativamente superiores a los niveles de aleatoriedad para la mayoría de los sujetos lo que implica que esta clasificación en tiempo real puede ser aplicada en futuros procedimientos de rehabilitación con exoesquelétos de miembro superior.

## 6.2 Trabajos Futuros

Los resultados obtenidos en esta tesis nos animan a emprender objetivos más ambiciosos. En trabajos futuros, se pueden diseñar entornos más realistas para realizar tareas de agarre de objetos cotidianos mediante la aplicación del clasificador basado en mapas EEG en el control de un brazo robot. El clasificador será mejorado mediante el estudio de diferentes tareas mentales y diferentes configuraciones de electrodos para adaptarlo a un mayor rango de usuarios. Las estrategias de control también serán mejoradas para reducir el error de posicionamiento, cuando sea necesario, y el tiempo empleado

en realizar los movimientos del efector final.

Respecto a los procedimientos de decodificación, la variabilidad de las señales cerebrales de los pacientes finales, en concreto aquellos que han sufrido un ictus, debe ser estudiada para probar la viabilidad de este método en procedimientos de rehabilitación. Esta investigación servirá como base de estudios futuros en relación a la decodificación de la cinemática del miembro superior, donde una investigación más profunda debe ser llevada a cabo para eliminar la influencia de los artefactos y mejorar la fiabilidad. Además, otros modelos de decodificación, como los no lineales y los adaptativos, pueden ser aplicados para reducir, o incluso eliminar, la influencia de los movimientos relativos del brazo. También, la fiabilidad de la decodificación discreta puede ser mejorada mediante la introducción de una serie de modificaciones en la metodología, como el uso de umbrales de incertidumbre para robustecer la clasificación o un análisis en detalle de los parámetros de decodificación. En trabajos futuros, la ampliación de esta metodología a un mayor número de direcciones debería mejorar las posibilidades de aplicación a procedimientos de rehabilitación más complejos. Además, otras aplicaciones asistivas que requieren la clasificación de estados discretos pueden beneficiarse de los métodos propuestos.



## BIBLIOGRAPHY

- [1] VI Framework Programme of Research and Development (2002-2006), Available: [http://ec.europa.eu/research/fp6/index\\_en.cfm](http://ec.europa.eu/research/fp6/index_en.cfm), last visit: 15 May 2014.
- [2] Las personas con discapacidad en España: Informe Olivenza 2010, *Observatorio Estatal de Discapacidad*, 2010.
- [3] Cardiovascular diseases: Key facts, Available: <http://www.who.int/mediacentre/factsheets/fs317/en/>, World Health Organization, last visit: 10 May 2014.
- [4] Encuesta sobre Discapacidades, Autonomía personal y situaciones de Dependencia (EDAD 2008), *Instituto Nacional de Estadística*, 2008.
- [5] Science Direct: Search for Journals, Available: <http://www.sciencedirect.com>, last visit: 6 May 2014.
- [6] A. Úbeda, E. Iáñez, J. M. Azorín and E. Fernández, “Analysis of EEG mapping images to differentiate mental tasks in brain-computer interfaces,” *International Work-conference on the Interplay between Natural and Artificial Computation (IWINAC)*, vol. 6686, pp. 246-255, 2011.
- [7] A. Úbeda, E. Iáñez and J. M. Azorín, “Mental tasks classification for BCI using image correlation,” *International IEEE EMBS Conference*, pp. 6303-6306, 2011.

- [8] A. Úbeda, E. Iáñez, J. M. Azorín, J. M. Sabater and E. Fernández, “Classification method for BCIs based on the correlation of EEG maps,” *Neurocomputing*, vol. 114, pp. 98-106, 2013.
- [9] A. Úbeda, E. Iáñez, J. M. Azorín and C. Perez-Vidal, “Endogenous brain-machine interface based on the correlation of EEG maps,” *Computer Methods and Programs in Biomedicine*, vol. 112(2), pp. 302-308, 2013.
- [10] A. Úbeda, J. M. Azorín, N. García, J. M. Sabater and C. Perez-Vidal, “Brain-machine interface based on EEG mapping to control an assistive robotic arm,” *IEEE RAS/EMBS International Conference on Biomedical Robotics and Biomechatronics (BioRob)*, pp. 1311-1315, 2012.
- [11] A. Úbeda, E. Iáñez, J. Badesa, R. Morales, J. M. Azorín and N. García, “Control strategies of an assistive robot using a brain-machine interface,” *IEEE/RSJ International Conference on Intelligent Robots and Systems (IROS)*, pp. 3553-3558, 2012.
- [12] A. Úbeda, J. M. Azorín, R. Chavarriaga and J. d. R. Millán, “Continuous and discrete decoding of the upper limb movements in center-out reaching tasks,” (Submitted to *Journal of Neural Engineering*)
- [13] A. Úbeda, E. Hortal, E. Iáñez and J. M. Azorín, “Assessing Movement Factors in Upper Limb Kinematics Decoding from EEG Signals,” (Submitted to *PLOS One*)
- [14] A. Úbeda, E. Hortal, A. Costa, D. Planelles, A. Rodríguez and J. M. Azorín, “Online detection of horizontal hand movements from low frequency EEG components,” (Under preparation)
- [15] C. S. Chung and L. R. Caplan, “Stroke and other neurovascular disorders,” *Textbook of Clinical Neurology 3rd Edition*, Elsevier, chap. 45, 2007.
- [16] A.D.A.M. Medical Encyclopedia, “Diseases and conditions,” 2013.
- [17] Stroke Recovery, Available: <http://www.strokeeducation.info/topics/recovery.htm>, Stroke Education: The Stroke Network, last visit: 25 May 2014.

- [18] P. W. Duncan, L. B. Goldstein, D. Matchar, G. W. Divine and J. Feussner, "Measurement of motor recovery after stroke. Outcome assessment and sample size requirements," *Stroke*, vol. 23, pp. 1084-1089, 1992.
- [19] J. J. Daly and J. R. Wolpaw, "Brain-computer interfaces in neurological rehabilitation," *Lancet Neurology*, vol. 7, pp. 1032-1043, 2008.
- [20] W. K. Tam, K. Tong, F. Meng and S. Gao, "A minimal set of electrodes for motor imagery BCI to control an assistive device in chronic stroke subjects: A multi-session study," *IEEE Transactions on Neural Systems and Rehabilitation Engineering*, vol. 19(6), pp. 617-627, 2011.
- [21] G. S. F. Ling, "Traumatic brain injury and spinal cord injury," *Goldmans Cecil Medicine 24th Edition*, Elsevier, chap. 406, 2011.
- [22] P. Shih and R. G. Fessler, "Trauma of the nervous system: Spinal cord trauma," *Bradley's Neurology in Clinical Practice 6th Edition*, Elsevier, chap. 50C, 2012.
- [23] M. A. Lebedev and M. A. L. Nicolelis, "Brain-machine interfaces: past, present and future," *Trends in Neurosciences*, vol. 29(9), pp. 536-546, 2006.
- [24] E. E. Fetz, "Operant conditioning of cortical unit activity," *Science*, vol. 163, pp. 955-958, 1969.
- [25] E. M. Schmidt, "Single neuron recording from motor cortex as a possible source of signals for control of external devices," *Annals of Biomedical Engineering*, vol. 8, pp. 339-349, 1980.
- [26] M. A. L. Nicolelis, L. A. Baccala, R. C. S. Lin and J. K. Chapin, "Sensorimotor encoding by synchronous neural ensemble activity at multiple levels of the somatosensory system," *Science*, vol. 268, pp. 1353-1358, 1995.
- [27] M. A. L. Nicolelis, "Actions from thoughts," *Nature*, vol. 409, pp. 403-407, 2001.
- [28] M. A. Lebedev MA, J. E. O'Doherty and M. A. L. Nicolelis, "Decoding of temporal intervals from cortical ensemble activity," *Journal of Neurophysiology*, vol. 99, pp. 166-186, 2008.

- [29] J. E. O’Doherty, M. A. Lebedev, P. J. Ifft, K. Z. Zhuang, S. Shokur, H. Bleuler and M. A. L. Nicolelis, “Active tactile exploration enabled by a brain-machine-brain interface,” *Nature*, vol. 479, pp. 228-231, 2011.
- [30] J. M. Carmena, M. A. Lebedev, R. E. Crist, J. E. O’Doherty, D. M. Santucci, D. F. Dimitrov, P. G. Patil, C. S. Henriquez and M. A. L. Nicolelis, “Learning to control a brain-machine interface for reaching and grasping by primates,” *PLoS Biology*, vol. 1(2), p. E42, 2003.
- [31] M. Velliste, S. Perel, M. C. Spalding, A. S. Whitford and A. B. T. Schwartz, “Cortical control of a prosthetic arm for self-feeding,” *Nature*, vol. 453, pp. 1098-1101, 2008.
- [32] L. R. Hochberg, D. Bacher, B. Jarosiewicz, N. Y. Masse, J. D. Simeral, J. Vogel, S. Haddadin, J. Liu, S. S. Cash, P. van der Smagt and J. P. Donoghue, “Reach and Grasp by People with Tetraplegia using a Neurally Controlled Robotic Arm,” *Nature*, vol. 485, pp. 372-375, 2012.
- [33] J. L. Collinger, B. Wodlinger, J. E. Downey, W. Wang, E. C. Tyler-Kabara, D. J. Weber, A. J. C. McMorland, M. Velliste, M. L. Boninger and A. B. Schwartz, “High-performance Neuroprosthetic Control by an Individual with Tetraplegia,” *The Lancet*, vol. 381(9866), pp. 557-564, 2013.
- [34] E. C. Leuthardt, G. Schalk, D. Moran and J. G. Ojemann, “The emerging world of motor neuroprosthetics: A neurosurgical perspective,” *Neurosurgery*, vol. 59(1), pp. 1-14, 2006.
- [35] E. C. Leuthardt, G. Schalk, J. R. Wolpaw, J. G. Ojemann and D. W. Moran, “A brain-computer interface using electrocorticographic signals in humans,” *Journal of Neural Engineering*, vol. 1(2), pp. 63-71, 2004.
- [36] J. A. Wilson, E. A. Felton, P. C. Garell, G. Schalk and J. C. Williams, “ECoG factors underlying multimodal control of a brain-computer interface,” *IEEE Transactions on Neural Systems and Rehabilitation Engineering*, vol. 14, pp. 246-250, 2006.

- [37] T. Pistohl, T. Ball, A. Schulze-Bonhage, A. Aertsen and C. Mehring, "Prediction of arm movement trajectories from ECoG-recordings in humans," *Journal of Neuroscience Methods*, vol. 167(1), pp. 105-114, 2008.
- [38] R. M. Demirer, M. S. Ozerdem and C. Bayrak, "Classification of imaginary movements in ECoG with a hybrid approach based on multi-dimensional Hilbert-SVM solution," *Journal of Neuroscience Methods*, vol. 178(1), pp. 214-218, 2009.
- [39] N. K. Logothetis, "The underpinnings of the BOLD functional magnetic resonance imaging signal," *Journal of Neuroscience*, vol. 23(10), pp. 3963-3971, 2003.
- [40] F. Matthews, B. A. Pearlmutter, T. E. Ward, C. Soraghan and C. Markham, "Hemodynamics for brain-computer interfaces," *IEEE Signal Processing Magazine*, vol. 25(1), pp. 87-94, 2008.
- [41] R. Sitaram, N. Weiskopf, A. Caria, R. Veit, M. Erb and N. Birbaumer, "fMRI brain-computer interfaces," *IEEE Signal Processing Magazine*, vol. 25(1), pp. 95-106, 2008.
- [42] N. Weiskopf, R. Sitaram, O. Josephs, R. Veit, F. Scharnowski, R. Goebel, N. Birbaumer, R. Deichmann and K. Mathiak, "Real-time functional magnetic resonance imaging: Methods and applications," *Magnetic Resonance Imaging*, vol. 25(6), pp. 989-1003, 2007.
- [43] J. H. Lee, J. Ryu, F. A. Jolesz, Z. H. Cho and S. S. Yo, "Brain-machine interface via real-time fMRI: Preliminary study on thought-controlled robotic arm," *Neuroscience Letters*, vol. 450(1), pp. 1-6, 2009.
- [44] J. Mellinger, G. Schalk, C. Braun, H. Peissl, W. Rosenstiel, N. Birbaumer and A. Kubler, "An MEG-based brain-computer interface (BCI)," *Neuroimage*, vol. 36(3), pp. 581-593, 2007.
- [45] F. Tecchio, C. Porcaro, G. Barbati and F. Zappasodi, "Functional source separation and hand cortical representation for brain-computer interface feature extraction," *Journal of Physiology*, vol. 580(3), pp. 703-721, 2007.

- [46] E. Buch, C. Weber, L. G. Cohen, C. Braun, M. A. Dimyan, T. Ard, J. Mellinger, A. Caria, S. Soekadar, A. Fourkas and N. Birbaumer, "Think to move: A neuro-magnetic brain-computer interface (BCI) system for chronic stroke," *Stroke*, vol. 39(3), pp. 910-917, 2008.
- [47] M. van Gerven and O. Jensen, "Attention modulations of posterior alpha as a control signal for two-dimensional brain-computer interfaces," *Journal of Neuroscience Methods*, vol. 179(1), pp. 78-84, 2009.
- [48] J. R. Wolpaw, N. Birbaumer, D. J. McFarland, G. Pfurtscheller and T. M. Vaughan, "Brain-computer interfaces for communication and control," *Clinical Neurophysiology*, vol. 113, pp. 767-791, 2002.
- [49] G. Pfurtscheller, G. R. Müller-Putz, R. Scherer and C. Neuper, "Rehabilitation with brain-computer interface systems," *Computer*, vol. 41(10), pp. 58-65, 2008.
- [50] J. N. Mak and J. R. Wolpaw, "Clinical applications of brain-computer interfaces: Current state and future prospects," *IEEE Rev. Biomed. Eng.*, vol. 2, pp. 187-199, 2009.
- [51] J. del. R. Millan et al., "Combining brain-computer interfaces and assistive technologies: state-of-the-art and challenges," *Frontiers in Neuroscience*, vol. 4:161, 2010.
- [52] E. Olbrich and P. Achermann, "Analysis of oscillatory patterns in the human sleep EEG using a novel detection algorithm," vol. 14(4), pp. 337-346, 2005.
- [53] C. Spironelli, A. Angrilli, A. Calogero and L. Stegagno, "Delta EEG band as a marker of left hypofrontality for language in schizophrenia patients," *Schizophrenia Bulletin*, vol. 37(4), pp. 757-767, 2011.
- [54] J. F. Cavanagh and M. J. Frank, "Frontal theta as a mechanism for cognitive control," *Trends in Cognitive Sciences*, in press.
- [55] L. V. Moran and L. Elliot Hong, "High vs low frequency neural oscillations in schizophrenia," *Schizophrenia Bulletin*, vol. 37(4), pp. 659-663, 2011.

- [56] P. W. Kaplan, D. Genoud, T. W. Ho and P. Jallon, "Etiology, neurologic correlations, and prognosis in alpha coma," *Clinical Neurophysiology*, vol. 110(2), pp. 205-213, 1999.
- [57] T. Hayashi, E. Okamoto, H. Nishimura, Y. Mizuno-Matsumoto, R. Ishii and S. Ukai, "Beta activities in EEG associated with emotional stress," *International Journal of Intelligent Computing in Medical Sciences and Image Processing*, vol. 3(1), pp. 57-68, 2009.
- [58] D. J. Serrien, A. H. Pogosyan and P. Brown, "Cortico-cortical coupling patterns during dual task performance," *Experimental Brain Research*, vol. 157(1), pp. 79-84, 2004.
- [59] D. J. McFarland, L. A. Miner, T. M. Vaughan and J. R. Wolpaw, "Mu and beta rhythm topographies during motor imagery and actual movements," *Brain Topography*, vol. 12(3), pp. 177-186, 2000.
- [60] American Electroencephalographic Society, "American Electroencephalography Society guidelines for standard electrode position nomenclature," *Journal of Clinical Neurophysiology*, vol. 8(2), pp. 200-202, 1991.
- [61] E. Iáñez, J. M. Azorín, A. Úbeda, J. M. Ferrández and E. Fernández, , "Mental tasks-based brain-robot interface," *Robotics and Autonomous Systems*, vol. 58(12), pp. 1238-1245, 2010.
- [62] B. Obermaier, G. R. Müller and G. Pfurtscheller, "Virtual keyboard controlled by spontaneous EEG activity," *IEEE Trans. Neural Syst. Rehabil. Eng.*, vol. 11, pp. 422-426, 2003.
- [63] S. Inoue, Y. Akiyama, Y. Izumi and S. Nishijima, "The development of BCI using alpha waves for controlling the robot arm," *IEICE Transactions on Communications*, vol. 91(7), pp. 2125-2132, 2008.
- [64] J. Decety and M. Lindgren, "Sensation of effort and duration of mentally executed actions," *Scandinavian Journal of Psychology*, vol. 32, pp. 97-104, 1991.

- [65] L. A. Farwell and E. Donchin, "Talking off the top of your head: Toward a mental prosthesis utilizing event-related brain potentials," *Electroenceph. Clin. Neurophysiol.*, vol. 70, pp. 510-523, 1998.
- [66] B. Z. Allison and J. A. Pineda, "ERPs evoked by different matrix sizes: Implications for a brain computer interface (BCI) system," *IEEE Trans. Neural Sys. Rehab. Eng.*, vol. 11, pp. 110-113, 2003.
- [67] I. Iturrate, J.M. Antelis, A. Kubler and J. Minguez, "A noninvasive brain-actuated wheelchair based on a P300 neurophysiological protocol and automated navigation," *IEEE Transactions on Robotics*, vol. 25(3), pp. 614-627, 2009.
- [68] E. Mugler, M. Bensch, S. Halder, W. Rosenstiel, M. Bogdan, N. Birbaumer and A. Kübler, "Control of an internet browser using P300 event-related potential," *Int. J. Bioelectromagn.*, vol. 10, pp. 56-63, 2008.
- [69] M. Bensch, A. A. Karim, J. Mellinger, T. Hinterberger, M. Tangermann, W. Rosenstiel and N. Birbaumer, "Nessi: An EEG-controlled web browser for severely paralyzed patients," *Computational Intelligence and Neuroscience*, 2007.
- [70] M. Eimer, "The N2pc component as an indicator of attentional selectivity," *Electroencephalography and clinical Neurophysiology*, vol. 99, pp. 225-234, 1996.
- [71] M. Kiss, J. Van Velzen and M. Eimer, "The N2pc component and its links to attention shift and spatially selective visual processing," *Psychophysiology*, vol. 45(2), pp. 240-249, 2008.
- [72] D. Regan, "Steady-state evoked potentials," *Journal of the Optical Society of America*, vol. 67(11), pp. 1475-1489, 1977.
- [73] R. B. Silberstein, P. L. Nunez, A. Pipingas, P. Harris and F. Danieli, "Steady state visually evoked potential (SSVEP) topography in a graded working memory task," *International Journal of Psychophysiology*, vol. 42(2), pp. 219-232, 2001.

- [74] J. Ding, G. Sperling and R. Srinivasan, "Attentional modulation of SSVEP power depends on the network tagged by the flicker frequency," *Cerebral Cortex*, vol. 16(7), pp. 1016-1029, 2006.
- [75] T. Hinterberger, S. Schmidt, N. Neumann, J. Mellinger, B. Blankertz, G. Curio and N. Birbaumer, "Brain-computer communication and slow cortical potentials," *IEEE Transactions on Biomedical Engineering*, vol. 51(6), pp. 1011-1018, 2004.
- [76] N. Birbaumer, N. Ghanayim, T. Hinterberger, I. Iversen, B. Kotchoubey, J. Perelmouter, E. Taub and H. Flor, "A spelling device for the paralysed," *Nature*, vol. 398, pp. 297-298, 1999.
- [77] T. J. Bradberry, R. J. Gentili and J. L. Contreras-Vidal, "Reconstructing three-dimensional hand movements from non-invasive electroencephalographic signals," *The Journal of Neuroscience*, vol. 30(9), pp. 3432-3437, 2010.
- [78] A. Presacco, L. W. Forrester and J. L. Contreras-Vidal, "Decoding lower-limb intra and inter-limb coordination during treadmill walking from scalp EEG signals," *IEEE Transactions on Neural Systems and Rehabilitation Engineering*, vol. 20(2), pp. 212-219, 2012.
- [79] G. Pfurtscheller and F. H. Lopes Da Silva, "Event-related EEG/MEG synchronization and desynchronization: basic principles," *Clinical Neurophysiology*, vol. 110(11), pp. 1842-1857, 1999.
- [80] D. Planelles, E. Hortal, A. Costa, E. Iáñez and J. M. Azorín, "First steps in the development of an EEG-based system to detect intention of gait initiation," *8th Annual IEEE International Systems Conference*, pp. 167-171, 2014.
- [81] G. R. Müller-Putz, R. Scherer, G. Pfurtscheller and R. Rupp, "Brain-computer interfaces for control of neuroprostheses: from synchronous to asynchronous mode of operation," *Biomedizinische Technik*, vol. 51, pp. 57-63, 2006.
- [82] K. -R. Müller and B. Blankertz, "Toward noninvasive brain-computer interfaces," *IEEE Signal Process. Mag.*, vol. 23, pp. 125-128, 2006.

- [83] J. L. Sirvent, E. Iáñez, A. Úbeda and J. M. Azorín, “Visual evoked potential-based brain—machine interface applications to assist disabled people,” *Expert Systems with Applications*, vol. 39(9), pp. 7908-7918, 2012.
- [84] E. W. Sellers and E. Donchin, “A P300-based brain-computer interface: Initial tests by ALS patients,” *Clinical Neurophysiology*, vol. 117(3), pp. 538-548, 2006.
- [85] T. Carlson and J. d. R. Millán, “Brain-controlled wheelchairs: a robotic architecture,” *IEEE Robotics and Automation Magazine*, vol. 20(1), pp. 65-73, 2013.
- [86] L. Tonin, R. Leeb, M. Tavella, S. Perdikis and J. d. R. Millán, “The role of shared-control in BCI-based telepresence,” *IEEE International Conference on Systems, Man, and Cybernetics*, 2010.
- [87] S. P. Kim, J. D. Simeral, L. R. Hochberg, J. P. Donoghue, G. M. Friehs and M. J. Black, “Point-and-click cursor control with an intracortical neural interface system by humans with tetraplegia,” *IEEE Transactions on Neural Systems and Rehabilitation Engineering*, vol. 19(2), pp. 193-203, 2011.
- [88] J. D. Simeral et al., “Neural control of cursor trajectory and click by a human with tetraplegia 1000 days after implant of an intracortical microelectrode array,” *Journal of Neural Engineering*, vol. 8(2), 2011.
- [89] J. R. Wolpaw and D. J. McFarland, “Control of a two-dimensional movement signal by a noninvasive brain-computer interface in humans,” *Proceedings of the National Academy of Sciences*, vol. 101, pp. 17849-17854, 2004.
- [90] D. J. McFarland, W. A. Sarnacki and J. R. Wolpaw, “Electroencephalographic (EEG) control of three-dimensional movement,” *Journal of Neural Engineering*, vol. 7(3), 2011.
- [91] G. Pfurtscheller, C. Guger, G. Muller, G. Krausz and C. Neuper, “Brain oscillations control hand orthosis in a tetraplegic,” *Neuroscience Letters*, vol. 292(3), pp. 211-214, 2000.

- [92] J. J. Daly and J. R. Wolpaw, "Brain-computer interfaces in neurological rehabilitation," *Lancet Neurology*, vol. 7, pp. 1032-1043, 2008.
- [93] G. R. Müller and G. Pfurtscheller, "Control of an electrical prosthesis with an SSVEP-based BCI," *IEEE Transactions on Biomedical Engineering*, pp. 361-364, 2008.
- [94] N. Sharma, V. M. Pomeroy and J-C. Baron, "Motor imagery: A backdoor to the motor system after stroke?," *Stroke*, pp. 1941-1952, 2006.
- [95] A. Bashashati, M. Fatourechi, R. K. Ward and G.E. Birch, "A survey of signal processing algorithms in brain-computer interfaces based on electrical brain signals," *Journal of Neural Engineering*, vol. 4(2), pp. 35-57, 2007.
- [96] D. Gutiérrez and D. I. Escalona-Vargas, "EEG data classification through signal spatial redistribution and optimized linear discriminants," *Computer Methods and Programs in Biomedicine*, vol. 97(1), pp. 39-47, 2010.
- [97] F. Lotte, M. Congedo, A. Lécuyer, F. Lamarche and B. Arnaldi, "A review of classification algorithms for EEG-based brain-computer interfaces," *Journal of Neural Engineering*, vol. 4, pp. 1-13, 2007.
- [98] C.-J. Lin and M.-H. Hsieh, "Classification of mental task from EEG data using neural networks based on particle swarm optimization," *Neurocomputing*, vol. 72(4-6), pp. 1121-1130, 2009.
- [99] A. Subasi and E. Erçelebi, "Classification of EEG signals using neural network and logistic regression," *Computer Methods and Programs in Biomedicine*, vol. 78(2), pp. 87-99, 2005.
- [100] H. J. Hwang, K. Kwon and C. H. Im, "Neurofeedback-based motor imagery training for brain-computer interface (BCI)," *Journal of Neuroscience Methods*, vol. 179(1), pp. 150-156, 2009.

- [101] W. Y. Hsu and Y. N. Sun, "EEG-based motor imagery analysis using weighted wavelet transform features," *Journal of Neuroscience Methods*, vol. 176(2), pp. 310-318, 2009.
- [102] W. Y. Hsu, "EEG-based motor imagery classification using neuro-fuzzy prediction and wavelet fractal features," *Journal of Neuroscience Methods*, vol. 189(2), pp. 295-302, 2010.
- [103] V. S. Prasad, J. M. K. Murthy and S. Sailaja, "Surface mapping of spike potential fields: Visual vs. quantitative EEG analysis," *Neurology India*, vol. 50, pp. 181-183, 2002.
- [104] M. V. Sebastián, M. A. Navascués and J.R. Valdizán, "Surface laplacian and fractal brain mapping," *Journal of Computational and Applied Mathematics*, vol. 189, pp. 132-141, 2006.
- [105] M. T. H. Wong and F. Lieh-Mak, "Topographic brain mapping of EEG and evoked potentials in chinese normal and psychiatric patients - Preliminary findings," *Hong Kong Journal of Psychiatry*, vol. 1, pp. 6-11, 1991.
- [106] R. Kennerly, "QEEG analysis of cranial electrotherapy: A pilot study," *Journal of Neurotherapy*, vol. 8(2), pp. 112-113, 2004.
- [107] A. Tzovara, M. M. Murray, G. Plomp, M. H. Herzog and C. M. Michel, "Decoding stimulus-related information from single-trial EEG responses based on voltage topographies," *Pattern Recognition*, vol. 45, pp. 2109-2122, 2012.
- [108] A. Tzovara, M. M. Murray, N. Bourdaud, R. Chavarriaga, J. del R. Millán and M. De Lucia, "The timing of exploratory decision-making revealed by single-trial topographic EEG analyses," *NeuroImage*, vol. 60, pp. 1959-1969, 2012.
- [109] A. Biasiucci, R. Chavarriaga, B. Hammer, R. Leeb, F. Pichiorri, F. De V. Fallani, D. Mattia and J. del. R. Millán, "Combining discriminant and topographic information in BCI: preliminary results on stroke patients," *IEEE EMBS Conference on Neural Engineering*, pp. 290-293, 2011.

- [110] J. P. Lewis, "Fast normalized cross-correlation," *Industrial Light and Magic*, 1995.
- [111] R. Brunelli and T. Poggio, "Face recognition: features versus templates," *IEEE Transactions on Pattern Analysis and Machine Intelligence*, vol. 15(10), pp. 1042-1052, 1993.
- [112] BCI Competitions 2003 Web Source: Data Set V results, viewed 5 July 2011, <<http://www.bbci.de/competition/iii/results/#martigny>>.
- [113] BCI Competitions 2003 Web Source: Data Set V description, viewed 5 July 2011, <[http://www.bbci.de/competition/iii/desc\\_V.html](http://www.bbci.de/competition/iii/desc_V.html)>.
- [114] D. T. Sandwell, "Biharmonic spline interpolation of GEOS-3 and SEASAT altimeter data," *Geophysical Research Letters*, vol. 2, pp. 139-142, 1987.
- [115] D. J. McFarland, L. M. McCane, S. V. David and J. R. Wolpaw, "Spatial filter selection for EEG-based communication," *Electroencephalography and Clinical Neurophysiology*, vol. 103(3), pp. 386-394, 1997.
- [116] C. Guger, A. Schlogl, C. Neuper, D. Walterspacher, T. Strein and G. Pfurtscheller, "Rapid prototyping of an EEG-based brain-computer interface (BCI)," *IEEE Transactions on Rehabilitation Engineering*, vol. 9(1), pp. 49-58, 2001.
- [117] F. J. Badesa, R. Morales, N. García-Aracil, J. M. Sabater, C. Pérez-Vidal and E. Fernández, "Multimodal interfaces to improve therapeutic outcomes in robot-assisted rehabilitation," *Transactions on Systems, Man, and Cybernetics-Part C: Applications and Reviews*, vol. 42(6), pp.1152-1158, 2012.
- [118] A. Llinares, F. J. Badesa, R. Morales, N. Garcia-Aracil, J. M. Sabater and E. Fernandez, "Robotic assessment of the influence of age on upper-limb sensorimotor function," *Clinical Interventions in Aging*, vol. 2013(8), pp. 879-888, 2013.
- [119] G. Schalk, J. Kubanek, K. J. Miller, N. R. Anderson, E. C. Leuthardt, "Decoding two-dimensional movement trajectories using electrocorticographic signals in human," *Journal of Neural Engineering*, vol. 4, pp. 264-275, 2012.

- [120] T. Pistohl, A. Schulze-Bonhage, A. Aertsen, C. Mehring and T. Ball, "Decoding natural grasp types from human ECoG," *Neuroimage*, vol. 59(1), pp. 248-260, 2012.
- [121] A. P. Georgopoulos, F. J. Langheim, A. C. Leuthold and A. N. Merkle, "Magnetoencephalographic signals predict movement trajectory in space," *Experimental Brain Research*, vol. 167, pp. 132-135, 2005.
- [122] S. Waldert, H. Preissl, E. Demandt, C. Braun, N. Birbaumer, A. Aertsen and C. Mehring, "Hand movement direction decoded from MEG and EEG," *The Journal of Neuroscience*, vol. 28(4), pp. 1000-1008, 2008.
- [123] P. Ofner and G. R. Müller-Putz, "Decoding of velocities and positions of 3D arm movement from EEG," *International Conference of the IEEE EMBS*, pp.6406-6409, 2012.
- [124] J. M. Antelis, L. Montesano, A. Ramos-Murguialday, N. Birbaumer and J. Minguéz, "On the usage of linear regression models to reconstruct limb kinematics from low frequency EEG signals," *PLoS ONE*, vol. 8(4), e61976, 2013.
- [125] T. J. Bradberry, R. J. Gentili and J. L. Contreras-Vidal, "Fast attainment of computer cursor control with noninvasively acquired brain signals," *Journal of Neural Engineering*, vol. 8(3), 2011.
- [126] R. Poli and M. Salvaris, "Comment on "Fast attainment of computer cursor control with noninvasively acquired brain signals" ," *Journal of Neural Engineering*, vol. 8(5), 2011.
- [127] T. J. Bradberry, R. J. Gentili and J. L. Contreras-Vidal, "Reply to comment on "Fast attainment of computer cursor control with noninvasively acquired brain signals" ," *Journal of neural engineering*, vol. 8(5), 2011.
- [128] K. Choi, "Reconstructing four joint angles on the shoulder and elbow from non-invasive electroencephalographic signals through electromyography," *Frontiers in Neuroscience*, vol. 7, a190, pp. 1-9, 2013.

- [129] N. J. Beuchat, R. Chavarriaga, S. Degallier and J. d. R. Millán, “Offline decoding of upper limb muscle synergies from EEG slow cortical potentials,” *International Conference of the IEEE EMBS*, pp. 3594-3597, 2013.
- [130] G. Garipelli, R. Chavarriaga and J. d. R. Millán, “Single trial analysis of slow cortical potentials: a study on anticipation related potential,” *Journal of Neural Engineering*, vol. 10(3), 2013.
- [131] H. A. Agashe and J. L. Contreras-Vidal, “Reconstructing hand kinematics during reach to grasp movements from electroencephalographic signals,” *International Conference of the IEEE EMBS*, pp. 5444-5447, 2011.
- [132] A. Úbeda, E. Hortal, E. Iáñez, D. Planelles and J. M. Azorín, “Passive robot assistance in arm movement decoding from EEG signals,” *International IEEE EMBS Neural Engineering Conference*, pp. 895-898, 2013.
- [133] P. S. Hammon, S. Makeig, H. Poizner, E. Todorov and V. R. de Sa, “Predicting reaching targets from human EEG,” *IEEE Signal Processing Magazine*, vol. 25, pp. 69–77, 2008.
- [134] N. Robinson, C. Guan, A. P. Vinod, K. K. Ang and K. P. Tee, “Multi-class EEG classification of voluntary hand movement directions,” *Journal of Neural Engineering*, vol. 10(5), 056018, 2013.
- [135] E. Lew, R. Chavarriaga, S. Silvoni and J. del R. Millán, “Single trial prediction of self-paced reaching directions from EEG signals,” *Frontiers in Neuroscience*, vol. 8, pp. 222, 2014.
- [136] E. Lew, R. Chavarriaga, S. Silvoni and J. d. R. Millán, “Detection of self-paced reaching movement intention from EEG signals,” *Frontiers in Neuroengineering*, vol. 5, p. 13, 2012.
- [137] N. Takeuchi and S.-I. Izumi, “Rehabilitation with poststroke motor recovery: A review with a focus on neural plasticity,” *Stroke Research and Treatment*, vol. 2013, ID: 128641, 2013.

- [138] R. S. Johansson, G. Westling, A. Bäckstöm and J. R. Flanagan, “Eye-hand coordination in object manipulation,” *The Journal of Neuroscience*, vol. 21(17), pp. 6917-6932, 2001
- [139] g.Tec Medical Engineering, Official Website, Available: <http://www.gtec.at>, last visit: 25 May 2014.
- [140] BioSemi, Official Website, Available: <http://www.biosemi.com>, last visit: 25 May 2014.



## Hardware and Equipment

### A.1 EEG Acquisition Devices

#### A.1.1 gUSBamp BMI System

The g.USBamp is a high-performance and high-accuracy biosignal amplifier and acquisition/processing system [139]. It allows investigation of brain-, heart- and muscle-activity, eye movements, respiration, galvanic skin response and many other physiological and physical parameters (Figure A.1).

The amplifier uses wide-range DC-coupled amplifier technology in combination with 24-bit sampling. The result is an input voltage range of +/- 250 mV with a resolution of < 30 nV. This means that any electrophysiological signal can be recorded directly without additional hardware. The use of digital filters avoids hardware-related variations between channels. An active electrode system can also be connected directly, as well as different sensors (e.g. GSR, skin temperature or blood pressure among others).

Each of the 16 analog to digital converters operates at 2.4576 MHz. Oversampling 64 times yields the internal sampling rate of 38.400 Hz. In addition, a floating point Digital Signal Processor performs oversampling and real-time filtering of the biosignal data (between 0 Hz - 2.400 Hz). This results in a very high signal to noise ratio.

In this thesis, two gUSBamp solutions for the recording of the EEG signals have been used: a passive 16-electrodes system (Figure A.2) and an active 16-electrodes system (Figure A.3). The main components of these systems are summarized next:

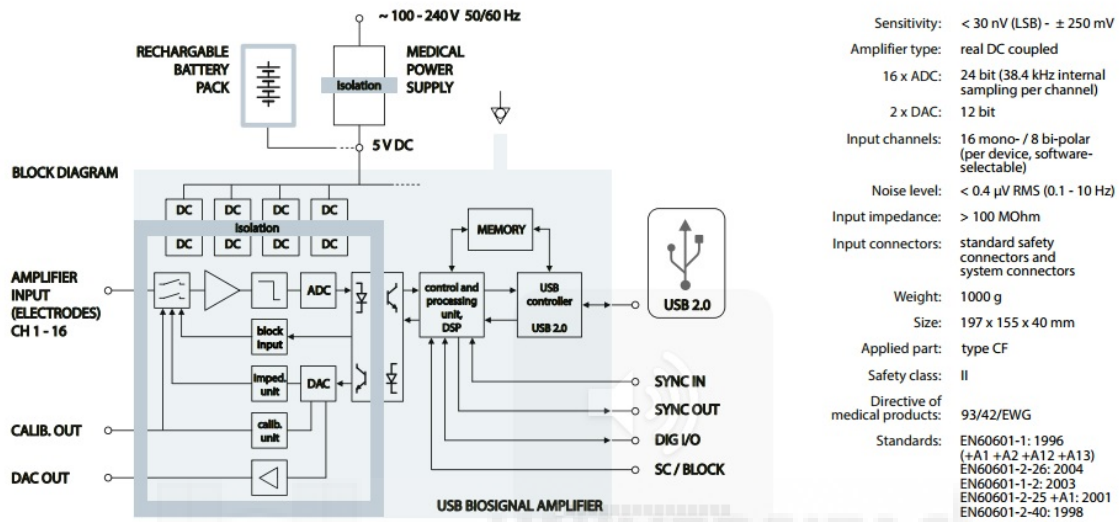


Figure A.1: gUSBamp technical specifications

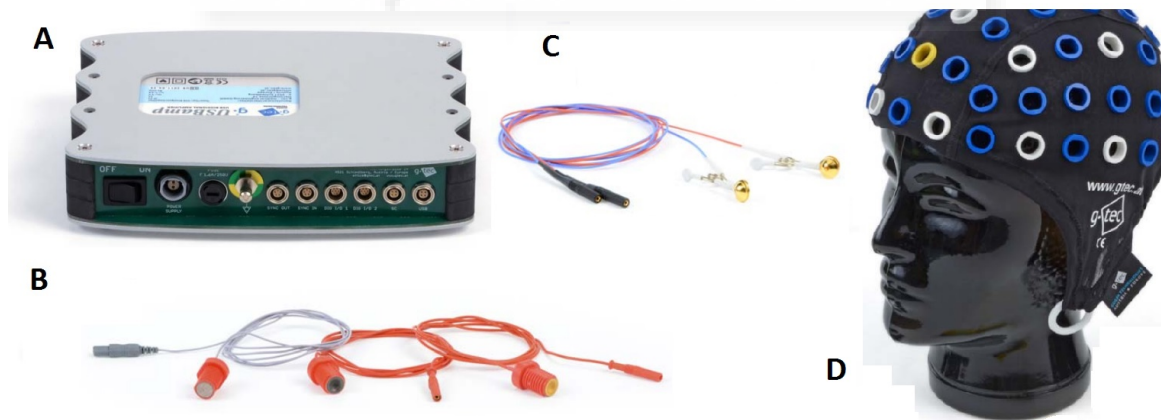


Figure A.2: gUSBamp passive 16-electrodes system. A-gUSBamp amplifier, B-g.EEGelectrode Au, C-Ear-clip electrode Au, D-g.EEGcap, 65 positions.

- gUSBamp amplifier: multi-modal biosignal amplifier (silver) with USB interface; 16 channels; 4 separated grounds.
- g.EEGelectrode Au: screwable passive gold EEG electrode, 100 cm lead, 1.5 mm safety connector.
- Ear-clip electrode Au: gold; to apply at the earlobes.
- g.LADYbird: active ring electrode, can be used with g.GAMMAcap2 (EEG) or with adhesive washer (ECG, EMG, EOG), sintered Ag/AgCl crown (for DC recordings), 125 cm lead, 2-pin safety connector.
- g.LADYbirdGND: passive ground ring electrode, can be used with g.GAMMAcap2 (EEG) or with adhesive washer (ECG, EMG, EOG), sintered Ag/AgCl crown (for DC recordings), 125 cm lead, 2-pin safety connector.
- g.GAMMAearclip Ag/AgCl: active earclip Ag/AgCl electrode (reference), sintered Ag/AgCl crown, 125 cm lead, 2-pin safety connector.
- g.EEGcap, 65 positions: electrode cap with 65 electrode positions; extended 10/20 system.

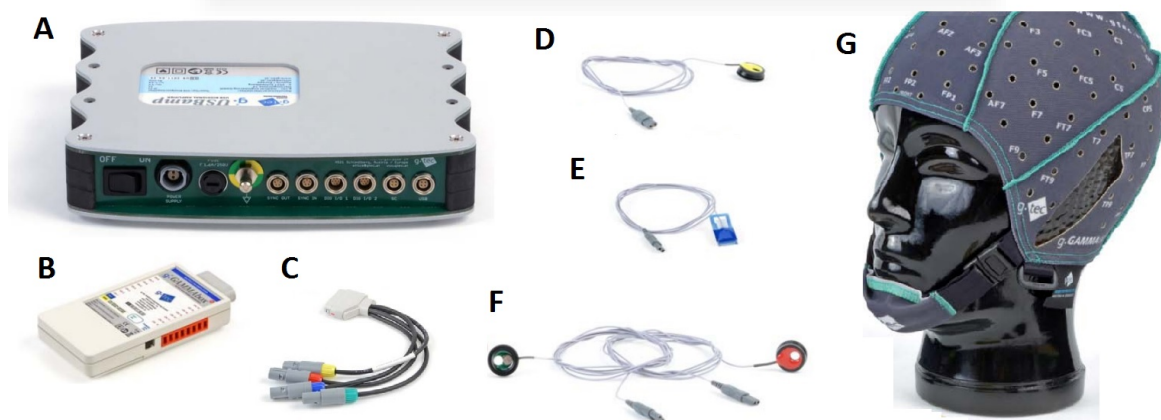


Figure A.3: gUSBamp active 16-electrodes system. A-gUSBamp amplifier, B-g.USBampGAMMAbox for 16 channels, C-g.USBampGAMMAconnector, D-g.LADYbirdREF, E-g.LADYbirdGND, F-g.LADYbird, G-g.GAMMAcap2, 74 position.

- g.GAMMAcap2, 74 position: electrode cap with 74 standard and 86 intermediate position; extended 10/10 system.
- g.USBampGAMMAbox for 16 channels: power supply and driver/interface box for 16 active electrodes.
- g.USBampGAMMAconnector: connector cable between the g.USBamp (system connector) and the g.GAMMAbox; 40 cm lead.

### A.1.2 BioSemi ActiveTwo BMI System

The ActiveTwo AD-box forms a compact, low power galvanically isolated front-end (close to the subject) in which up to 256 sensor-signals are digitized with 24 bit resolution [140]. These sensors can be Active electrodes but also BioSemi Bufferboxes with normal passive electrodes, as well as a range of additional active sensors measuring parameters like respiration, temperature, force etc. Each AD-box channel consists of a low noise DC coupled post-amplifier, with a first order anti-aliasing filter, followed by a Delta-Sigma modulator with an oversampling rate of 64, and decimation filter with a steep fifth order sinc response and high resolution 24-bit output. The digital outputs of all the AD converters (up to 256) are digitally multiplexed and sent to the PC via a single optical fiber without any compression or other form of data reduction.

The main features of this biomedical device are:

- Special input stage matched with the output of the new 2-wire Active electrodes.
- Powersupply to active electrodes has auto-shutdown for optimal safety.
- ADC per channel offers synchronized sampling, no skew, zero-reference principle.
- 24 bit sampling, 31nV digital resolution with guaranteed no missing codes.
- Sigma-Delta converter technology for unsurpassed linearity and dynamic range.
- Configurable/upgradeable number of channels: 8 up to 256 channels.
- Up to 16 kHz sample-rate per channel, user selectable (1.5MByte/sec total throughput).

- Full DC operation, with input range as large as found in AC designs.
- Battery powersupply with fiber optic link offers optimal interference rejection and subject safety.
- Low power design: 5 hour battery life for 256 channels, 1 week for 8 channels.

In this thesis, a Biosemi ActiveTwo 64-electrodes solution for the recording of the EEG signals has been used (Figure A.4). The main components of this system are summarized next:

- ActiveTwo AD-box: a compact, low power galvanically isolated front-end (close to the subject) in which up to 256 sensor-signals are digitized with 24 bit resolution.
- BioSemi headcap, 64 electrodes: consists of an elastic cap with plastic, electrode holders.
- Pin-Type Active-electrodes: sintered Ag-AgCl electrode, extremely low-noise measurements free of interferences.



Figure A.4: BioSemi ActiveTwo active 64-electrodes system. A-ActiveTwo AD-box, B-BioSemi headcap, C-Pin-Type Active-electrodes.

## A.2 Planar Robot Arm

The planar robot arm used in this thesis is the PuPArm, a force-controlled planar robot designed and developed by the nBio research group at the Miguel Hernández University of Elche (Spain). It is based on a four bar mechanism similar to the MIT-MANUS rehabilitation robot [117, 118]. The mechanism is configured as a generic planar two-dimensional manipulator and optimized for delivering rehabilitation therapies, in which end-point impedance must be minimized. The pneumatic rehabilitation robot is composed of several parts as it can be seen in Figure A.5. It consists of a two-dimensional manipulator fixed to a table, a tactile monitor with a custom developed software which is used as a Graphical User Interface.

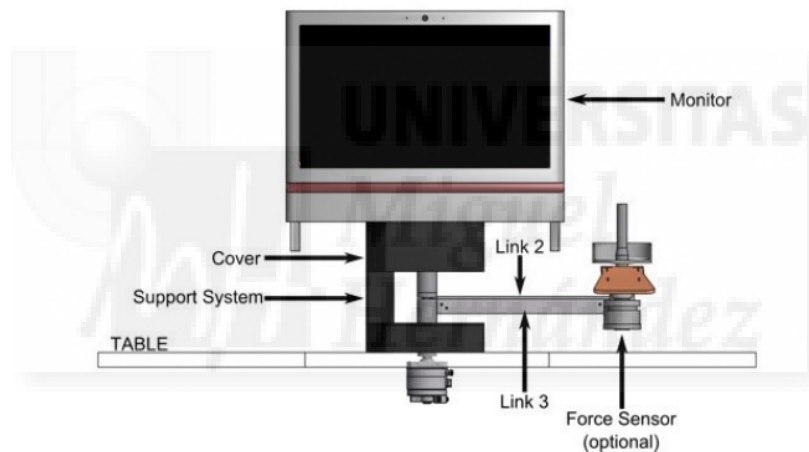


Figure A.5: Pneumatic planar robot: Parts.

The technical characteristics of the PuPArm robot are the following (see Figure A.6):

- A pneumatic swivel module with angular displacement encoder (DSMI-25-270-A-B of Festo) has been used as actuator for each two joints. This kind of actuators can exert enough driving power despite being lightweight and having a small size because the ratio of its output power to its weight is large. The semi-rotative drives are controlled by two proportional pressure valves (MPPE manufactured by Festo) to achieve a maximum torque of 5 Nm at 6 bar and a maximum swivel angle

of  $270^\circ$ . The valve MPPE is designed so that pressure output is proportional to voltage input through a proportional electromagnet. With this configuration (two proportional valves and a pneumatic actuator), the pressure of the two chambers of the pneumatic drive can be regulated to get a desired output force.

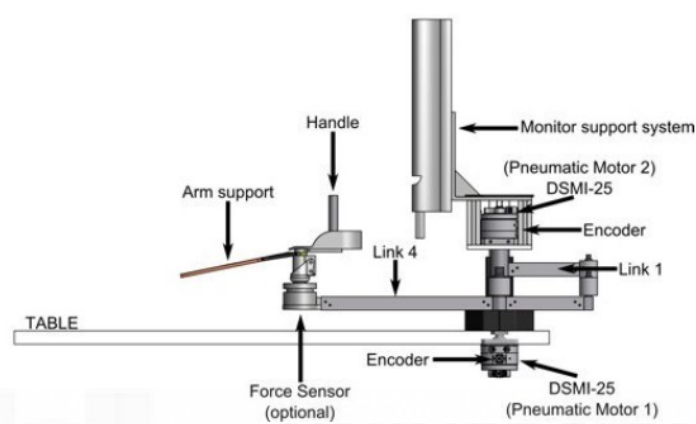


Figure A.6: Pneumatic planar robot: Components.

- The core of the control system is a motion controller board (DMC-40) manufactured by Galil. It operates stand-alone or interfaces to a PC with Ethernet 10/100Base-T or RS232. The controller includes optically isolated I/O, high-power outputs capable of driving brakes or relays, and analog inputs for interfacing to analog sensors. Four analog outputs from the DMC-40 board are used to control each pneumatic actuator through two proportional pressure valves. An electronic board, called distributor, has been designed to convert the control signal from each joint into two voltage inputs for its respective proportional pressure valves (it is assumed that the valves behavior is identical).